ÄSPÖLABORATORIET

INTERNATIONAL COOPERATION REPORT

95-01

Simulations of pressure and salinity fields at Äspö

Jari Löfman, Veikko Taivassalo
VTT Energy, Espoo, Finland

June 1995

Supported by TVO, Finland

SVENSK KÄRNBRÄNSLEHANTERING AB
SWEDISH NUCLEAR FUEL AND WASTE MANAGEMENT CO
BOX 5864 S-102 40 STOCKHOLM
TEL. +46-8-665 28 00 TELEX 13108 SKB TELEFAX +46-8-661 57 19

9603010261 960214
PDR WASTE
WM-11 PDR

ISSN 1104-3210
ISRN SKB-ICR--95/01--SE

SIMULATIONS OF PRESSURE AND SALINITY FIELDS AT ÄSPÖ

Jari Löfman, Veikko Taivassalo

VTT Energy, Espoo, Finland

June 1995

Supported by TVO, Finland

This document concerns a study which was conducted within an Äspö HRL joint project. The conclusions and viewpoints expressed are those of the author(s) and do not necessarily coincide with those of the client(s). The supporting organization has reviewed the document according to their documentation procedure.

SIMULATIONS OF PRESSURE AND SALINITY FIELDS AT ÄSPÖ

Jari Löfman
Veikko Taivassalo

VTT Energy
Espoo, Finland

Supported by TVO, Finland

June 1995

ABSTRACT

The primary objective of this study was to examine whether the geochemical field data from the Äspö site can be interpreted and understood by means of numerical simulations for flow and transport. A site-specific simulation model for the coupled system of groundwater flow and salt transport was developed on the basis of the field investigations. Both steady-state and transient analyses were performed. In the transient simulations, land uplift and matrix diffusion were taken into account.

Two conceptual models for solute transport in a fractured medium were applied. In the equivalent-continuum approach, a rock mass is treated as a homogeneous continuum with representative hydraulic characteristics. The dual-porosity model is able to take into account the diffusion of solute particles between moving water and stagnant water. It assumes that the medium consists of two overlapping continuums for the fractures with flowing water and matrix blocks with stagnant water. The dual-porosity approach was implemented in the FEFLOW code used in the simulations.

A finite element mesh of 42000 elements was created for the Äspö site. In order to examine the sensitivity of the results on the input parameters, various salinity models and several parameter values were applied. The transient simulations were carried out for a period that started 3000 years ago (at the end of the Litorina stage) when the highest hills at Äspö rose above sea level. The simulation period continued until the present day.

The pressure and salinity field computed for various assumptions and parameter values were compared with each other and with the experimental data from Äspö. The pressure proved to depend strongly on a salinity model used as an initial state. The pressure and salt concentration calculated for a salinity model with a constant initial salinity of 10 g/l coincide best with the values measured in the cored boreholes. The salt concentrations computed both for the equivalent-continuum and dual-porosity models agreed equally well with the field data. The location of the fracture zones could not be identified in the results of the equivalent-continuum approach, while they could clearly be recognized in the salinity fields computed applying the dual-porosity model. Regarding the general behavior along the boreholes, the field data resemble the equivalent-continuum results more than the dual-porosity results. On the other hand, dual-porosity results that better agree with the experimental data would obviously be obtained by varying the salinity model and input parameters. Despite the scarcity of prior information about the input parameters, the dual-porosity model proved to be a useful approach when simulating solute transport in a fractured rock mass. The approach makes it possible to predict the concentration not only in flowing water but also in the rock matrix with stagnant water.

TABLE OF CONTENTS

		Page
	EXECUTIVE SUMMARY	iv
1	**INTRODUCTION**	**1**
1.1	BACKGROUND	1
1.2	GROUNDWATER FLOW CONDITIONS AT ÄSPÖ	1
1.3	MODELLING GROUNDWATER FLOW IN FRACTURED BEDROCK	2
1.4	OVERVIEW OF THIS REPORT	8
2	**SIMULATION OF FLOW AND TRANSPORT**	**9**
2.1	FEFLOW CODE	9
2.2	EQUIVALENT-CONTINUUM APPROACH	12
2.2.1	Conceptual model	12
2.2.2	Governing equations	12
2.2.3	Numerical solution method	14
2.3	DUAL-POROSITY APPROACH	17
2.3.1	Conceptual model	17
2.3.2	Governing equations	17
2.3.3	Numerical solution method	20
2.3.4	Verification	24
3	**SIMULATION MODEL FOR THE ÄSPÖ SITE**	**38**
3.1	FLOW MODEL	38
3.1.1	Geometry of the fracture zones	38
3.1.2	Properties of the bedrock	46
3.2	FINITE ELEMENT MESH	50
3.3	INITIAL AND BOUNDARY CONDITIONS	52
3.3.1	Pressure	52
3.3.2	Salinity	54
4	**RESULTS AND DISCUSSION**	**58**
4.1	PRESSURE	58
4.2	SALINITY	67
5	**CONCLUSIONS**	**83**
	ACKNOWLEDGEMENTS	**87**
	REFERENCES	**88**

APPENDICES:

Appendix A: Simulated and measured pressure along the cored boreholes as a function of depth. Steady-state and transient simulations for the equivalent-continuum and the dual-porosity models with deterministic and stochastic hydraulic conductivities, and for the salinity model with a constant initial salinity of 10 g/l.

Appendix B: Simulated and measured salt concentration along the cored boreholes as a function of depth. Steady-state and transient simulations with deterministic and stochastic hydraulic conductivities. Simulations performed applying the equivalent-continuum model and the salinity model with a constant initial salinity of 10 g/l.

Appendix C: Simulated and measured salt concentration along the cored boreholes as a function of depth in the fracture domain. Transient simulations with the dual-porosity model for three different values of the matrix porosity and the salinity model with a constant initial salinity of 10 g/l.

Appendix D: Simulated and measured salt concentration along the cored boreholes as a function of depth in the fracture domain. Transient simulations with the dual-porosity model for four different values of the matrix block thickness and the salinity model with a constant initial salinity of 10 g/l.

Appendix E: Simulated salt concentration along the cored boreholes as a function of depth and with different distances from the center of the matrix blocks. A transient simulation with the dual-porosity model for a matrix block thickness of 40 m and the salinity model with a constant initial salinity of 10 g/l.

Appendix F: Simulated salt concentration along the cored boreholes as a function of depth and with different distances from the center of the matrix blocks. A transient simulation with the dual-porosity model for a matrix block thickness of 10 m and the salinity model with a constant initial salinity of 10 g/l.

Appendix G: Simulated salt concentration along the cored boreholes as a function of depth at the center of the matrix blocks. Transient simulations with the dual-porosity model for four different values of the matrix block thickness and the salinity model with a constant initial salinity of 10 g/l.

Appendix H: Simulated salt concentration along the cored boreholes as a function of depth at the center of the matrix blocks. Transient simulations with the dual-porosity model for three different values of the matrix block porosity and the salinity model with a constant initial salinity of 10 g/l.

EXECUTIVE SUMMARY

Background and objectives

The Äspö Hard Rock Laboratory (HRL) is constructed below the Äspö island. The main goal of the HRL project is to study various methods of investigating and modelling a fractured crystalline bedrock and the phenomena involved. Extensive field investigations have been carried out to study the properties of the bedrock at Äspö.

The primary objective of this study was to examine whether the geochemical field data from Äspö could be interpreted and understood by means of numerical simulations for flow and transport. A site-specific simulation model for groundwater flow and salt transport was developed on the basis of the field investigations. Both steady-state and transient simulations of flow and transport were performed. In the transient simulations, land uplift and the effect of diffusion into/from the matrix blocks with stagnant water were taken into account. The computational results were evaluated on the basis of the experimental values for the pressure and salt concentration.

Modelling approach

A fractured rock mass consists of solid rock cut by a network of fractures. Water flow occurs primarily along the interconnected and water-bearing fractures, which account for only a small portion of all fractures. Most of the water in rock masses does not move.

Two conceptual models developed for solute transport in a fractured medium were applied in this study. In the equivalent-continuum (EC) approximation, the fractured medium is treated as a homogeneous continuum with representative characteristics. In the dual-porosity (DP) approach, the medium is assumed to consist of two overlapping continuums: the fractures with flowing water and the matrix blocks with essentially stagnant water. The DP model is thus able to take into account the influence of the diffusion of solute particles between moving water and stagnant water.

In the EC approach, the system of water flow and mass transport is described by a mathematical model that comprises two coupled and non-linear partial differential equations. The first equation is for the flow of groundwater with a variable density under the influence of pressure. The second equation is for the amount of mass transported with flowing water. The difference between the EC and DP models is that in the DP representation solute transport is described by a multi-dimensional equation in the water-bearing fracture system and by a one-dimensional equation in

the matrix with stagnant water. The two equations are coupled by a source/sink term representing the mass transfer between two subsystems.

The DP approach was implemented in the FEFLOW code employed in the simulations. FEFLOW is a finite-element program package for the coupled analyses of groundwater flow, heat transfer and solute transport.

Simulations

A finite element mesh was constructed on the basis of the same Äspö flow model which was applied when simulating the long-term pumping test LPT2. The mesh contains 42000 elements with three-dimensional hexahedral elements representing the intact rock and two-dimensional quadrilateral and triangular elements for the fracture zones.

Three different salinity models were examined with the EC and DP approaches. The transient simulations were carried out for a period that started 3000 years ago (at the end of the Litorina stage) when the highest hills at Äspö rose above sea level. The simulation period continued until the present day. As an initial state in all the salinity models, the whole solution domain was assumed to be saturated with saline sea water. The uplift rate of the water table was assumed to be 1 mm/year. With the DP model, several values of the matrix porosity and the matrix block thickness were applied.

Results and conclusions

The simplest salinity model (the whole modelling domain was assumed to be initially saturated with water having a constant salt concentration of 10 g/l) gave the best results for both pressure and salinity compared to the values measured in the cored boreholes. The pressure proved to depend strongly on the salinity model employed as an initial state. The contours of the salinity field computed with the simplest salinity model and the DP model with a matrix porosity of 0.01 and matrix block thickness of 40 m are presented in the figure on page vii for four different time steps.

The salinity fields computed both with the EC and DP models agree equally well with the field data. A difference between the two models can be recognized when plotting the salt concentration along the boreholes and comparing the values at the intersections with fracture zones. The fracture zones cannot be identified in salt distributions computed with the EC approach whereas they can clearly be seen in the results of the DP model. This follows from the fact that the EC approximation cannot take into account retardation caused by the diffusion of salt from the rock blocks with stagnant water.

The simulation results are sensitive to several input parameters. Especially in the DP model, there are input parameters relating to the properties of the

medium for which field data are scarce. In this study, various values were used for the most important parameters (the matrix block porosity and thickness).

Although the DP representation is a more realistic approach to describe a fractured rock mass than the EC approximation, the general behavior of the experimental data along the boreholes resembles the behavior of the EC results more than that of the DP results. The DP model has more input parameters than the EC model. Accordingly, DP results which would agree better with the field data could obviously be found if more simulations with different salinity models and input parameter values were performed than was possible in this study.

The DP approximation is nevertheless a useful approach when simulating solute transport in a fractured rock mass. Concentrations both in the moving water and in the parts of a system with stagnant water can be simulated with it. Only the water-bearing subsystems can be analyzed with the EC model. The Äspö results of the DP model indicate that, for some values of the matrix block thickness and porosity, the matrix blocks even close to the surface can still contain water with as high a salt concentration as 3000 years ago. Unfortunately, the simulation results for the matrix blocks cannot be evaluated by comparison with the experimental data, because the salt concentrations measured mainly represent the salt content in the water-bearing fractures in the bedrock.

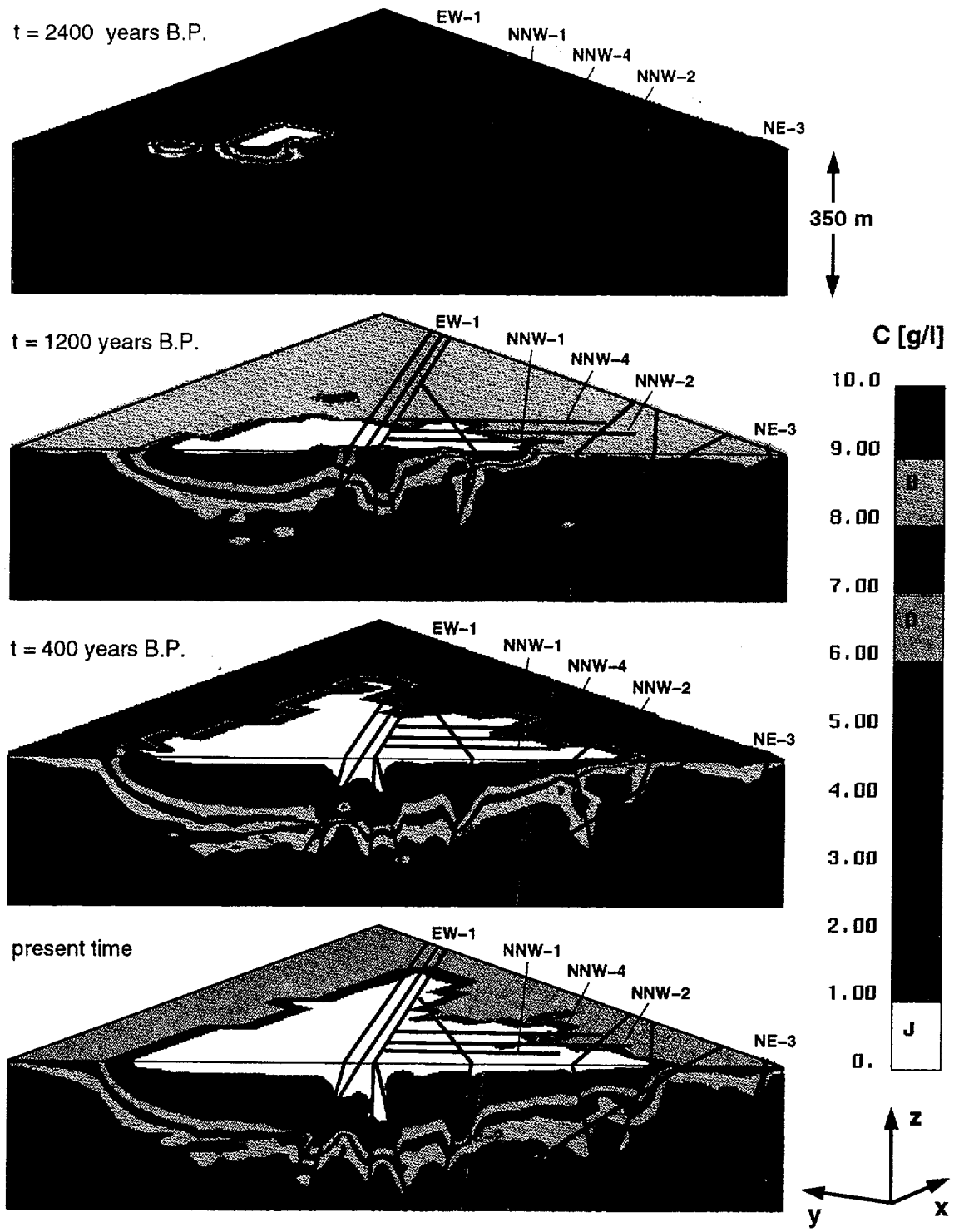

Figure. *Contours of the simulated salt concentration at four different time steps. The simulations were started 3000 years before the present and performed with the dual-porosity model with a matrix block porosity of 0.01 and a matrix block thickness of 40 m.*

1 INTRODUCTION

1.1 BACKGROUND

The Swedish Nuclear Fuel and Management Company (SKB) is excavating an underground research laboratory called the Äspö Hard Rock Laboratory (HRL). The laboratory will be constructed below the Äspö island, which is located in southeastern Sweden, about 20 km north of the town of Oskarshamn. The HRL project is a part of SKB's program aimed at supporting the design and construction of a deep repository for nuclear waste and identifying and investigating a suitable site for the repository. The main goal of the HRL project is to study various methods of investigating and modelling a fractured crystalline bedrock and the phenomena involved. In addition, some optional construction techniques for deep excavations are tested in practice. The goals, objectives and execution of the HRL project are discussed in detail in a background report to SKB's RD&D-Programme 92 (SKB, 1992).

The HRL project is divided into three main phases. In the pre-investigation phase, the Äspö island was selected to be the location of the underground laboratory. Field investigations were conducted on the island, both on the surface and in a number of boreholes. The pre-investigation phase also included a study on making preliminary predictions for the conditions in the excavation area. The laboratory was excavated in the construction phase 1992 - 1994. During and after the excavation, the predictions and also the pre-investigation methods are evaluated. The updated characterization of the bedrock was taken into account in the final layout of the laboratory and when locating various experimental areas. The third phase, the operating phase, started in the beginning of 1995.

1.2 GROUNDWATER FLOW CONDITIONS AT ÄSPÖ

During the hydrogeochemical investigations at Äspö, the salt content of the groundwater samples from the boreholes was measured (Wikberg et al., 1991). The experimental salt concentration increases with depth. High salt concentrations have also been found relatively close to the surface. Especially deep in the bedrock, the salt concentration exceeds the value prevailing today in the Baltic sea (7 g/l), which strongly suggests a relict sea-water source and/or groundwater-rock interaction (Wikberg et al., 1991). Furthermore, there are large spatial variations in the salt content and, obviously, the depth is not the only factor that influences the salinity field.

Since the end of the last glaciation about 12000 years before the present (B.P.), the Äspö island was covered by freshwater lakes and saline seas (Figure 1-1). The salt content of the sea water was highest during the Litorina stage (about 7000 - 3000 B.P.). The highest hills on the Äspö island rose above sea level some 3000 years ago, and since then the average rate of land uplift has been about 2 mm/year.

The land uplift process enlarges the area of the island. The water table rises with the land, which in turn increases the flow of fresh water into the bedrock. That is a transient process and with time the fresh water flows deeper and deeper into the bedrock forcing the saline water deeper too. The salinity field is thus also changing as a function of time. The fact that the salt distribution affects the flow field makes the system of water flow and salt transport coupled. The transient behavior thus originates from land uplift and may, together with the heterogeneity of the bedrock, cause the large and local variations found in the experimental salt concentrations (Wikberg et al., 1991).

Since the salt content of the groundwater at Äspö varies, a realistic simulation of groundwater flow calls for coupled modelling of water flow and solute transport. In addition, in order to take into account the effects of land uplift since the Litorina stage, transient simulations are required.

1.3 MODELLING GROUNDWATER FLOW IN FRACTURED BEDROCK

Groundwater flow in a fractured rock mass

The proportion of groundwater in the bedrock is typically very small even in the saturated zone. The flow of water is mainly controlled by pressure differences, which under natural, hydraulically undisturbed conditions are attributed to the undulating water table. Precipitation sustains the undulation of the water table. The portion of the rainfall infiltrating into the bedrock depends on the level of the water table and on the hydraulic properties of the soil and bedrock. For instance, the calculations concerning the regional area surrounding the Äspö site (i.e. the Simpevarp area) and based on various methods give 10 mm (Grundfelt et al., 1990) and up to 60–125 mm (Liedholm, 1987) for the average annual infiltration rate into the bedrock.

Besides the pressure differences, the variation in the density of the groundwater may significantly affect the groundwater flow since the heavier water seeks to penetrate lower. The largest differences in the density are commonly caused by the varying salt concentration.

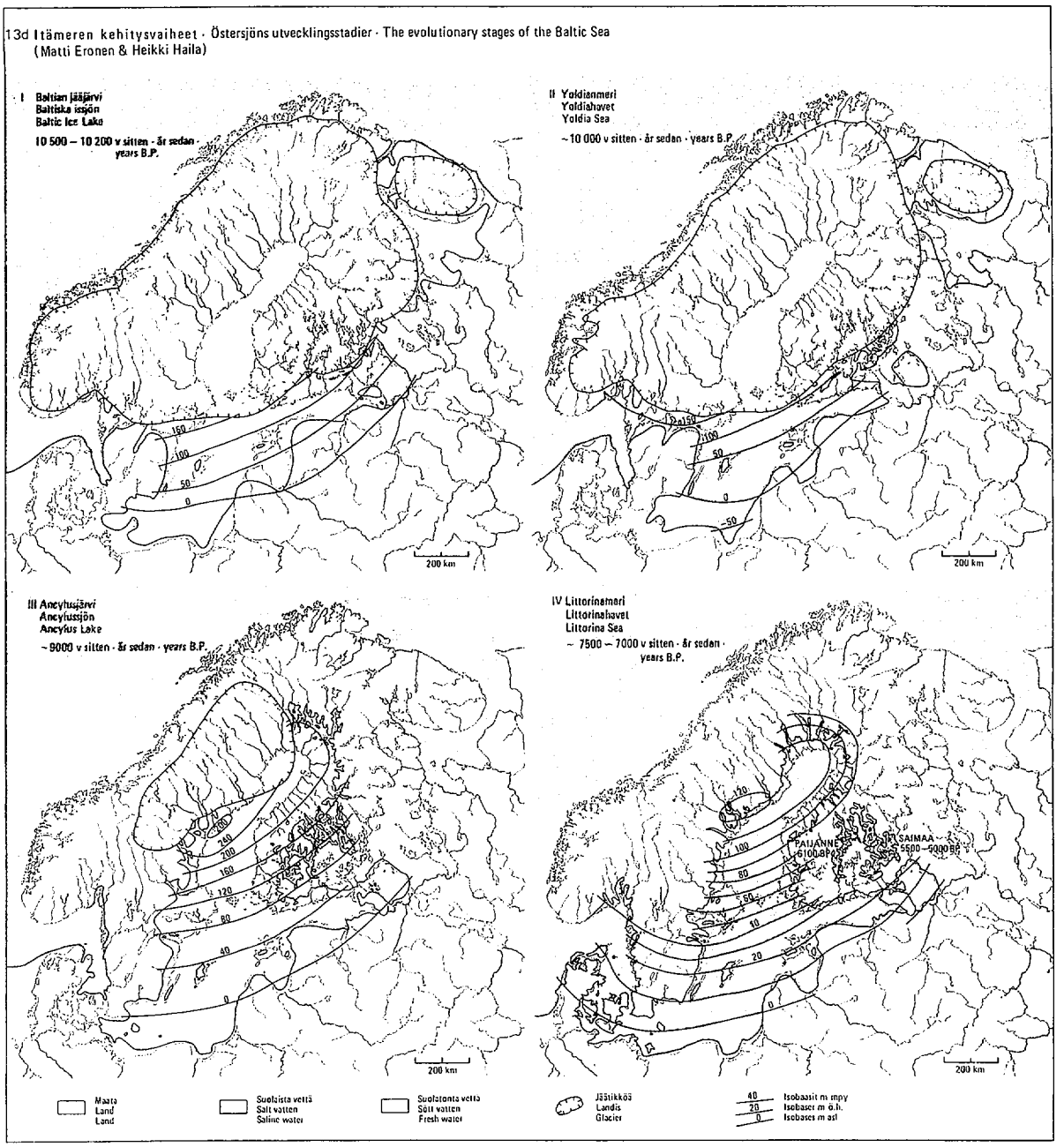

Figure 1-1. The evolutionary stages of the Baltic Sea (Alalammi, 1992).

Differences in the temperature result in density differences, too. The temperature also affects the flow characteristics of water through the viscosity. Although the temperature of the bedrock increases with depth, its influence is insignificant compared to that of the salinity.

In a crystalline rock, water flows unevenly through an intricate network of preferred paths formed by fracture intersections and the flow channels on fracture planes (Figure 1-2). Field investigations (e.g., Neretnieks et al., 1987) indicate that groundwater flow may be very discretely distributed over the rock, i.e. water flows along paths with little contact to other paths. Consequently, there are scales on which the hydraulic properties of the crystalline bedrock are evidently different from those of a homogenous medium.

A crystalline rock mass consists of solid rock cut by fractures. The fracture density in rock masses varies. Zones with a high fracture density are often called fracture(d) zones. They also usually possess a great ability to conduct water even though the correlation between the fracture density and the hydraulic conductivity is not always clear. In this study, the remaining part of a rock mass is termed intact rock, in which the fracture density is low, resulting in heterogenous and discontinuous characteristics with low hydraulic conductivity. The fracture zones are also commonly heterogenous. The same applies to an individual fracture, the hydraulic properties of which may vary on a very small scale. The variations in the properties of the fractures and in the fracture density actually cause the hydrological heterogeneity of the bedrock.

Individual fractures can be classified as water-bearing and non-bearing. Water flows along a network formed by the water-bearing fractures. However, with given boundary conditions, water does not move in all of the fractures. For various reasons, no driving force exists in a number of fractures. For instance, water does not flow in fractures which are "dead-ends". Moreover, water flows only in small parts, i.e. flow channels, of the fractures which form the active flow routes. Thus, only a small proportion of the total volume of water in the bedrock moves along water-bearing fractures separated by rock blocks with stagnant water.

When analyzing groundwater flow and mass transport in the bedrock, the characteristics of the bedrock need to be considered. From a conceptual point of view, the study of water flow in fractured rock may be carried out by adopting various models. The selection of the modelling approach is affected by the type of results aimed for, the data available and some practical limitations like computational resources. The results required also determine the scale of interest, which may influence the feasibility of alternative methods.

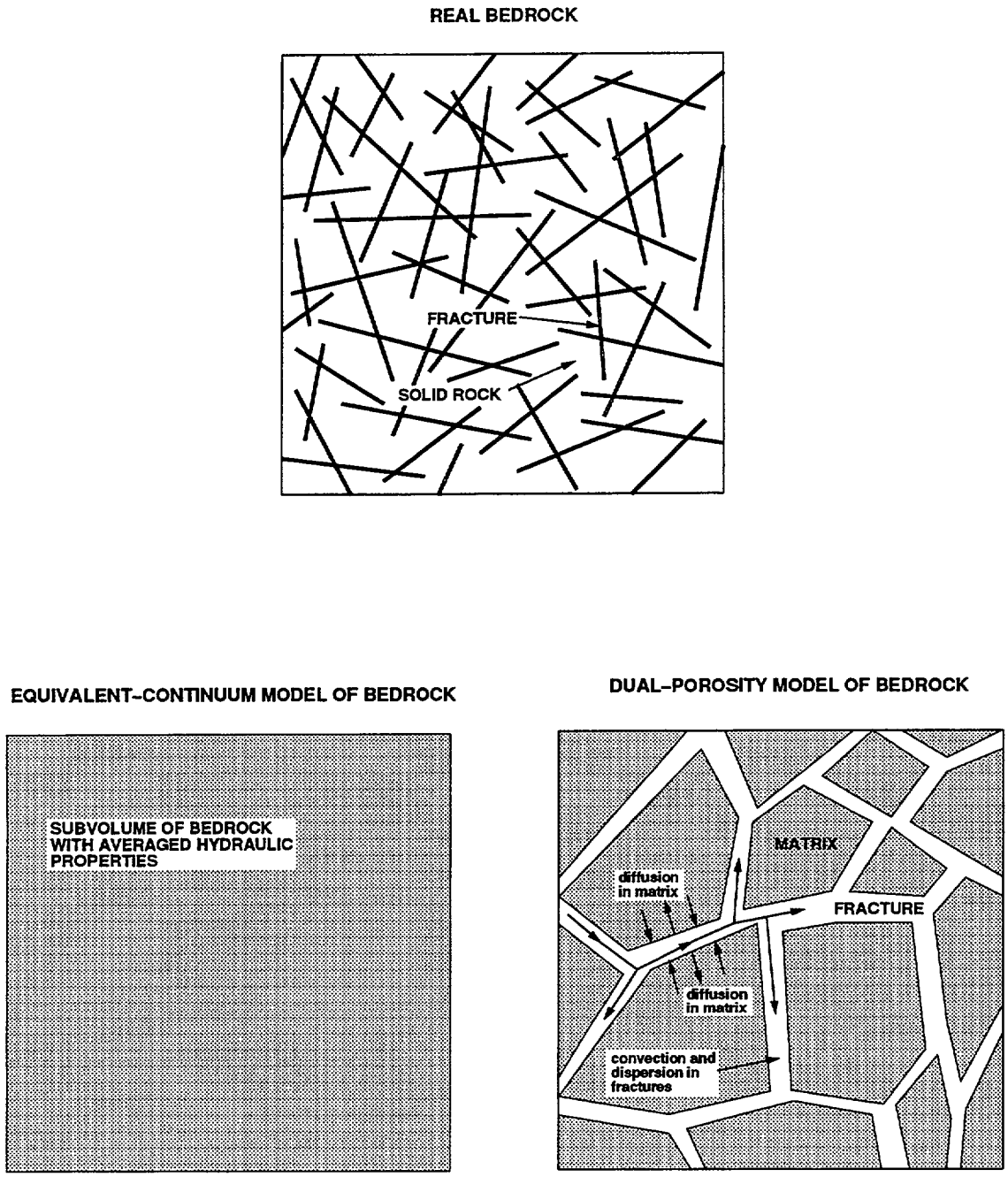

Figure 1-2. *A schematic description of the real bedrock (top) with its equivalent-continuum (EC) (bottom left) and dual-porosity (DP) (bottom right) representations.*

Equivalent-continuum model

The hydraulic properties of the bedrock often vary significantly on a local scale but it may be unnecessary to include the small-scale heterogeneities in a model if water flow on a large scale is analyzed. It is then assumed that a subvolume of the bedrock can be treated as a continuum. In this equivalent-continuum (EC) approximation, the hydraulic properties are assumed to be macroscopic averages over a subvolume containing a large number of fractures on the microscale. The parameter values are chosen so that the real volume concerned and the corresponding EC representation as a whole behave similarly, considering flow and transport (Figure 1-2). The smallest volume with that feature is called the representative elementary volume (REV). The equivalent properties depend on several fracture parameters (permeability, density, size and orientation distribution).

The justification of the EC approximation is often questionable in practical applications. One reason for this is the scarcity of field data (see, e.g., Carlsson et al., 1987). The selection of equivalent hydraulic properties is difficult and constitutes a major source of uncertainty in simulations. On the other hand, a study by Herbert & Gale (1989) dealing with a densely fractured hard rock concludes that it might be possible to define a relatively small volume of fractured rock on which the EC approximation is valid.

Modelling results must be interpreted taking into account the assumptions of the approach applied. From the standpoint of the groundwater flow itself, the EC approach is not too restrictive. The pressure field and average flux can be reliably computed. However, the EC approximation becomes more restricting when transport phenomena are also taken into account.

There are modelling approaches that deal with the bedrock more realistically than the EC model. In fracture network modelling, for instance, the fracture system of the bedrock is modelled. Each significant fracture is simulated in principle. Due to practical limitations, fractures are treated with statistical methods and the values characterizing the appropriate distributions are based on the interpretations of field investigations. Commonly, the dominating conceptual model that considers the impact of each fracture is the parallel-plate approach, i.e. there is no channelling inside an individual fracture. In this type of fracture network modelling, the continuum approximation is thus also employed but on a fracture scale.

Dual-porosity model

The real bedrock thus consists of solid rock cut by a network of water-bearing and non-bearing fractures. A realistic analysis of solute transport through a fractured medium requires taking into account the fact that most of the fluid is located in disjointed blocks of solid rock and in fractures in which water does not move, and that most of the moving fluid is in a small portion of interconnected and water-bearing fractures. Transport in water that is not moving is dominated by molecular diffusion. Water flows in some of

the fractures, in which the dominant processes are convection and dispersion. Mass transport in this kind of system includes the molecular diffusion of solute particles from fractures with mobile water to matrix blocks which include essentially stagnant water, and vice versa. This diffusion process is called matrix diffusion. It acts as a dynamic storage mechanism for the mass in the system. It constitutes a process that can be effective in removing mass from the moving subsystem into the matrix and thus in retarding transport process through the system. On the other hand, diffusion can also transfer mass from the matrix back into the fracture.

The conventional simulation methods for solute transport, which usually employ the EC representation of a medium (see Section 2.2), cannot take into account the special features of fractured systems discussed above. Therefore, the simulation results can be quite different compared with the experimental values and those computed by more realistic models. For fractured systems, alternative and more realistic approaches have been developed. In the dual-porosity (DP) representation, the medium is assumed to consist of two overlapping continuums: the fractures with flowing water and the matrix blocks with essentially stagnant water representing the rest of a system (Figure 1-2).

Several methods that utilize the DP concept have been developed for simulating mass transport in a fractured porous medium. The dual porosity approach has been studied and applied, for example, by Bibby (1981), Dykhuizen (1990), Grisak and Pickens (1980), Huyakorn et al. (1983) as well as Sudicky and Frind (1982). Most of the models deal with a system of parallel water-bearing fractures. Mass transport in the matrix blocks with stagnant water is treated numerically and/or analytically.

The approach developed by Grisak and Pickens (1980) assumes a system of parallel fractures in which water flows. Each matrix-fracture unit is modelled by applying the standard finite element method. A finite element mesh includes elements explicitly for both the fractures and the matrix blocks. Consequently, the simulation of one-dimensional transport requires a two-dimensional finite element mesh and, correspondingly, a two-dimensional system needs a three-dimensional mesh. The transfer of the solute mass between the fractures and matrix blocks is handled automatically by the special features of the finite element method. In addition to the fact that it is not possible to simulate three-dimensional transport, this approach is computationally a costly modelling technique.

In the approach by Bibby (1981), two-dimensional transport can be simulated without constructing a three-dimensional mesh. A parallel fracture system is again assumed. A two-dimensional finite element mesh is constructed to represent the fracture domain. Transport in the fractures is modelled by the finite element method. For matrix blocks with stagnant water, only one-dimensional diffusion (perpendicular to a water-bearing fracture) is considered and approximated using a convolution of a simple analytic solution for diffusion. With this technique it would be difficult to extend the model to handle convection and dispersion in the matrix and

multispecies transport because of more complex analytic expressions related to transport in the matrix blocks.

The method developed by Huyakorn et al. (1983) combines the favorable aspects of the two schemes discussed above. Transport in a water-bearing fracture is described by a multi-dimensional equation and transport in a matrix block by a one-dimensional equation. The two equations are implicitly coupled with a term for the leakage flux. The coupled system is solved numerically, employing an efficient finite element algorithm. The method has been applied, for example, in the FTRANS code (FTRANS, 1983). The method by Huyakorn et al. (1983) was also implemented and applied in this study.

Yet there are some problems associated with the DP model. For example, results computed with the DP approach comprise values both for the fracture system and the matrix blocks. The values in the fracture domain represent the mass distribution in moving water and they can be directly compared with the field data. However, comparison of the values obtained for the matrix blocks is not usually possible because of missing experimental data. In addition, the source term which couples the two systems is proportional to the difference in the values of the systems through a coefficient whose physical significance is not well defined except for very simple geometries. As far as a detailed geometrical description of the processes is not of interest, those deficiencies can be considered insignificant and the dual porosity model can be applied as a practical tool for modelling flow and transport in a fractured medium.

1.4 OVERVIEW OF THIS REPORT

As part of the modelling of the long-term pumping test LPT2, Taivassalo et al. (1994) also performed coupled simulations for the pressure and salinity fields in the bedrock below the Äspö island. Those simulations were carried out for a steady-state with the EC model. The modelling results were also compared with the experimental data.

This report provides a more detailed and comprehensive description of the coupled simulation methods as well as computational results for the pressure and salinity fields at Äspö. Simulations in this study were performed with two conceptual models and various initial and boundary conditions. Transient as well as steady-state simulations were carried out. In the transient simulations, the impact of land uplift and the effect of matrix diffusion were taken into account.

The report is organized in the following manner. The two modelling approaches employed as well as the computer code used are introduced in Chapter 2. Chapter 3 presents the simulation model specific to the Äspö site. Chapters 4 and 5 summarize the results and conclusions, respectively.

2 SIMULATION OF FLOW AND TRANSPORT

When simulating solute transport at Äspö, two conceptual models for a fractured medium were applied: the equivalent-continuum (EC) and dual-porosity (DP) models. These two representations and the corresponding mathematical models are discussed in this chapter. We start with a short introduction into the FEFLOW code, into which the DP approach was implemented and which was employed in the simulations for the Äspö site.

2.1 FEFLOW CODE

The FEFLOW code (Taivassalo et al., 1991; Löfman and Taivassalo, 1993; Laitinen, 1995) is a finite element program package for the analyses of groundwater flow. It has been developed at the Technical Research Center of Finland (VTT). FEFLOW is capable of modelling flow, heat transfer and solute transport in a medium. The different phenomena can also be coupled. Problems to be simulated can be steady-state or transient. The FEFLOW code can be utilized in a deterministic or stochastic mode.

The mathematical model consists of the partial differential equations for the hydraulic head/pressure, temperature and solute concentration. The equations are coupled by means of the Darcy velocity as well as temperature and concentration dependent properties such as the fluid density. When solving the concentration, the effect of matrix diffusion can be taken into account too (see Section 2.3). Highly convective cases can be handled with different kinds of upwind methods (Laitinen, 1995). The core of FEFLOW comprises programs FPH1, FPH2 and FPH3 (Figure 2–1), which solve the desired quantities.

FEFLOW uses linear one-, two- and three-dimensional elements. Two-dimensional elements can also be applied in a three-dimensional mesh and one-dimensional elements in two- and three-dimensional meshes. For example, in three-dimensional groundwater flow simulations, the intact rock itself can be described by three-dimensional elements, whereas fracture zones or other planar structures can be represented by two-dimensional elements. The time discretization in FEFLOW is based on the finite difference approximation. The linear matrix equations resulting from the finite element formulation can be solved either using the direct frontal solver or various iterative solvers. In coupled cases, a set of nonlinear algebraic equations is solved applying an iterative approach with options for the relaxation process.

For each output quantity, the program offers a wide selection of nodal boundary conditions including prescribed values, sources, sinks and/or

fluxes. Nodal boundary conditions may be constant or they can vary as a function of time. FEFLOW is able to take into account various properties of a medium depending on the type of the problem to be solved. Properties include the hydraulic conductivity/transmissivity, permeability, specific storage/storativity, fluid density and viscosity, porosity, longitudinal and transversal dispersion lengths, molecular diffusion coefficient, specific heat, and thermal conductivity. The hydraulic conductivity and permeability may be constant, vary exponentially or logarithmically as a function of depth, or follow a lognormal distribution.

The FEFLOW package also comprises several programs to compute derived output parameters as well as to facilitate modelling work and the analyses of simulation results (Figure 2-1). The derived quantities include flow paths computed with the FPATH program, the Darcy velocity calculated with the DVELO program and the flow rate obtained with the FRATE code. In addition, the comparison of measured and calculated values is carried out with program GOODNESS, which outputs a value for a pre-defined goodness-of-fit function. The INTER program can be employed when assigning boundary conditions for the top nodes of a mesh. It interpolates values to surface nodes using the digitized equivalue contours of a water table. A commonly applied technique in the field of numerical hydrogeological modelling is the use of a system of several nested element meshes so that the boundary conditions for the bordering faces of a smaller model are extracted from a solution computed with a larger model. The HBOUND program facilitates the labourless application of this technique. In addition, a set of advanced routines has been developed to enhance and facilitate the element mesh creation process (Figure 2-1).

Despite several simple test cases, the code has also been tested and verified by computing more complicated coupled test cases, which were studied in the international HYDROCOIN project (HYDROCOIN, 1988, 1990, 1991 and 1992).

The FEFLOW package was applied in the safety analyses and site investigations undertaken by the Finnish power companies operating the nuclear power plants (Taivassalo et al., 1994; Taivassalo and Mészáros, 1994; Taivassalo and Saarenheimo, 1991; Vieno et al., 1992). It was also used to simulate coupled flow and solute transport at Äspö, Sweden, relating to the simulations of LPT2 pumping test within the Hard Rock Laboratory project (Taivassalo et al., 1994).

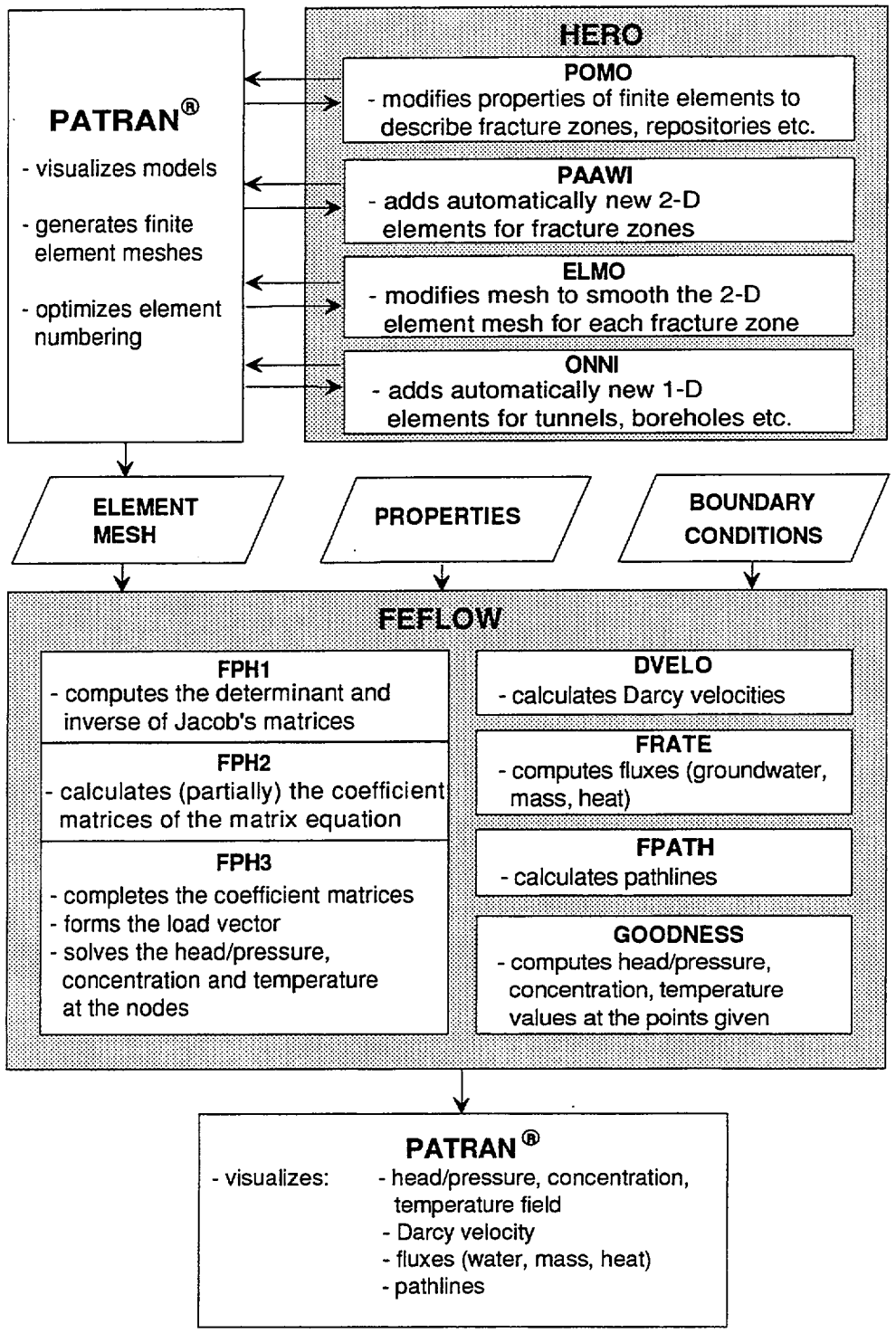

Figure 2-1. *The main components of the FEFLOW program package. PATRAN (1989) is a commercial pre- and postprocessing software for finite element codes.*

2.2 EQUIVALENT-CONTINUUM APPROACH

2.2.1 Conceptual model

The hydraulic properties of rock masses often vary significantly on a local scale. The small-scale heterogeneities may, however, be omitted if the primary interest is on a large scale. It is then assumed that a rock unit (intact rock, fracture or fracture zone) can be treated as a continuum. In this equivalent-continuum (EC) approximation, the hydraulic properties are assumed to be macroscopic averages over subvolumes containing a large number of small scale heterogeneities. The properties are chosen so that the real rock volume concerned and its EC representation as whole behave identically considering the flow and transport (Figures 1-2 and 1-3). The smallest volume with that feature is commonly called a representative elementary volume (REV). The equivalent properties are influenced by many parameters. For instance, in the case of the intact rock, the properties depend on several fracture parameters (permeability, density, size and orientation distribution).

2.2.2 Governing equations

Flow and transport in a porous medium can be described by a mathematical model that comprises two coupled and non-linear partial differential equations. An equation is for the flow of water under the influence of the pressure field in the presence of density variations. Another equation describes the amount of mass transported along with flowing water.

The flow equation can be expressed for the residual pressure, i.e. the actual pressure minus the hydrostatic component of fresh water. Assuming Darcy's law to be valid and taking into account the law of conservation of mass, the flow equation can be written as follows (e.g., Bear, 1979; Huyakorn and Pinder, 1983; de Marsily, 1986)

$$\nabla\cdot\left(\frac{\rho \boldsymbol{k}}{\mu}\nabla(p+(\rho-\rho_o)gz)\right) = \frac{\partial(\rho\phi)}{\partial t}, \qquad (2\text{-}1)$$

where
- p is the residual pressure (Pa),
- ρ is the density of water (kgm^{-3}),
- ρ_o is the density of fresh water (kgm^{-3}),
- μ is the viscosity of water ($kgm^{-1}s^{-1}$),
- $\boldsymbol{k}$ is the permeability tensor of the medium (m^2),
- g is the gravitational acceleration (ms^{-2}) and
- ϕ is the total porosity (-).

The right hand side of Equation (2-1) represents the change in the fluid density and the compressibility of the medium (the change in the porosity).

The transport equation can be written for the concentration of a solute as (e.g., Huyakorn and Pinder, 1983)

$$\nabla\cdot(\boldsymbol{D}\nabla c) - \nabla\cdot(\boldsymbol{q}c) - \lambda c = \frac{\partial(\phi_f R c)}{\partial t}, \tag{2-2}$$

where
- c is the concentration of a solute (kgm^{-3}),
- $\boldsymbol{D}$ is the hydrodynamic dispersion tensor (m^2s^{-1}),
- $\boldsymbol{q}$ is the Darcy velocity (ms^{-1}),
- λ is the first order decay coefficient (1/s) (employed only in the first verification case in Section 2.3.4),
- ϕ_f is the flow porosity (-) and
- R is the retardation coefficient (-).

The first term in the left-hand side of Equation (2-2) represents the dispersive mass transport. The second term characterizes transport caused by flow. The term in the right-hand side takes into account the change in the kinematic porosity and in the concentration.

The components of the hydrodynamic dispersion tensor in Equation (2-2) are

$$D_{ij} = \varepsilon_T|\boldsymbol{q}|\delta_{ij} + (\varepsilon_L - \varepsilon_T)\frac{q_i q_j}{|\boldsymbol{q}|} + \phi_d \tau D^o, \tag{2-3}$$

where
- ε_L is the longitudinal dispersion length (m),
- ε_T is the transversal dispersion length (m),
- D^o is the molecular diffusivity (m^2s^{-1}),
- δ_{ij} is the Kronecker delta function,
- ϕ_d is the diffusion porosity (-) and
- τ is the tortuosity (-).

Equations (2-1) and (2-2) are coupled through the Darcy velocity

$$\boldsymbol{q} = -\frac{\boldsymbol{k}}{\mu}\nabla(p + (\rho - \rho_o)gz) \tag{2-4}$$

and the density

$$\rho = \rho_o + a_c c, \tag{2-5}$$

where a_c is the coefficient of density dependence on the solute concentration. For salt in water a_c is 0.71 (Lide, 1990). The pressure dependence is missing in Equation (2-5) since the fluid is assumed to be incompressible.

The permeability $\boldsymbol{k}$ in Equations (2-1) and (2-4) can be expressed in terms of the hydraulic conductivity $\boldsymbol{K}$

$$k = \frac{K\mu}{\rho g} .$$

The dependence of the total porosity (dependence of the flow porosity is analogous) on the pressure is given by the expression

$$\phi = \phi_o + \frac{S_s}{\rho g}(p - p_o),$$

where S_s is the specific storage of the medium (m^{-1}),
p_o is the reference pressure (Pa) and
ϕ_o is the porosity in the reference pressure (-).

Equations (2-1) and (2-2) are written in reduced forms (without terms representing sinks and sources) as they are applied in this study. A more general formulation of the equations is given by, e.g., Löfman and Taivassalo (1993).

2.2.3 Numerical solution method

The coupling of Equations (2-1) and (2-2) by the Darcy velocity (2-4) and the density (2-5) results in a system of two non-linear partial differential equations. Coupled cases can rarely be solved analytically. Therefore numerical methods have to be employed. The FEFLOW code utilizes the finite element method (see Section 2.1).

When applying the finite element method, a modelling domain is divided into a number of subvolumes, finite elements, that are connected to each other at a discrete number of nodal points. The finite element approximation p' of the pressure is of the form

$$p'(x,y,z,t) = \sum_{i=1}^{n} p_i(t) w_i(x,y,z), \qquad (2\text{-}6)$$

where $p_i(t)$ is the nodal value of the pressure at the time t,
$w_i(x,y,z)$ is the basis function at the point (x,y,z) (related to node i and defined by the elements with node i) and
n is the number of nodes in the system.

Applying the conventional Galerkin method of weighted residuals to Equation (2-1) and applying the approximation (2-6), a global matrix equation for the pressure is obtained (Löfman and Taivassalo, 1993)

$$\boldsymbol{A}_p\boldsymbol{P} + \boldsymbol{B}_p\frac{\partial \boldsymbol{P}}{\partial t} + \boldsymbol{U}_p = \boldsymbol{0}, \tag{2-7}$$

where n x n -matrices $\boldsymbol{A}_p$ and $\boldsymbol{B}_p$ are stiffness matrices, n-vector $\boldsymbol{U}_p$ is a load vector containing the boundary conditions and $\boldsymbol{P}$ is a n-vector containing the unknown nodal values.

The time derivative in Equation (2-7) is approximated by the expression

$$\frac{\partial \boldsymbol{P}}{\partial t} = \frac{\boldsymbol{P}^{k+1} - \boldsymbol{P}^{k}}{\Delta t}, \tag{2-8}$$

where $\boldsymbol{P}^{k+1}$ is the pressure at the current time step, $\boldsymbol{P}^{k}$ is the pressure at the previous time step and Δt is the time increment

$$\Delta t = t^{k+1} - t^{k}.$$

Substitution of the approximation (2-8) into Equation (2-7) yields

$$(\boldsymbol{A}_p + \frac{\boldsymbol{B}_p}{\Delta t})\boldsymbol{P}^{k+1} - \frac{\boldsymbol{B}_p}{\Delta t}\boldsymbol{P}^{k} + \boldsymbol{U}_p = \boldsymbol{0}. \tag{2-9}$$

Equation (2-9) can be solved using any standard solver for matrix equations. For matrices $\boldsymbol{A}_p$ and $\boldsymbol{B}_p$, and vector $\boldsymbol{U}_p$ in Equations (2-7) and (2-9) we obtain

$$A_{p,ij} = \int_V \sum_{\alpha,\beta} \frac{\rho k_{\alpha\beta}}{\mu} \frac{\partial w_i}{\partial \alpha} \frac{\partial w_j}{\partial \beta} dV, \qquad i,j=1,\ldots,n, \tag{2-10}$$

$$B_{p,ij} = \frac{S_s}{g} \int_V w_i w_j dV, \qquad i,j=1,\ldots,n \tag{2-11}$$

and

$$\begin{aligned} U_{p,j} = & \int_V \left(\sum_{\alpha,\beta} \frac{\rho k_{\alpha\beta}}{\mu} \frac{\partial w_j}{\partial \alpha} \frac{\partial(\rho g z)}{\partial \beta} \right) w_j dV \\ & - \oint_{\partial V} \rho q_n w_j dA + \oint_{\partial V} \rho_{inp} q_{n,inp} w_j dA, \qquad j=1,\ldots,n, \end{aligned} \tag{2-12}$$

where $k_{\alpha\beta}$ is a component of the permeability tensor, and α and β refer to the summation with respect to coordinates x, y and z over the solution

domain V. The first term in vector (2-12) represents the buoyancy phenomena caused by the variations in the density, the second term is the effect of the concentration on the flow and the last terms describe the flux of water flowing through the boundaries of the system.

Application of the Galerkin method to the transport equation (2-2) leads, correspondingly, to a system of equations

$$(\boldsymbol{A}_c + \frac{\boldsymbol{B}_c}{\Delta t})\boldsymbol{C}^{k+1} - \frac{\boldsymbol{B}_c}{\Delta t}\boldsymbol{C}^{k} + \boldsymbol{U}_c = \boldsymbol{0} \ . \tag{2-13}$$

Here matrices $\boldsymbol{A}_c$ and $\boldsymbol{B}_c$ and vector $\boldsymbol{U}_c$ are given by

$$\begin{aligned} A_{c,ij} = & \int_V \sum_{\alpha,\beta} (D_{\alpha\beta} \frac{\partial w_i}{\partial \alpha} \frac{\partial w_j}{\partial \beta} - q_\alpha \frac{\partial w_i}{\partial \alpha} w_j + (\frac{S_s}{\rho g} \frac{\partial p}{\partial t} + \lambda) w_i w_j) dV \\ & + \oint_{\partial V} q_n w_i w_j dA, \end{aligned} \tag{2-14}$$

$$B_{c,ij} = \phi_f R \int_V w_i w_j dV \tag{2-15}$$

and

$$U_{c,j} = -\oint_{\partial V} q_{n,inp} c_{inp} w_j dA. \tag{2-16}$$

The first and second terms in matrix (2-14) are the dispersion and convection terms. The third term represents the influence of the change of the porosity of the medium. The third term takes into account radioactive decay, too.

The FEFLOW code solves the two sets of non-linear equations, (2-9) and (2-13) applying the Picard iterative scheme (Huyakorn and Pinder, 1983) with underrelaxation. In the Picard scheme, for each time step the finite element procedure is employed for both equations sequentially until the convergence criterion or the maximum allowed number of iterations is attained. The code uses also a linear time extrapolation formula to obtain an initial estimate of the nodal values of the pressure and concentration at the beginning of the current time step.

The discussion above was based on the conventional Galerkin method. In highly convective cases, the FEFLOW code, however, employs different kinds of upwind methods. The formulation of the equations in those situations is given by Laitinen (1995).

2.3 DUAL-POROSITY APPROACH

2.3.1 Conceptual model

In the dual-porosity (DP) concept, it is assumed that two overlapping continuums and two porosities are associated with the medium in which fluid flows (e.g. Bibby, 1981; Dykhuizen, 1990; Grisak and Pickens, 1980; Huyakorn et al., 1983; Sudicky and Frind, 1982). The primary porosity is that of a subsystem with low permeability and high storage capability. The secondary porosity is related to features with higher permeability and low storage capability.

In a fractured rock mass, water flows along a subset of fractures (water-bearing fractures), while most of the fractures (non-bearing fractures) and other void volumes of the rock contain essentially stagnant water. The secondary porosity is related to the water-bearing fractures. The rest of the volume of the water represent the primary porosity. The rock blocks with stagnant or almost stagnant water are called matrix blocks.

When solute transport occurs through a fractured medium, convection and dispersion are the dominant processes within the water-bearing fractures, whereas molecular diffusion is the dominant process in the matrix blocks. Transport in such a system is accompanied by the exchange of solute particles to and from the surrounding porous matrix blocks, i.e. the matrix blocks act as sources (and sinks) that feed (and drain) the water-bearing fractures in which fluid flows (Figure 1-2).

In this study, the water in the matrix blocks is assumed to be practically stagnant. The DP approach is applied only on salt transport, but not on groundwater flow.

2.3.2 Governing equations

Consider a fractured porous medium which is assumed to be macroscopically uniform. The medium can be approximated by the parallel fracture model (Figure 2-2). The parallel fracture model employs a rectangular prismatic block idealization. The system of fractures and matrix blocks is assumed to consist of equally spaced and parallel water-bearing fractures separated by the blocks of saturated porous rock with stagnant water. Because the fracture/matrix geometry repeats itself and because each fracture is symmetrical, only one half of a fracture and one half of the intervening porous matrix block have to be considered when developing a mathematical model.

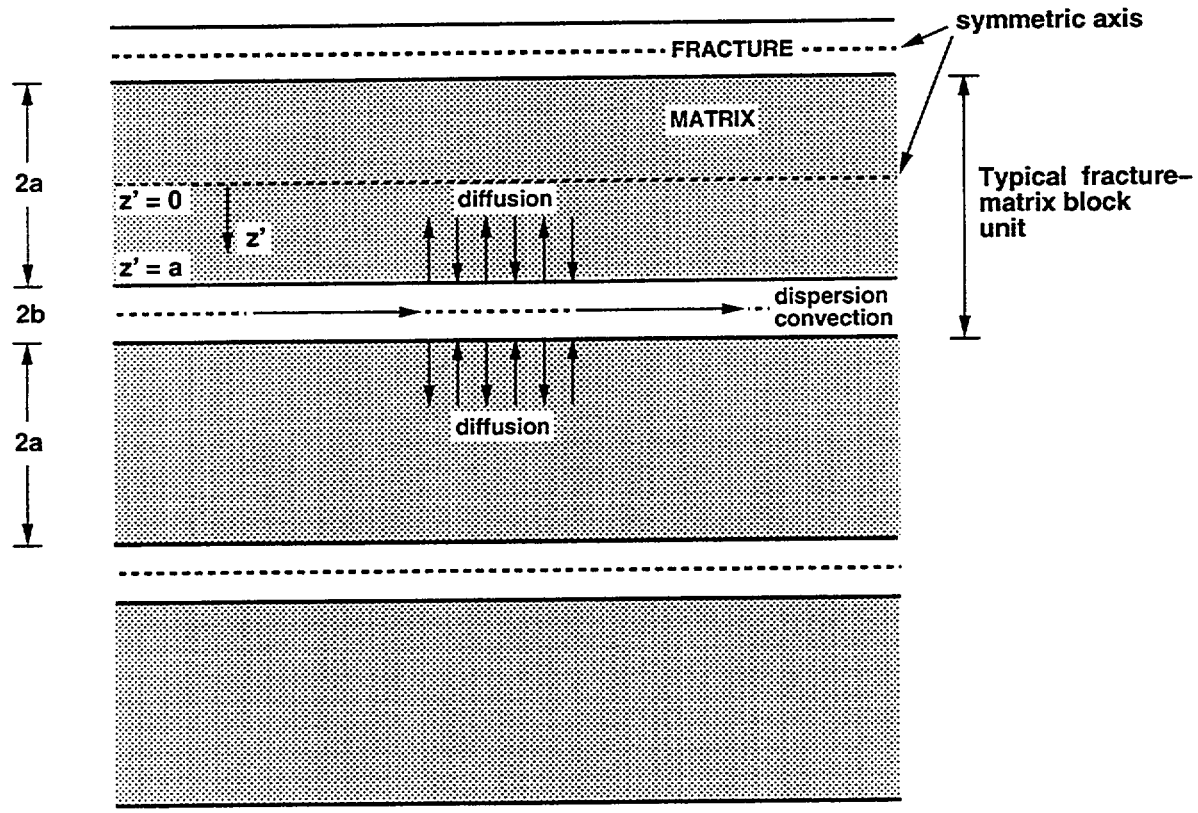

Figure 2-2. A parallel fracture representation of a dual porosity medium.

Flow and transport in the DP medium is described by a mathematical model that comprises three coupled and non-linear partial differential equations. The first equation is for the flow of water with variable density in the fracture domain. The second equation describes the amount of mass transported with flowing water in the fracture domain. The third equation represents the amount of mass transported by molecular diffusion in the matrix blocks. The exchange of the solute particles between the water-bearing fractures and the porous matrix blocks with stagnant water is represented by a term that describes the rate of mass transfer. Groundwater flow is simulated only in the fracture domain because the water in the matrix blocks is assumed to be stagnant and to have no influence on the flow pattern.

The flow equation is the same used with the EC model (Equation 2-1 in Section 2.2.2). Transport of solute particles in a DP system is described by a multi-dimensional equation for fractures and a one-dimensional equation for matrix blocks. The matrix system is perpendicular to the fractures. Transport of solute particles in the matrix parallel to the fractures is assumed to be negligible. The two equations are coupled by a source/sink term that results from the solution of the equation for the matrix blocks and that is

proportional to the concentration difference between the matrix and fracture systems.

The equation describing mass transport in the water-bearing fractures contains terms for dispersion and convection. The transport equation can be written as follows (Huyakorn et al., 1983)

$$\nabla\cdot(\boldsymbol{D}\nabla c) - \nabla\cdot(\boldsymbol{q}c) + (1-\theta)\Gamma - \theta\lambda c = \theta R\frac{\partial c}{\partial t}, \qquad (2\text{-}17)$$

where
- c is the concentration of the solute (kgm^{-3}),
- $\boldsymbol{D}$ is the hydrodynamic dispersion coefficient (includes dispersion and diffusion) (m^2s^{-1}),
- $\boldsymbol{q}$ is the Darcy velocity (ms^{-1}),
- θ is the fracture porosity (-),
- Γ is the rate of solute transfer from the matrix block to the fracture ($kgm^{-3}s^{-1}$),
- λ is the first order decay coefficient (1/s) (employed only in the first verification case in Section 2.3.4) and
- R is the retardation coefficient (-).

The first and second term in the left-hand side of Equation (2-17) represent mass transport by dispersion and convection per unit volume of the system. The third term represents the rate of mass transfer from a matrix block to a fracture per unit volume. The right-hand term takes into account the temporal change in the concentration.

The fracture porosity is defined as the volume of fractures per unit volume of the entire system

$$\theta = \frac{b}{a+b}, \qquad (2\text{-}18)$$

where a is half the matrix block thickness and b is half the fracture aperture (Figure 2-2).

Mass transport in the matrix blocks is dominated by the molecular diffusion and it can be described with a one-dimensional diffusion equation

$$\frac{\partial}{\partial z'}(\tau'\phi' D^{o}\frac{\partial c'}{\partial z'}) = \phi' R'\frac{\partial c'}{\partial t} + \lambda\phi' R' c', \qquad (2\text{-}19)$$

where
- c' is the concentration of the solute (kgm^{-3}),
- τ' is the tortuosity (-),
- D^{o} is the coefficient of molecular diffusion (m^2s^{-1}),
- ϕ' is the porosity in the matrix blocks (-) and
- R' is the retardation coefficient (-).

Equation (2-19) is subject to the initial condition

$$c' = c'_0, \qquad t = 0 \tag{2-20}$$

and the boundary condition

$$c' = c, \qquad z' = a \tag{2-21}$$

describing the continuity of the concentration at the interface of the fracture and the matrix block (cf. Figure 2-2). In addition, the condition

$$\frac{\partial c'}{\partial z'} = 0, \qquad z' = 0 \tag{2-22}$$

is employed to describe the no-flow boundary at the center of the matrix block due to symmetry.

Equations (2-17) and (2-19) are coupled by the continuity of the diffusive mass flux at the interface of the fracture and the matrix block. The rate of solute transfer from the matrix block to the fracture can be expressed by applying Fick's law (de Marsily, 1986). For a typical rectangular matrix block unit (Figure 2-2), the mass transfer term is given by

$$\Gamma = -(\tau\phi' D^{o} \frac{\partial c'}{\partial z'}|_{z'=a})\sigma, \tag{2-23}$$

where σ is the specific surface of the matrix block. The specific surface of the matrix block is defined as the surface to the volume ratio of the block

$$\sigma = \frac{2 \cdot l \cdot d}{2a \cdot l \cdot d} = \frac{1}{a}, \tag{2-24}$$

where l and d are the length and width of the area across which the mass flux occurs. Substituting Equation (2-24) into Equation (2-23), we obtain for the mass transfer term

$$\Gamma = -\frac{1}{a}(\tau\phi' D^{o} \frac{\partial c'}{\partial z'}|_{z'=a}). \tag{2-25}$$

On the other hand, Equations (2-1) and (2-17) are coupled by the Darcy velocity (2-4) and the density (2-5) as described in Section 2.2.2.

2.3.3 Numerical solution method

As the flow equation employed with the DP model is the same as presented in Section 2.2.3 for the flow equation (2-1) of the EC approach, only the numerical solution of the transport equations is considered below. Furthermore, the iterative scheme for the coupled partial differential

equations (2-1) and (2-17) to determine the pressure and concentration is the same employed with the EC model.

Finite element formulation

The standard Galerkin finite element method with linear basis functions is applied to the transport equation (2-17). Introducing a trial function $\hat{c}$

$$\hat{c} = \sum_{i=1}^{n} c_i w_i, \qquad i=1,2,\ldots,n,$$

application of the weighted residual technique, Green's theorem, the backward difference time-stepping scheme and rearranging yield a set of algebraic equations (e.g., Huyakorn and Pinder, 1983) (compare with Equation (2-13))

$$(\boldsymbol{A} + \theta R \frac{\boldsymbol{B}}{\Delta t} + \lambda \boldsymbol{B})\boldsymbol{C}^{k+1} - \theta R \frac{\boldsymbol{B}}{\Delta t}\boldsymbol{C}^{k} + \boldsymbol{U} - \boldsymbol{B}\Gamma = \boldsymbol{0}, \tag{2-26}$$

Here $\boldsymbol{C}$, $\boldsymbol{U}$ and Γ are vectors of size n containing the nodal concentrations in flowing system, the boundary conditions and the nodal values of the mass transfer term, respectively. $\boldsymbol{A}$ and $\boldsymbol{B}$ are n by n matrices, indexes k and $k+1$ refer to previous and current time steps, respectively, and

$$\Delta t = t^{k+1} - t^{k}. \tag{2-27}$$

For linear elements, the vectors and matrices above are expressed as follows

$$A_{ij} = \int_V \sum_{\alpha,\beta} (D_{\alpha\beta} \frac{\partial w_i}{\partial \alpha}\frac{\partial w_j}{\partial \beta} - q_\alpha \frac{\partial w_i}{\partial \alpha} w_j)\, dV + \oint_{\partial V} q_n w_i w_j dA, \tag{2-28}$$

$$B_{ij} = \int_V w_i w_j dV \tag{2-29}$$

and

$$U_j = -\oint_{\partial V} q_{n,inp} C_{inp} w_j dA\ . \tag{2-30}$$

Parameters $D_{\alpha\beta}$ and q_α are components of the hydrodynamic dispersion tensor (2-3) and those of the Darcy velocity (2-4), respectively. Parameters α and β refer to the summation with respect to coordinates x, y and z over the solution domain V.

The standard Galerkin finite element technique is also employed when solving the one-dimensional equation describing transport in the matrix block

without flow. For the prismatic matrix block (Figure 2-2) used in this study, application of the Galerkin method to Equation (2-19) yields to the equation

$$\int_0^a \tau\phi' D^o \frac{\partial w_i}{\partial z'}\frac{\partial w_j}{\partial z'} c_j' dz' + \int_0^a \phi' R' w_i w_j \frac{\partial c_j'}{\partial t} dz' +$$
$$\int_0^a \lambda\phi' R' w_i w_j c_j' dz' - \tau\phi' D^o \frac{\partial \hat{c}'}{\partial z'}\Big|_{z'=a} = 0, \quad i=1,2,\ldots,n', \tag{2-31}$$

where n' is the number of nodes in the one-dimensional domain for the matrix block, w_i is the standard linear basis function and $\hat{c}'$ is a trial function given by the expression

$$\hat{c}' = \sum_{j=1}^{n'} c_j' w_j.$$

By using the boundary condition (2-22) and the mass transfer term (2-25), the following tridiagonal set of equations is obtained for the porous matrix block associated with node J in the fracture domain:

$$\begin{aligned} \beta_1 c_1'^{k+1} + \gamma_1 c_2'^{k+1} &= d_1, \\ \alpha_i c_{i-1}'^{k+1} + \beta_i c_i'^{k+1} + \gamma_i c_{i+1}'^{k+1} &= d_i, \\ \alpha_{n'} c_{n'-1}'^{k+1} + \beta_{n'} c_{n'}'^{k+1} &= d_{n'} - a\Gamma_J^{k+1}, \; i=2,3,\ldots,n'-1, \end{aligned} \tag{2-32}$$

The superscript $k+1$ is used to denote the current time step and J ranges from 1 to n. The coefficients in Equation (2-32) are given by

$$\begin{aligned} \alpha_i &= -\frac{\tau\phi' D^0}{\Delta z_{i-1}'} + \frac{\lambda\phi' R' \Delta z_{i-1}'}{6} + \frac{\phi' R' \Delta z_{i-1}'}{6\Delta t} \\ \beta_i &= \frac{\tau\phi' D^0}{\Delta z_{i-1}'} + \frac{\tau\phi' D^0}{\Delta z_i'} + \frac{\lambda\phi' R'}{3} + \frac{\phi' R' (\Delta z_{i-1}' + \Delta z_i')'}{3\Delta t} \\ \gamma_i &= -\frac{\tau\phi' D^0}{\Delta z_i'} + \frac{\lambda\phi' R' \Delta z_i'}{6} + \frac{\phi' R' \Delta z_i'}{6\Delta t} \\ d_i &= \frac{\phi' R'}{6\Delta t}(\Delta z_{i-1}' c_{i-1}'^{k} + 2(\Delta z_{i-1}' + \Delta z_i') c_i'^{k} + \Delta z_i' c_{i+1}'^{k}), \\ & i=2,3,\ldots,n'-1 \; , \end{aligned} \tag{2-33}$$

$$\beta_1 = \frac{\tau\phi' D^o}{\Delta z_1'} + \frac{\lambda\phi' R' \Delta z_1'}{3} + \frac{\phi' R' \Delta z_1'}{3\Delta t}$$
$$\gamma_1 = -\frac{\tau\phi' D^o}{\Delta z_1'} + \frac{\lambda\phi' R' \Delta z_1'}{6} + \frac{\phi' R' \Delta z_1'}{6\Delta t} \qquad (2\text{-}34)$$
$$d_1 = \frac{\phi' R' \Delta z_1'}{6\Delta t}(2c_1'^{\,k} + c_2'^{\,k}),$$

and

$$\alpha_{n'} = -\frac{\tau\phi' D^0}{\Delta z'_{n'-1}} + \frac{\lambda\phi' R' \Delta z'_{n'-1}}{6} + \frac{\phi' R' \Delta z'_{n'-1}}{6\Delta t}$$
$$\beta_{n'} = \frac{\tau\phi' D^0}{\Delta z'_{n'-1}} + \frac{\lambda\phi' R' \Delta z'_{n'-1}}{3} + \frac{\phi' R' \Delta z'_{n'-1}}{3\Delta t} \qquad (2\text{-}35)$$
$$d_{n'} = \frac{\phi' R' \Delta z'_{n'-1}}{6\Delta t}(c'^{\,k}_{n'-1} + 2c'^{\,k}_{n'}),$$

The spatial increments in Equations (2-33) - (2-35) are defined as follows

$$\Delta z_i' = z'_{i+1} - z_i', \qquad i = 1, 2, \ldots, n'-1.$$

Solution scheme

There are two alternative schemes to solve the coupled set of equations (2-26) and (2-32): an iterative and a direct solution scheme (Huyakorn et al., 1983). In order to avoid a time-consuming iteration loop, an efficient direct solution scheme was employed here.

Applying the general algorithm (e.g., Press et al., 1986) for solving tridiagonal matrix equations, the matrix in Equation (2-32) can be factorized into a product of lower and upper bidiagonal matrices. After performing a forward elimination, the following relation for the mass transfer term $\Gamma_J^{\,k+1}$ connected to the fracture node J can be derived

$$-\Gamma_J^{k+1} = \frac{1}{a}[l_n c_{n'}'^{\,k+1} + (\alpha_{n'} g_{n'-1} - d_{n'})_J], \qquad (2\text{-}36)$$

where $c_{n'}'^{\,k+1} = c_J^{k+1}$ according to the boundary condition (2-21). The coefficients in Equation (2-36) are

$$
\begin{aligned}
l_1 &= \beta_1, \\
u_{i-1} &= \frac{\gamma_{i-1}}{l_{i-1}}, && i=2,3,\ldots,n', \\
l_i &= \beta_i - \alpha_i u_{i-1}, && i=2,3,\ldots,n', \\
g_1 &= \frac{d_1}{l_1}, \\
g_i &= \frac{(d_i - \alpha_i g_{i-1})}{l_i}, && i=2,3,\ldots,n'-1.
\end{aligned}
\tag{2-37}
$$

When the elimination process is completed for all the fracture nodes J, all the coefficients in Equation (2-36) are known. Substitution of Γ in Equation (2-26) yields

$$
[A + \theta R\frac{B}{\Delta t} + (\lambda + l_{n'})B]C^{k+1} - \theta R\frac{B}{\Delta t}C^{k} + U - B\Gamma' = 0, \tag{2-38}
$$

where

$$
\Gamma_J' = \frac{1}{a}[(\alpha_{n'} g_{n'-1} - d_{n'})_J].
$$

The current nodal values of the concentration in the fracture domain c_J^{k+1} can thus be determined directly by using a standard direct or iterative solver for the asymmetric matrix equation (2-38).

Knowing the concentration values in the fractures c_J^{k+1}, the concentration in the matrix block c'^{k+1} can easily be determined by performing a backward substitution into the reduced form of Equation (2-32):

$$
\begin{aligned}
c_{n'}'^{k+1} &= c_J^{k+1} \\
c_i'^{k+1} &= g_i - u_i c_{i+1}'^{k+1}, && i=n'-1, n'-2, \ldots, 1.
\end{aligned}
\tag{2-39}
$$

This completes the solution cycle for a given time step and iteration loop. The same solution sequence is repeated for subsequent time-steps and iteration loops.

The finite element algorithm described above (called the Huyakorn method after Huyakorn et al. (1983) in this section) was implemented to the FEFLOW code.

2.3.4 Verification

The Huyakorn method can easily be verified. Mass transport in a DP medium can also be simulated with Equation (2-2) describing mass transport in an EC medium. When applying that approach (called here the Grisak-Pickens method after Grisak and Pickens (1980)) both the fracture domain

and the matrix blocks have to be described explicitly with finite elements. Equation (2-2) is applied for transport within the water-bearing fractures as well as the matrix blocks with stagnant water. The equation can be solved using the finite element method and assigning the fracture and matrix properties into appropriate elements.

Two test problems were selected to test the implementation of the finite element algorithm and the applied numerical scheme for simulation of solute transport in a DP medium. The first case consists of a simple one-dimensional problem of longitudinal transport in a fracture with transverse diffusion in porous matrix. The second problem concerns a coupled system of two-dimensional groundwater flow and solute transport below a hypothetical island surrounded by a sea. Both problems were computed with the Huyakorn and Grisak-Pickens methods and the results were compared. An analytical solution is also available for the first test case and the results of the both numerical approaches were compared against it.

One-dimensional transport

The case concerns solute transport from a source located at the fracture inlet ($x = 0$, $z' = 0$) into a fracture. Figure 2-3 schematically depicts the problem. In the fracture, the solute particles are transported with flowing water. Dispersion in the direction of flow is considered. The flow particles migrate with diffusion into the porous matrix enclosing the fracture. The analytical solution to the problem is reported by Tang et al. (1981). The values of the material parameters in Tables 2-1 and 2-2 were chosen to be the same as those used by Tang et al. (1981) in order to facilitate comparison of the present numerical solution with their analytical solution. The problem was solved with the two numerical methods. Applying the Huyakorn method, transport in the fracture and matrix blocks are described by the one-dimensional equations (2-17) and (2-19), respectively. With the Grisak-Pickens method, transport is described by the two-dimensional equation (2-2) both in the fractures and matrix.

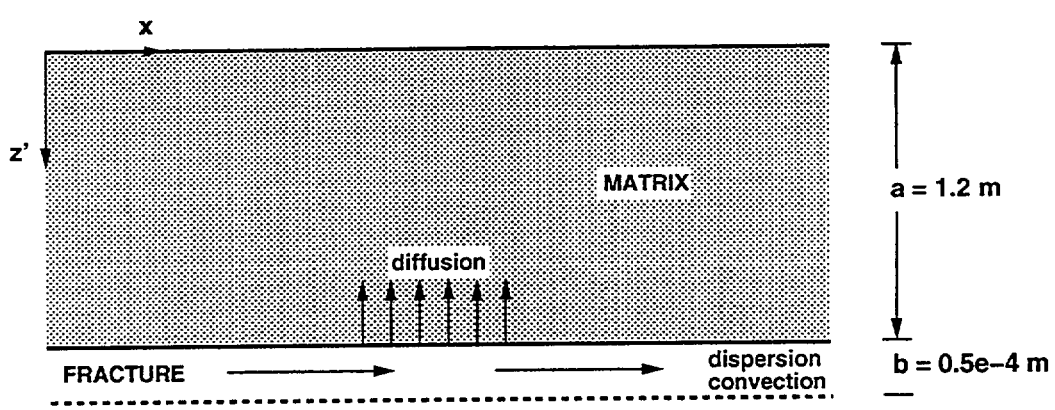

Figure 2-3. Longitudinal mass transport in a fracture with transverse matrix diffusion.

Table 2-1. Properties of the fracture system in the test case with one-dimensional transport. Flow porosity is employed only with the Grisak-Pickens method (see Eq. 2-2).

Symbol	Parameter	Value
q	Darcy velocity	$1.16 \cdot 10^{-7}$ m/s
ϕ_d	Diffusion porosity	1
ϕ_f	Flow porosity	1
ε_L	Longitudinal dispersion length	0.5 m
D^o	Molecular diffusion coefficient	$1.6 \cdot 10^{-9}$ m^2/s
R	Retardation	1
τ	Tortuosity	1
$2b$	Fracture aperture	10^{-4} m

Table 2-2. Properties for the matrix in the test case with one-dimensional transport.

Symbol	Parameter	Value
$2a$	Matrix block thickness	2.4 m
ϕ'	Matrix porosity	0.01
D^o	Molecular diffusion coefficient	$1.6 \cdot 10^{-9}$ m^2/s
λ	Decay coefficient	$1.78 \cdot 10^{-9}$ 1/s
τ'	Tortuosity	1
R'	Retardation coefficient	1

In the Huyakorn method, the x axis represents the fracture domain and it was discretized into 50 one-dimensional elements. When solving the system, the code assumes a vertical line of length 1.2 m in the z' direction for each node in the elements created for the fracture. Moreover, the code discretizes (not explicitly) each line into ten one-dimensional elements. The discretization of modelled region is illustrated in Figure 2-4.

With the Grisak-Pickens method, a two-dimensional finite element mesh was constructed in the xz' plane (Figure 2-5). In this case both the fracture and the porous matrix are discretized explicitly into two-dimensional rectangular elements. The two-dimensional transport equation (2-2) was is used to describe transport within the fracture as well as the matrix. In order to obtain results consistent with the assumptions (Section 2.3.1), the transversal dispersion length (ε_T), diffusion coefficient (D^o) and Darcy velocity (q) in the x direction were set equal to zero in the elements representing the matrix blocks.

The initial conditions are

$$c(x,t) = c'(x,z',t) = 0, \qquad t=0$$

and the boundary conditions are

$$\begin{aligned} c(x,t) &= 1\ kg/m^3, & x&=0, \\ \frac{\partial c}{\partial x}(x,t) &= 0, & x&=10\ m, \\ c'(z',t) &= c(x,t), & z'&=1.2\ m, \\ \frac{\partial c'}{\partial z'}(z',t) &= 0, & z'&=0. \end{aligned}$$

The contours of the concentration computed with the Grisak-Pickens method for the two-dimensional area are presented in Figure 2-6. The concentration values computed both by the Huyakorn method and the Grisak-Pickens method as well as the analytic solution along the fracture and in the matrix are shown in Figures 2-7 and 2-8. The results of both numerical methods agree almost identically with the analytical solution.

Although the nature of the first test problem is one-dimensional, it was also computed by applying two- and three-dimensional elements in order to test the capability of the code to employ elements of different dimensions. In the case of the Grisak-Pickens method, the three-dimensional modelling was not possible because of the requirement of the one additional dimension to represent the matrix. The results were the same regardless of the type of the elements used.

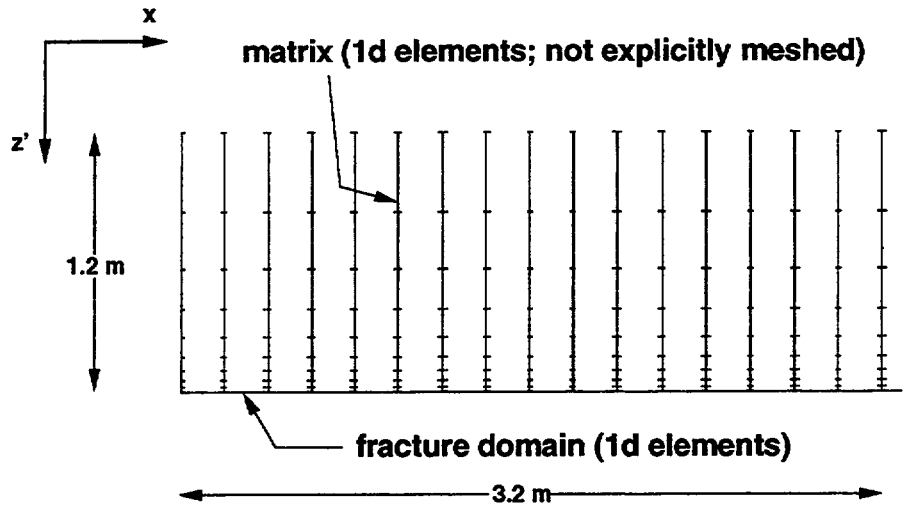

Figure 2-4. Discretization of part of the modelled domain for the Huyakorn method in the one-dimensional verification case (cf. Figure 2-3).

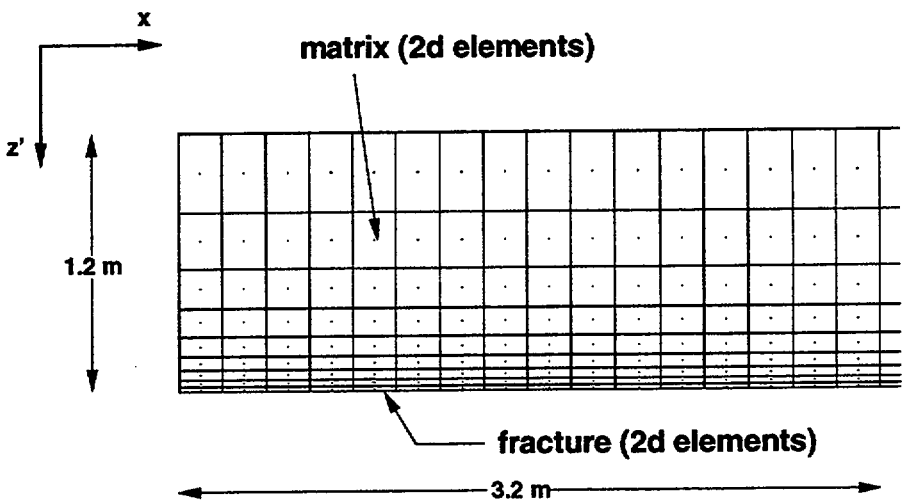

Figure 2-5. Part of the two-dimensional mesh applied in simulating the one-dimensional transport case (Figure 2-3) with the Grisak-Pickens method.

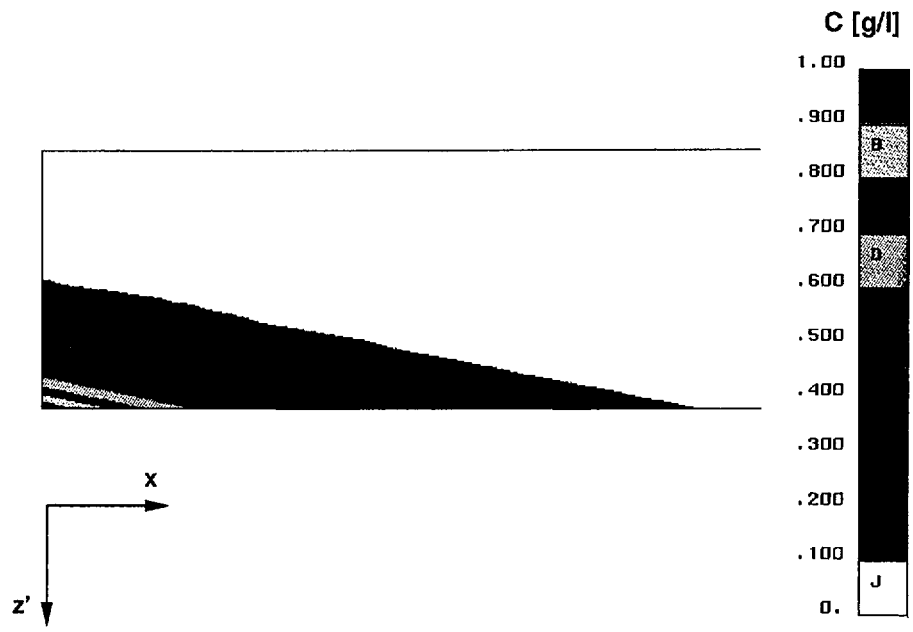

Figure 2-6. Contours of the solute concentration computed with the Grisak-Pickens method in the two-dimensional domain after 9991 days (cf. Figures 2-3 and 2-5).

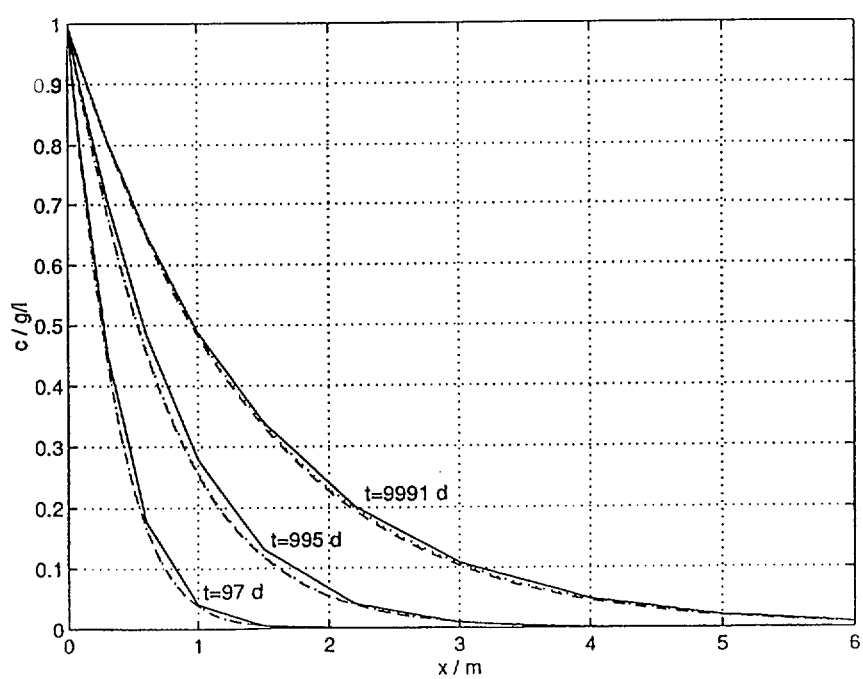

Figure 2-7. Concentration values along the fracture for the one-dimensional test case in Figure 2-3 (solid line - analytic, dashed line - Huyakorn method, dotted line - Grisak-Pickens method).

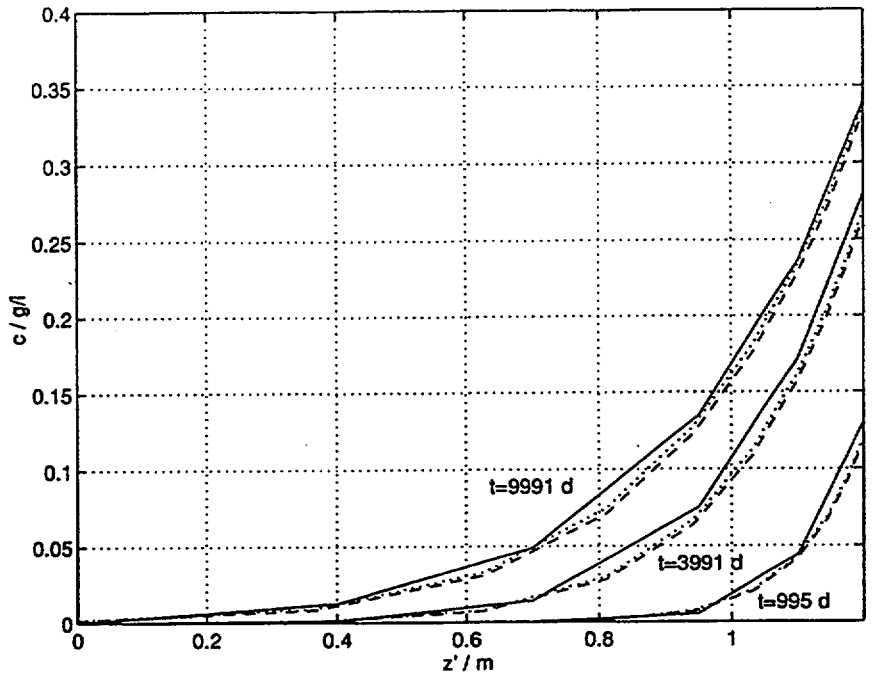

Figure 2-8. Concentration values in the matrix at a distance of 1.5 m from the inlet for the one-dimensional test case in Figure 2-3 (solid line - analytic, dashed line - Huyakorn method, dotted line - Grisak-Pickens method).

Coupled simulation of flow and transport

The second test case concerns groundwater flow and salt transport below a hypothetical island surrounded by a sea. The objective is to verify the implemented dual porosity model with this simple case before computing more complicated coupled problems.

The test case is depicted schematically in Figure 2-9. The problem is two-dimensional and transient because of land uplift. Only a half of the system has to be considered, because the geometry is assumed to be symmetric with respect to the vertical center line of the island. A transient simulation was carried out starting when the highest point of the island rises above sea level. The simulation was performed for a time period of about 700 years. The initial salt concentration in the bedrock below the sea is 10 g/l. The concentrations of the fresh and sea water are 0 and 5 g/l, respectively. The pressure gradient caused by the uplift of the water table makes the fresh water flow into the system. The domain to be modelled is a vertical cross section with a length of 900 m and a depth of 300 m. The rate of the uplift of the water table is 7 mm/year.

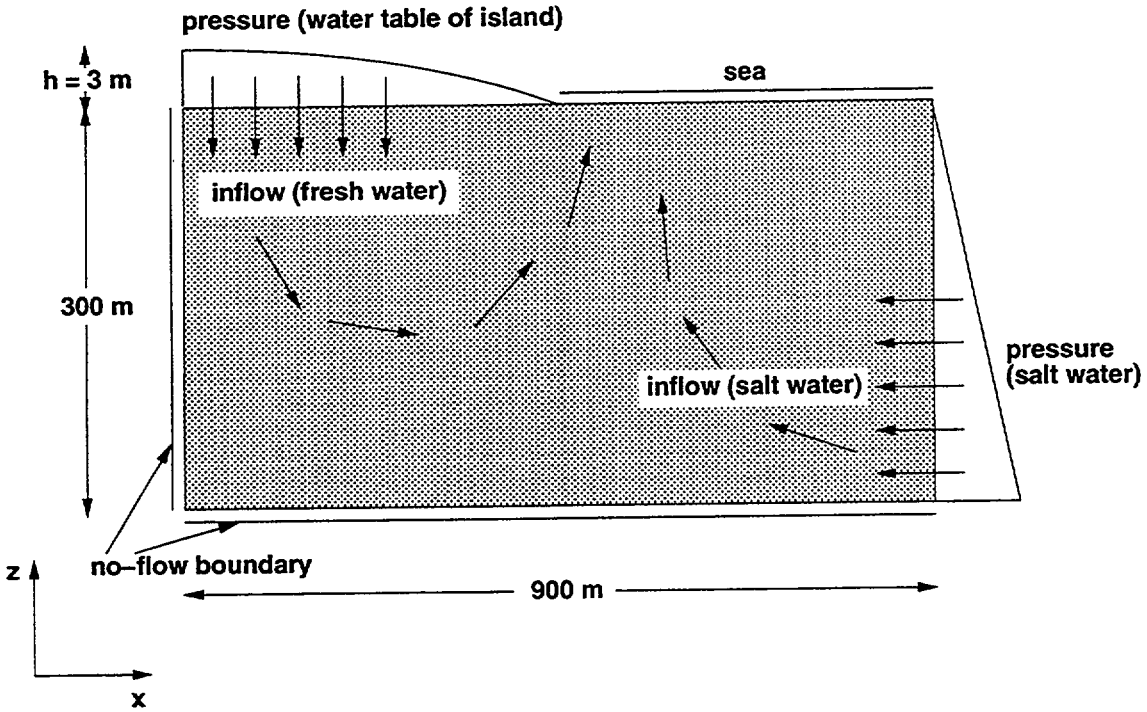

Figure 2-9. Schematic description of the test case for coupled flow and transport.

The rock is taken as homogeneous and isotropic. The modelling domain is also assumed to contain fracture zones with a higher hydraulic conductivity than the remaining intact rock (cf. Figure 2-10). Water flow was assumed to take place only in water-bearing fractures in the intact rock and fracture zones. The water in the matrix blocks does not move and the matrix contributes only on salt transport. The properties of the water-bearing fractures and the matrix are presented in Tables 2-3 and 2-4.

The initial and boundary conditions applied in the numerical simulations are given in the following in more detail. The boundary condition for the salt concentration on the water inflow boundary ($0 \leq x \leq 450$ m and z=0; cf. Figure 2-9) is

$$c = 0.$$

The salt concentration for the sea area ($450 \leq x \leq 900$ m and z=0; cf. Figure 2-9) is

$$c = 5 \ g/l.$$

The rest of the boundaries are taken as impermeable to salt transport. The initial condition for the salt concentration below the sea ($z < 0$ m; cf. Figure 2-9) is

$$c = 10 \ g/l.$$

Table 2-3. Properties of the fracture system in the test case for coupled flow and transport. Flow porosity is employed only with the Grisak-Pickens method (see Eq. 2-2).

Symbol	Parameter	Value
T_{2d}	Transmissivity (intact rock)	$2 \cdot 10^{-10}$ m^2/s
T_{1d}	Hydraulic conductivity multiplied with the area of cross-section (fracture zones)	$2 \cdot 10^{-6}$ m^3/s
ϕ_d	Diffusion porosity	10^{-3}
ϕ_f	Flow porosity	1
ε_L	Longitudinal dispersion length	100 m
ε_T	Transversal dispersion length	10 m
D^o	Molecular diffusion coefficient	10^{-9} m^2/s
R	Retardation	1
τ	Tortuosity	1
$2b$	Fracture aperture	10^{-3} m

Table 2-4. Properties of the matrix in the test case for coupled flow and transport.

Symbol	Parameter	Value
$2a$	Matrix block thickness	40 m
ϕ'	Matrix porosity	0.1
τ'	Tortuosity	1
R'	Retardation coefficient	1

The boundary condition for the pressure corresponding the water table of the island ($0 \leq x \leq 450$ m and z=0; cf. Figure 2-9) follows the parabola

$$p(x) = p_o(t)(1 - (\frac{x}{450\ m})^2),$$

where p_o (= 30000 Pa) is the maximum value of the pressure caused by the uplift of the water table of the island. The pressure on the boundary corresponding the sea ($450 \leq x \leq 900$ m and z=0; cf. Figure 2-9) is

$$p = 0.$$

The pressure on the boundary through which the salt water flows in (x=900 m and $0 \leq z \leq -300$ m; cf. Figure 2-9) is assigned according to the additional pressure caused by the varying fluid density

$$p = (\rho_0 - \rho)gz.$$

The left hand side wall and the bottom boundary are assumed to be impermeable to water.

No analytical solution exists for the problem. This test case was thus simulated applying the Huyakorn method and the Grisak-Pickens method. The latter provides a "correct" numerical solution with which the solution of Huyakorn method can be compared. Both the approaches employ Equation (2-1) for groundwater flow.

With the Grisak-Pickens method, transport is described by the three-dimensional equation (2-2) both in the water-bearing fractures and in the matrix with stagnant water. A three-dimensional mesh was constructed for numerical simulations (Figure 2-10). Both the fracture system and the matrix are discretized explicitly by three-dimensional rectangular elements (6 x 18 x 10 elements in zxz' directions, respectively). As the three-dimensional transport equation (2-2) is used to describe transport in the matrix, too, the transversal dispersion length (ε_T), diffusion coefficient (D^o) and Darcy velocity (q) in the x and z directions have to be set to zero in the elements representing the matrix.

When applying the Huyakorn method, transport in the fracture system is described by the two-dimensional equation (2-17) and in the matrix blocks by the one-dimensional equations (2-19). Here the xz direction (explicitly meshed) represents the fracture domain and the z' direction the matrix (not explicitly meshed). The area to be modelled was divided into 108 square elements (6 x 18 elements in zx directions, respectively) (Figure 2-10). The two horizontal and four vertical zones with a high hydraulic conductivity were modelled with the one dimensional bar elements.

The contours of the concentration in the water-bearing fracture domain (xz plane) are presented in the top part of Figure 2-11, which demonstrates that

the fresh water moves faster in the fracture zones than in the intact rock because of the larger hydraulic conductivities. On the other hand, the bottom part of Figure 2-11 shows clearly how after 700 years the matrix still contains saline water while only fresh water flows in the fracture domain. The salt concentrations computed by both the methods were compared at seven horizontal lines at depths of 0, 50, 100, 150, 200, 250 and 300 m both in the fracture domain and at a distance of 4.3 m from the water-bearing fracture system into the matrix. The agreement of the results is good. The salt concentration at a depth of 100 m is presented in Figures 2-12 and 2-13.

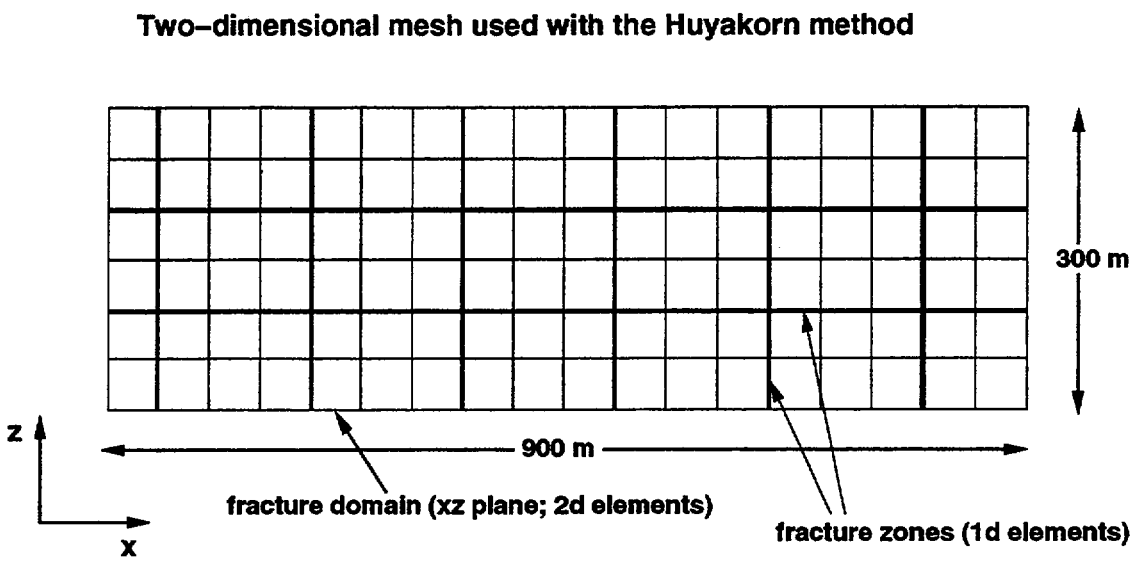

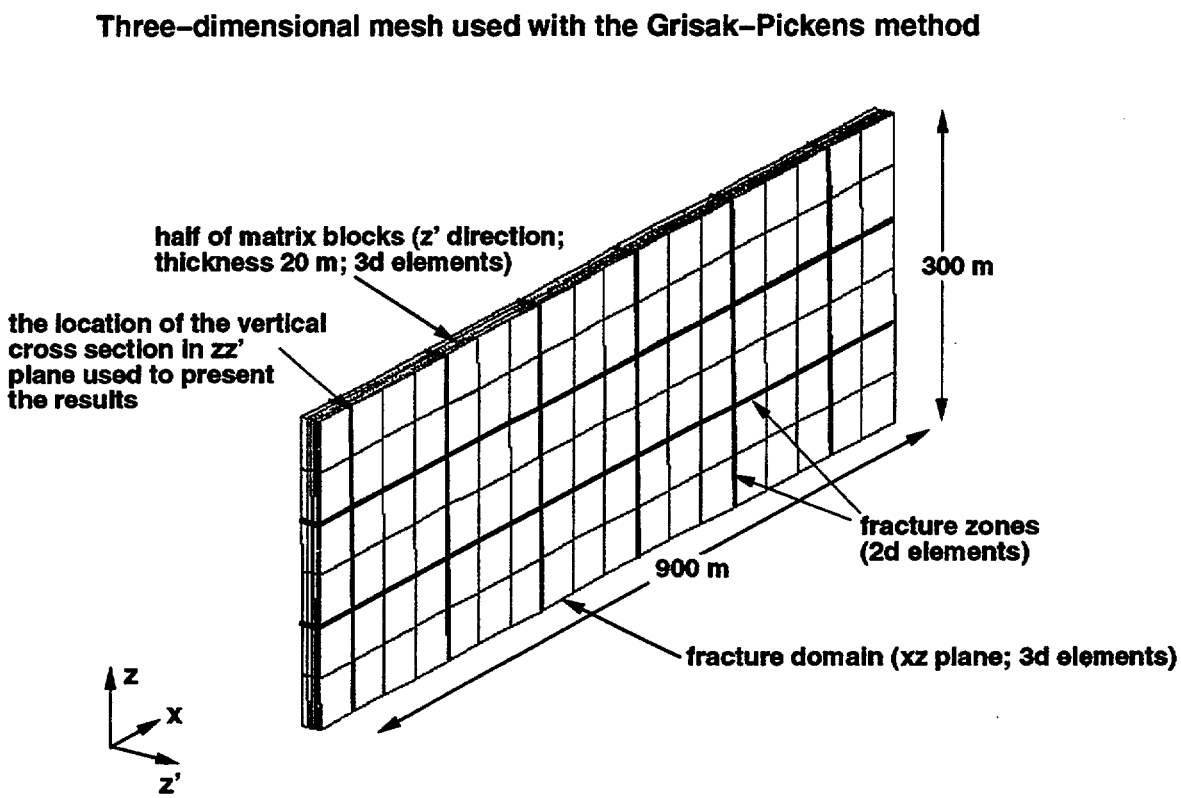

Figure 2-10. A two-dimensional mesh used with the Huyakorn method (top) and a three-dimensional mesh used with the Grisak-Pickens method (bottom) to simulate the test case of coupled flow and transport (cf. Figure 2-9).

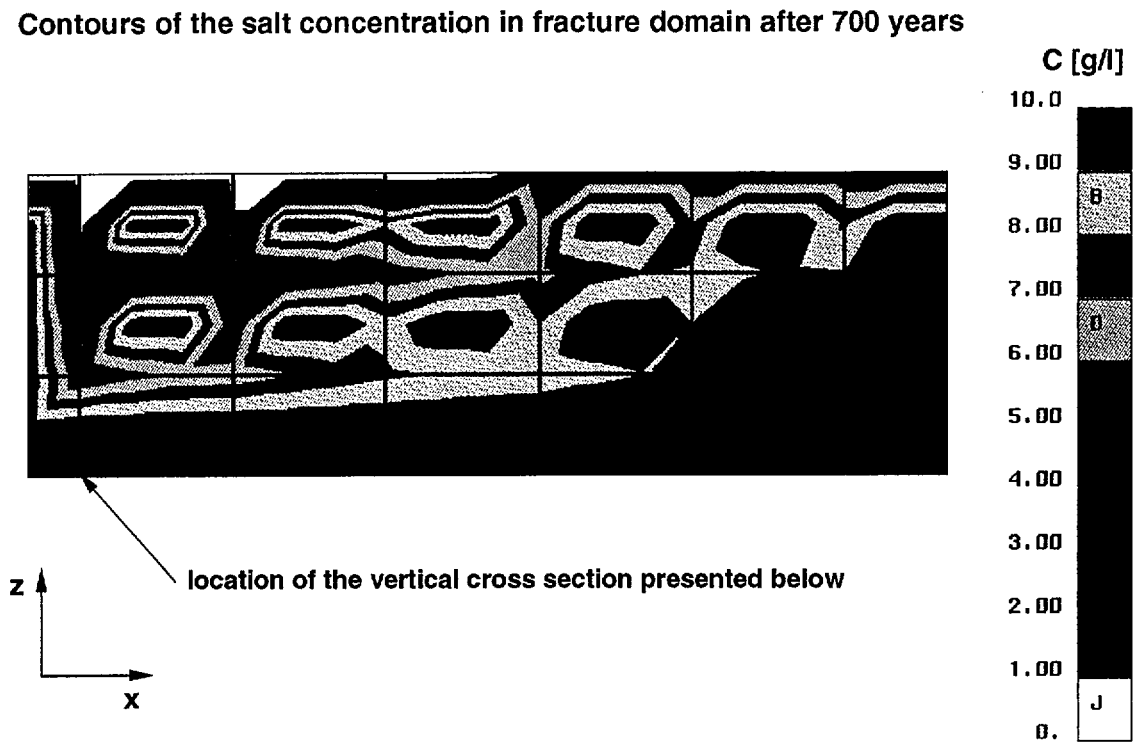

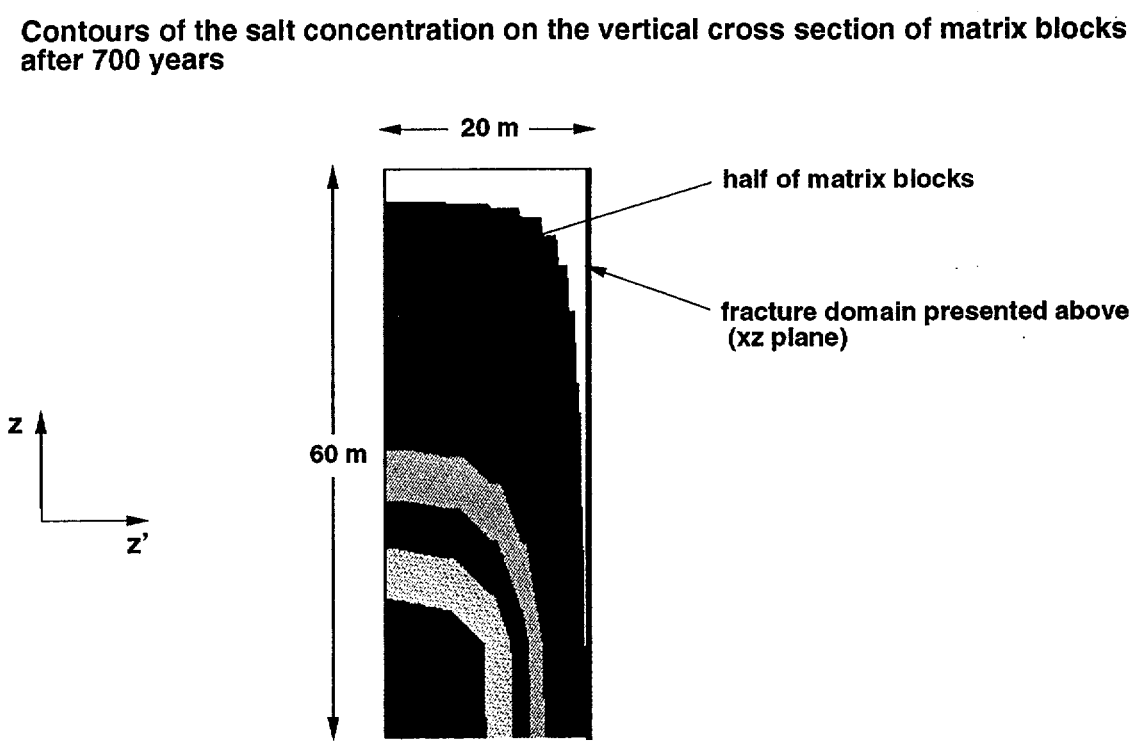

Figure 2-11. Contours of the salt concentration in the fracture domain (top) and in the matrix at a distance of 4.3 m from the fracture domain (bottom) after 700 years for the test case of coupled flow and transport (cf. Figure 2-9).

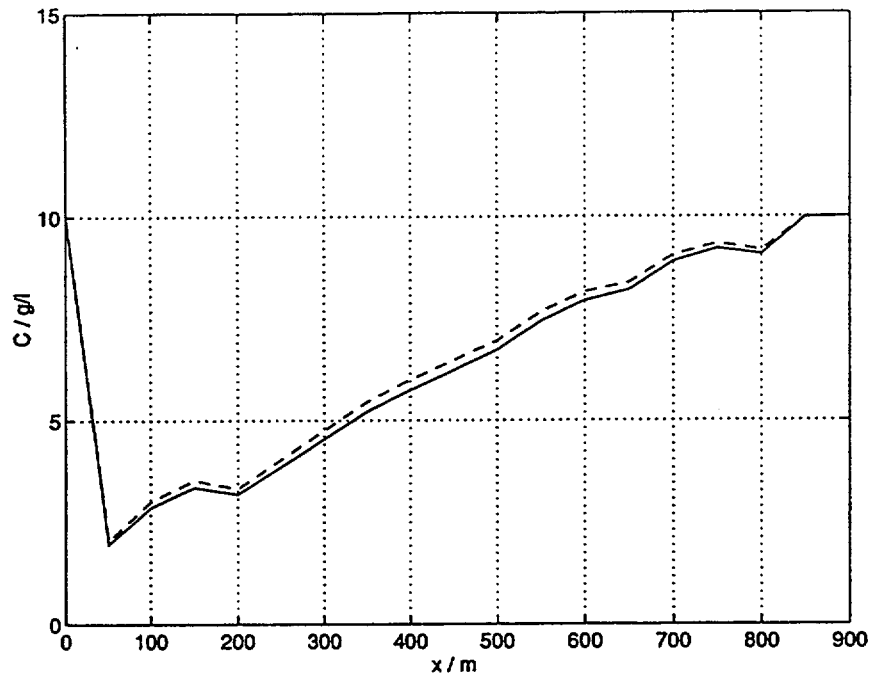

Figure 2-12. *Salt concentration at a depth of 100 m in the fracture domain after 700 years for the test case of coupled flow and transport (cf. Figure 2-9) (solid line - Huyakorn method, dashed line - Grisak-Pickens method).*

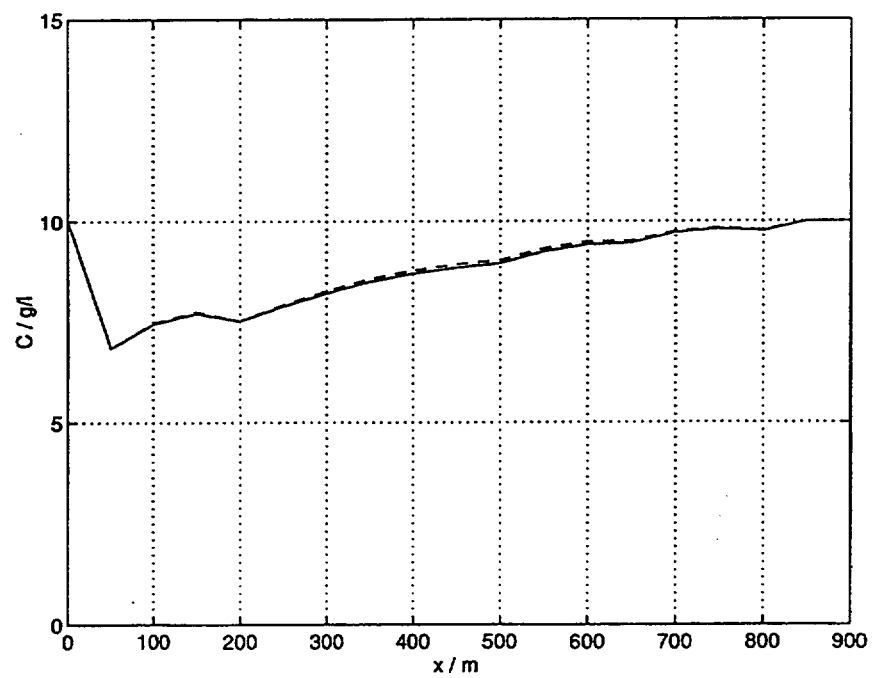

Figure 2-13. *Salt concentration at a depth of 100 m in the matrix at a distance of 4.3 m from the fracture domain after 700 years (solid line - Huyakorn method, dashed line - Grisak-Pickens method). The test case of coupled flow and transport (cf. Figure 2-9).*

3 SIMULATION MODEL FOR THE ÄSPÖ SITE

The coupled system of groundwater flow and salt transport at the Äspö site was simulated with the FEFLOW code. The equivalent-continuum (EC) and dual-porosity (DP) approaches were applied to represent the bedrock. The DP model is equivalent to the Huyakorn approach. It was implemented in FEFLOW and verified as discussed earlier. A three-dimensional mesh was constructed for the simulations taking into account the experimental data available, flow model and the special features of the FEFLOW code (see Section 2.1).

The flow model, finite element mesh as well as initial and boundary conditions employed in the simulations are introduced in this chapter. The results are presented in the next chapter.

3.1 FLOW MODEL

The concept of a flow model was utilized in this study. A flow model refers to a representation of a real system. It includes geometrical parameters (the geometry of fracture zones) and hydraulic properties. In practical applications, a flow model is a simplification of the real system concerned. In this study, the flow model of the Äspö site is the same applied when simulating the long-term pumping test LPT2 (Taivassalo et al., 1994).

3.1.1 Geometry of the fracture zones

The geometry of the flow model is based on the updated structural model reported by Ström (1993). The layouts of the structural model at the ground level and at a depth of 300 m are shown in Figures 3-1 and 3-2. The fracture zones with labels are assumed to be more than about 5 m wide and they extend over several hundred meters. Even though several fracture zones are classified as "certain" at the Äspö site, their regional extensions are not generally known as indicated in Figures 3-1 and 3-2. The depth extent of the zones is not explicitly reported.

It is assumed that the bedrock includes zones with a higher hydraulic conductivity than the intact rock comprising the rest of the bedrock. Thus, the domain to be modelled was divided into hydraulic units: the intact rock with low hydraulic conductivity and fracture zones with high hydraulic conductivities. The flow model includes 15 fracture zones. The zones extend to the bottom of the model in the vertical direction. The depth of the flow model was chosen to be 1500 m. Figure 3-3 illustrates the geometry of the fracture zones. The horizontal cut planes for the flow model corresponding

those in Figures 3-1 and 3-2 for the structural model are presented in Figure 3–4. The dip angles and directions of the zones are given in Table 3-1.

Figure 3-5 shows the occurrence of the zones in the cored boreholes according to the field investigations (Wikberg et al., 1991) and, on the other hand, the intersections of the boreholes and the zones in the flow model. The most significant differences in the figure are the following (references to the field data in this list are based on the compilation by Wikberg et al. (1991)):

- KAS02 does not intersect NE–1 in the flow model.
- According to the field data, neither KAS03, KAS08 nor KAS13 intersect EW–5 as they do in the flow model.
- According to the field data, KAS11 does not intersect NE–1A and NE-1B as it does in the flow model.
- KAS13 does not quite intersect NNW–1 in the flow model although the distance between them is very small at the ground surface.
- According to the field data, KAS14 does not intersect NNW–3.

The discrepancies above are mainly due to the simplifications made while constructing the flow model. The fracture zones in the flow model are smooth planes while their real shape is more or less rugged. These differences must be considered when interpreting and comparing the experimental and computational results.

Table 3–1. Dip angles and directions of the fractures zones in the flow model. Multiple dip angles indicate that a fracture zone consists of two or more subzones (cf. Figures 3-3 and 3–4).

Fracture zone	Dip angle (°) and direction
NW-1	30 NE
EW-1A, B, C, D	60 NW, 88 NW, 78 SE, 75 NW
EW-3	79 S
EW-5	37 N
NE-1A, B	70 NW, 75 NW
NE-2	78 NW
NE-3A, B	80 NW, 70 NW
NE-4A, B	78 SE, 71 SE
NNW-1	vertical
NNW-2	vertical
NNW-3	vertical
NNW-4	vertical
NNW-5	vertical
NNW-6	vertical
EW-7A, B	81 S, 52 SE

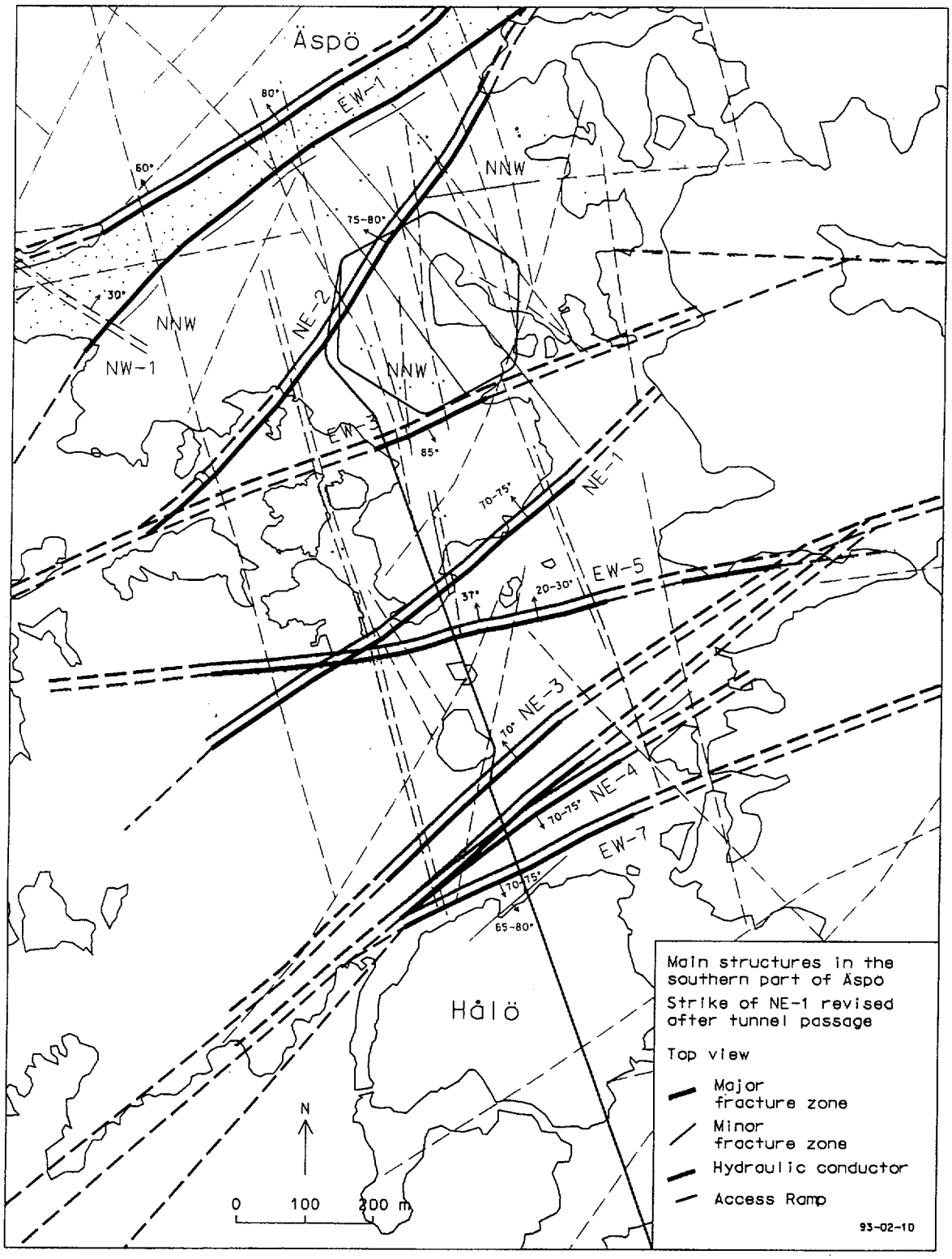

Figure 3–1. *Updated structural model for the Äspö area at the ground level (Ström, 1993). A solid line means that a fracture zone is confirmed by borehole or surface investigations. A blue line indicates a certain hydraulic conductor and a dashed blue line is a possible hydraulic conductor. Fracture zone EW-5 is drawn 50 m to the south of its estimated location (Ström, 1993a).*

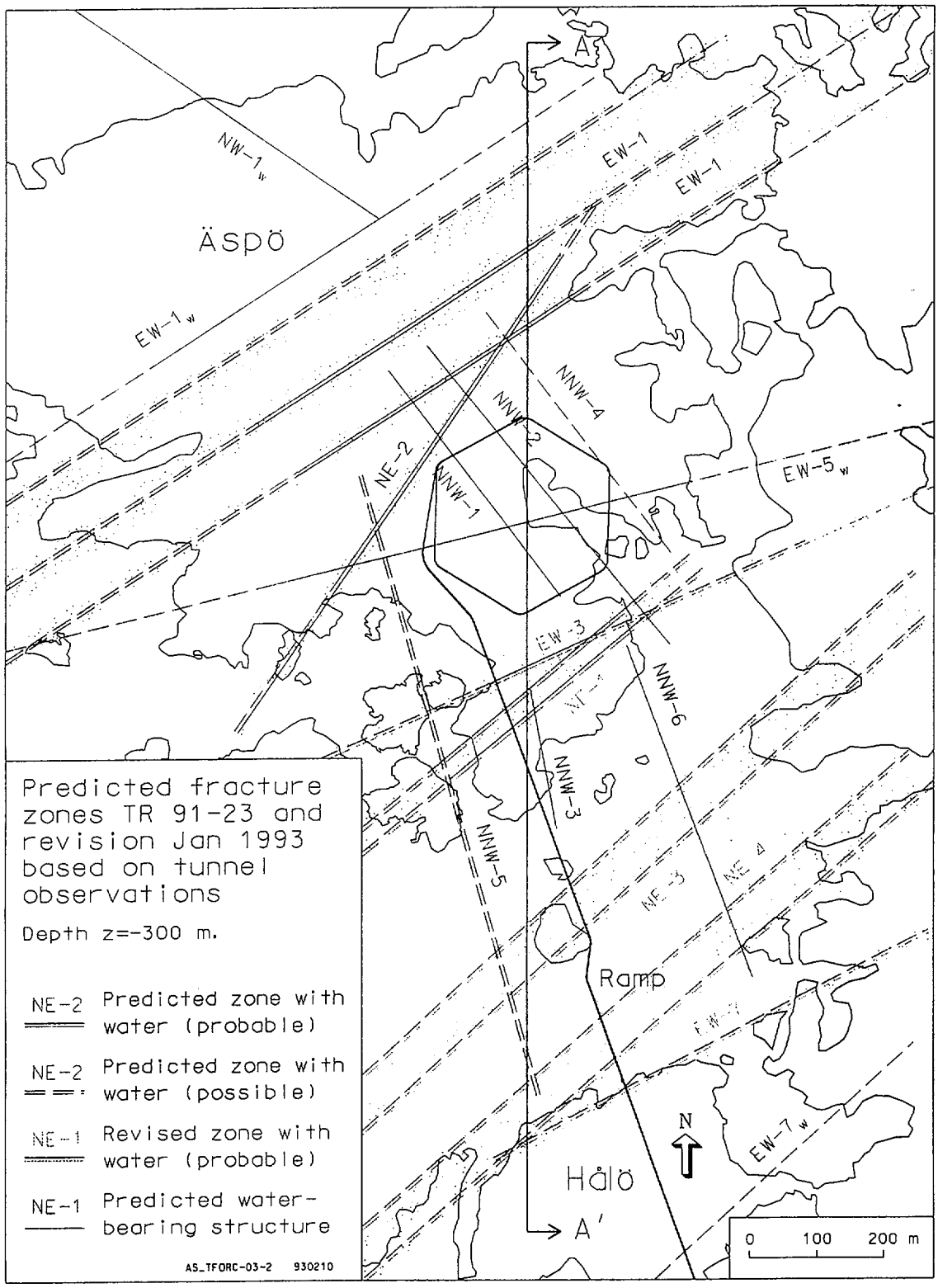

Figure 3–2. *Updated structural model for the Äspö area at the depth of 300 m (Ström, 1993). A solid line means that a fracture zone is confirmed by borehole or surface investigations. A blue line indicates a certain hydraulic conductor and a dashed blue line is a possible hydraulic conductor. Compare with Figure 3–1.*

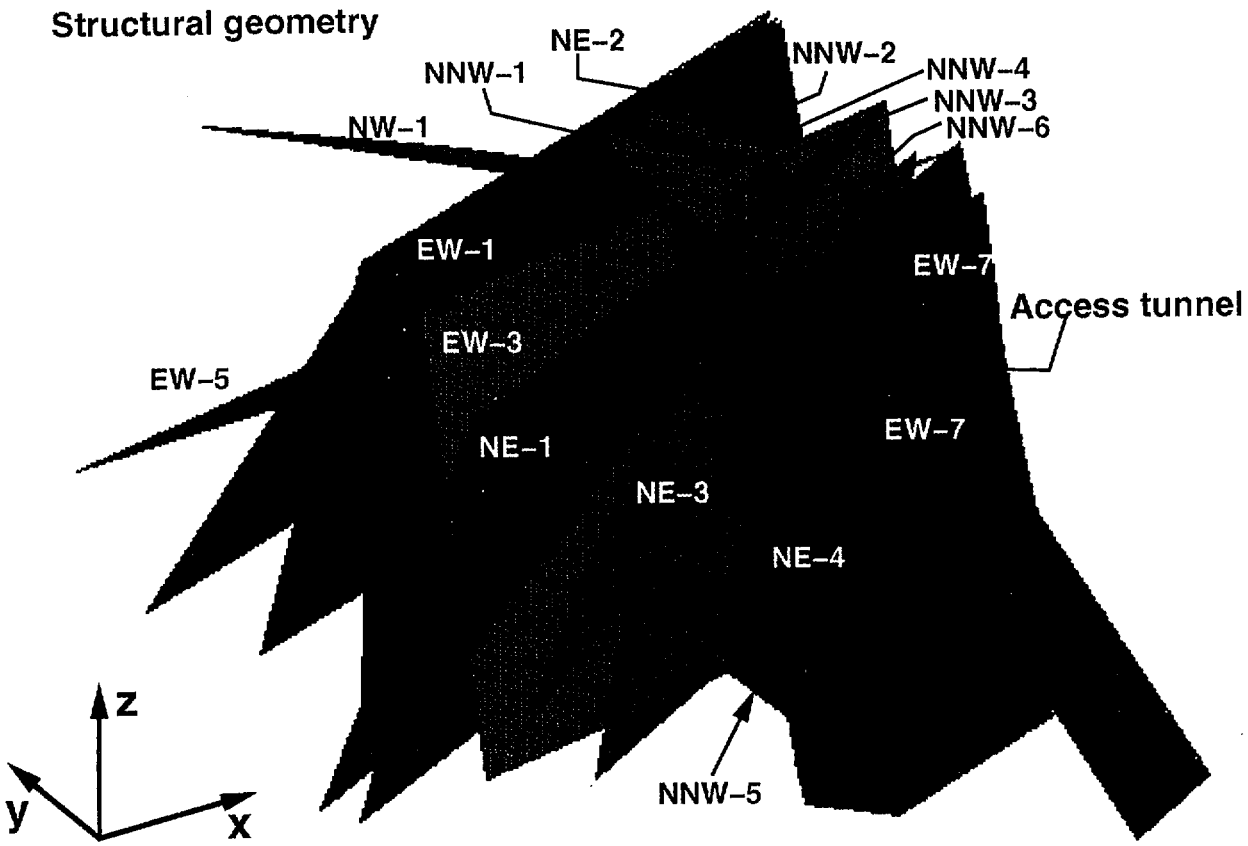

Figure 3-3. Zone geometry of the flow model for the Äspö site.

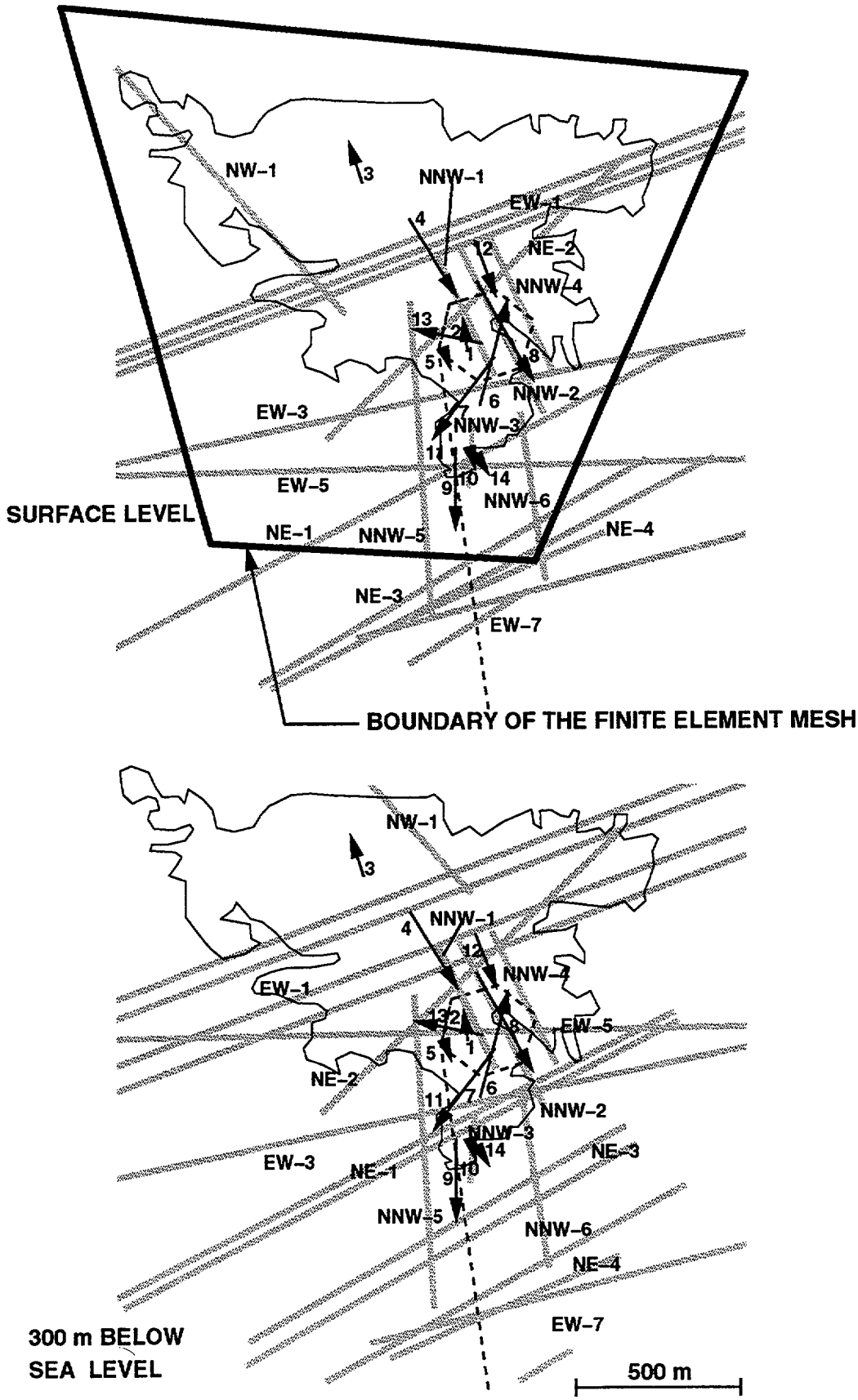

Figure 3–4. Outlines of the site model and the zone geometry in the flow model at the ground surface (top) and at a depth of 300 m (bottom). Compare with Figures 3–1 and 3–2.

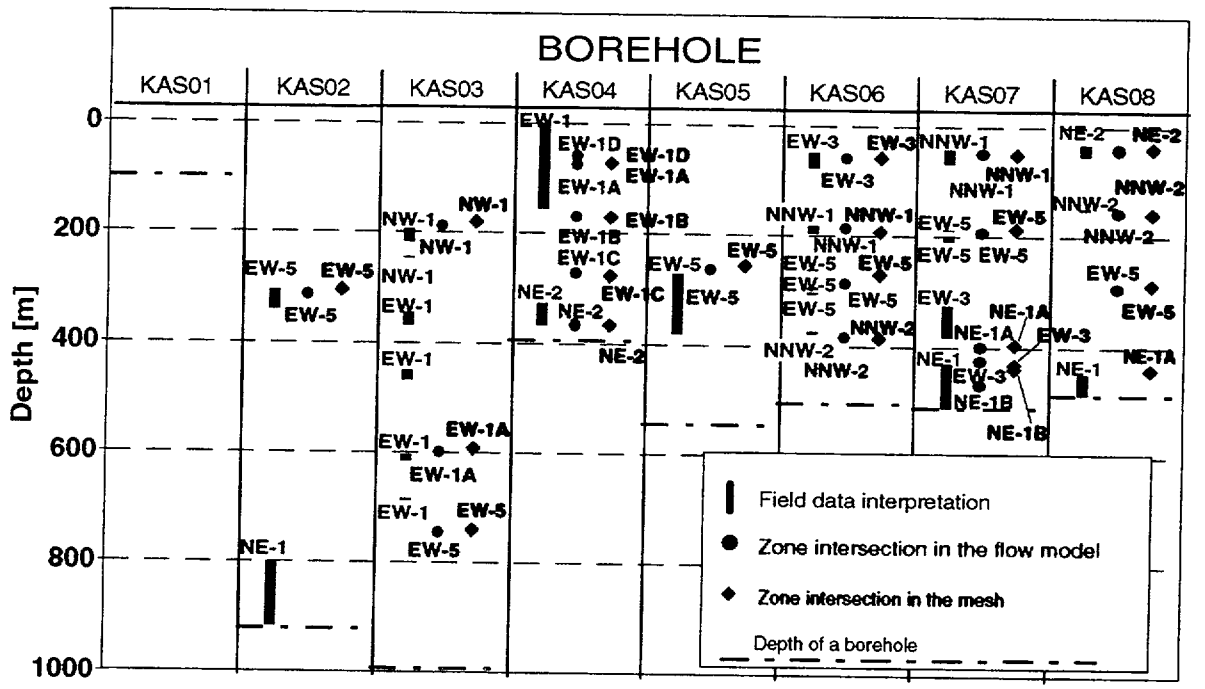

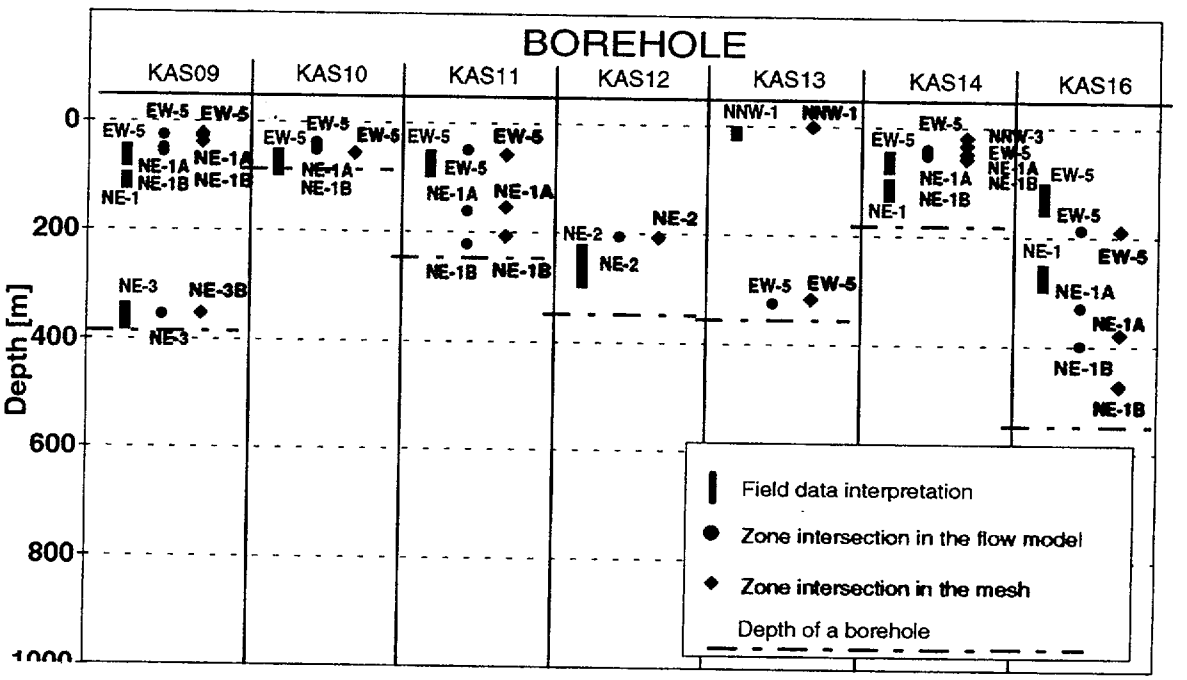

Figure 3–5. *Intersections of the cored boreholes and the fracture zones according to the field data interpretations (Wikberg et al., 1991), the flow model geometry and the corresponding finite element mesh.*

3.1.2 Properties of the bedrock

Although the hydraulic properties of the fracture zones and the intact rock may vary in space, the scale of heterogeneity in both of them was assumed to be small compared with the areas/volumes of the modelled domain. Values for the pressure and concentration computed from the equivalent properties are therefore average values for areas/volumes significantly greater than the scale of the heterogeneity.

Each hydrogeologic unit in the flow model, a fracture zone or the intact rock, is assumed to be homogeneous and isotropic. It is likely that anisotropy is present due to, e.g., lithostatic mechanical stresses and an anisotropic fracture network in the bedrock. These phenomena, however, include considerable uncertainties preventing any quantitative evaluation of their influences.

The values of the property parameters were chosen on the basis of prior information. The hydraulic conductivity of the intact rock and the transmissivity of the fracture zones were taken equivalent to those found in the calibration phase of the LPT2 modelling study (Taivassalo et al., 1994). As no site-specific data were available for several parameters, general knowledge was utilized to select their values. Poorly known parameters were allowed to vary in the simulations. When applying the DP model, in addition to the properties corresponding the water-bearing fracture system used in the EC approach, parameters characterizing the matrix blocks are needed.

Equivalent-continuum approach

The properties needed when simulating with the EC model (see Section 2.2) comprise

- transmissivity for the fracture zones,
- hydraulic conductivity of the intact rock,
- thickness of the fracture zones,
- specific storage,
- density of the fresh water,
- total, flow and diffusion porosities,
- longitudinal and transversal dispersion lengths and
- molecular diffusivity of salt in water.

The values of the transmissivities of the fracture zones and of the hydraulic conductivity of the intact rock are shown in Table 3–2. The selected values are based on the report by Wikberg et al. (1991) and the calibration process by Taivassalo et al. (1994). The thickness of the fracture zones was assumed to be 10 m.

Stochastic hydraulic conductivities and transmissivities were also used in one simulation. Lognormally distributed values were determined with a standard deviation of 1 for the logarithm of the hydraulic conductivity. The values in

the Table 3-2 are the corresponding mean values (the equivalent hydraulic conductivities in the stochastic simulations are thus about one order of magnitude smaller than those in Table 3-2).

Table 3–2. Transmissivity of the fracture zones and the hydraulic conductivity of the intact rock. Values are based on the report by Wikberg et al. (1991) and the calibration process by Taivassalo et al. (1994).

Fracture zone	Transmissivity (10^{-5} m^2/s)
NW–1	0.7
EW–1A	2
EW–1B	0.2
EW–1C	0.2
EW–1D	2
EW–3	1
EW–5	1
NE–1A	10
NE–1B	10
NE–2	0.4
NNW–1	0.75
NNW–2	4
NNW–3	2
NNW–4	4
NNW–5	5
NNW–6	5
NE–3A	3
NE–3B	3
NE–4A	35
NE–4B	35
EW–7A	0.7
EW–7B	0.7
Hydraulic conductivity of the intact rock is 10^{-9} m/s	

Values taken for the other input parameters are presented in Table 3-3. The specific storage was chosen on the basis of the transient simulations performed for the LPT2 pumping test (Taivassalo et al., 1994). Values considered representative for a crystalline rock mass were selected for the porosities (Valkiainen, 1992). The longitudinal dispersion length was chosen to be 100 m. Commonly the longitudinal dispersion length is assumed to be about 10% of the length of a transport route (e.g., de Marsily, 1986). The value used is a compromise between values for short (starting from zero) and long, over 1000 m long transport routes. The transversal dispersion length is 10% of the longitudinal dispersion length. The density of the fresh water and the molecular diffusion coefficient of salt in water are well known parameters (Lide, 1990). The effect of the retardation of salt was considered negligible in this study. The tortuosity of the transport routes was neglected, too.

Table 3-3. Properties of the bedrock and water related to the equivalent-continuum (EC) model. The symbols refer to the equations presented in Section 2.2.2.

Symbol	Parameter	Value
S_s	Specific storage	10^{-7} 1/m
ϕ_d	Diffusion porosity	$5 \cdot 10^{-2}$
ϕ_f	Flow porosity	10^{-4}
ε_L	Longitudinal dispersion length	100 m
ε_T	Transversal dispersion length	10 m
R	Retardation	1
τ	Tortuosity	1
ρ_o	Density of fresh water	1000 kg/m^3
D^o	Molecular diffusivity for salt water	10^{-9} m^2/s

Dual-porosity approach

Properties employed with the EC model (see Table 3-3; except the flow porosity) are also needed when simulating with the DP model. In this case they characterize the water-bearing fracture system. In addition, the properties characterizing the matrix blocks with stagnant water and the aperture of the water-bearing fractures are required with the DP model. The additional properties needed when simulating with the DP model consist of

- fracture aperture,
- matrix block thickness,
- matrix porosity,
- tortuosity coefficient and
- retardation coefficient.

The values applied for the additional parameters above are shown in Table 3-4. The fracture aperture was selected to be consistent with the hydraulic conductivity of the intact rock. Several alternative values of the matrix block thickness and porosity were employed because of the missing field data and in order to study the importance of these parameters. The simulation with a matrix block porosity of 10^{-2} and a matrix block thickness of 40 m was selected as a "base case" for the simulations with the dual-porosity model. Most of the simulations were performed with the base case. The other cases were utilized in sensitivity studies. The effect of the retardation of salt and the tortuosity both in fracture system and matrix blocks were considered negligible in this case, too.

Table 3-4. Properties of the bedrock related to the dual-porosity (DP) model. The symbols refer to the equations presented in Section 2.3.2. Other properties of the bedrock (and water) related to the DP model are in Table 3-3 (flow porosity is not employed with the DP model).

Symbol	Parameter	Value(s)
$2b$	Fracture aperture	10^{-4} m
$2a$	Matrix block thickness [1)]	10, 20, 40, 80 m
ϕ'	Matrix porosity [2)]	10^{-2}, $5 \cdot 10^{-3}$, 10^{-3}
τ'	Tortuosity	1
R'	Retardation coefficient	1

[1)] Four values of the matrix block thickness $2a$ were used in the simulations. In the base case the thickness was 40 m.
[2)] Three values of the matrix porosity ϕ' were used in the simulations. In the base case the porosity was 10^{-2}.

3.2 FINITE ELEMENT MESH

The modelled domain covers the Äspö island in such a way that the distance of the vertical boundaries from the shoreline of the island is about 150 m. The depth of the modelled domain is 1200 m (Figure 3-4). The domain was discretized into a finite element mesh.

The base mesh consisting of only three-dimensional linear hexahedral elements representing the intact rock was created with PATRAN (1989). The base mesh was modified to correspond to the geometry of the flow model (Section 3.1) by adding two-dimensional quadrilateral and triangular elements for the fractures zones. The two-dimensional elements were added in an optimal way on the faces or diagonals of three-dimensional elements by means of the PAAWI program (Figure 2-1). Due to the finite resolution of the original three-dimensional base mesh, the new elements cannot naturally be located along the plane of an arbitrary-oriented fracture zone. The ELMO program (Figure 2-1) was employed to optimize the planarity of a set of two-dimensional elements representing a planar part of the fracture zone.

The total number of finite elements is about 42000. The average element volume of three-dimensional elements is about 30x30x30 m^3. The mesh is illustrated in Figure 3-6.

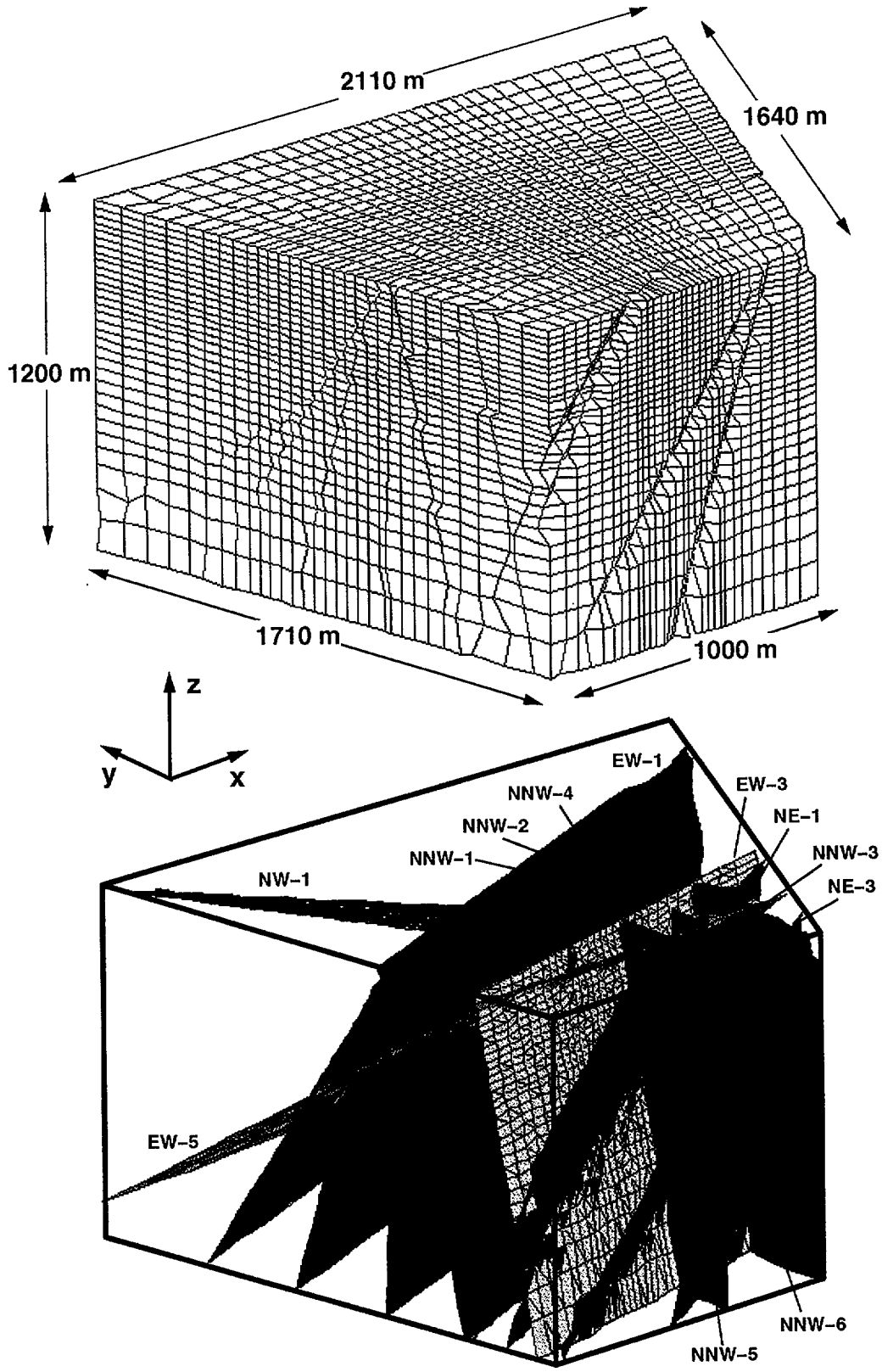

Figure 3-6. Finite element mesh of the Äspö site for the numerical simulations. The three-dimensional elements for the intact rock are shown in the top part and the two-dimensional elements for the fracture zones in the bottom part.

3.3 INITIAL AND BOUNDARY CONDITIONS

3.3.1 Pressure

For the upper boundary of the model domain, the boundary condition associated to the pressure was interpolated from the equicontour map of the water table reported by Wikberg et al. (1991). This map is based on the average water levels measured in the boreholes in 1987–1989 (Figure 3-7). For the areas not covered by the borehole measurements, the water table was estimated from a regression curve representing the relationship between the water table and the topography. During 1987–1989, the level of the Baltic sea ranged from -0.5 to +0.8 m with a reference to its mean value. The normal fluctuations are ±0.3 m. The importance of the sea-level variations is small compared to the effects of the uncertainties associated with the other modelling assumptions, and they were not considered in the numerical simulations.

In transient simulations, the effects of land uplift are taken into account. The simulations were carried out for a period that started 3000 years ago when the highest hills at Äspö rose above sea level (Wikberg et al., 1991). The simulation period continued until the present day. The rate of the uplift of the water table is assumed to be 1 mm/year being about a half of the average rate of land uplift at Äspö (Figure 3-8) (Kakkuri, 1986; Alalammi, 1992). The water table is assumed to rise linearly from zero to a level corresponding the equicontour map mentioned above.

The vertical faces of the model domain were thus defined to follow the sea around the Äspö island. The pressure on the vertical boundaries was assumed to be hydrostatic. The drawback of this assumption is that it requires knowledge on the salinity field on the boundaries. A residual pressure value assigned to a node on a vertical boundary was calculated according to a salinity model (see the next section) as follows

$$p_{BC} = a_c C g h, \tag{3-1}$$

where p_{BC} is the residual pressure on a boundary (Pa),
C is the salt concentration (kgm^{-3}),
a_c is the coefficient of density dependence on the concentration (= 0.71 (Lide,1990)) and
h is the depth of the node on the boundary (m).

The depth of the model domain for the simulation was 1200 m. At that depth, the no-flow boundary condition is presumed to be valid. This is based on the assumption that the amount of the infiltrated water flowing deeper than 1200 m is insignificant.

In the rest of the domain the initial values of the residual pressure were computed according to the salinity model applied with Equation (3-1). In

transient simulations, the pressure values on the vertical boundaries were kept as fixed in the initial state.

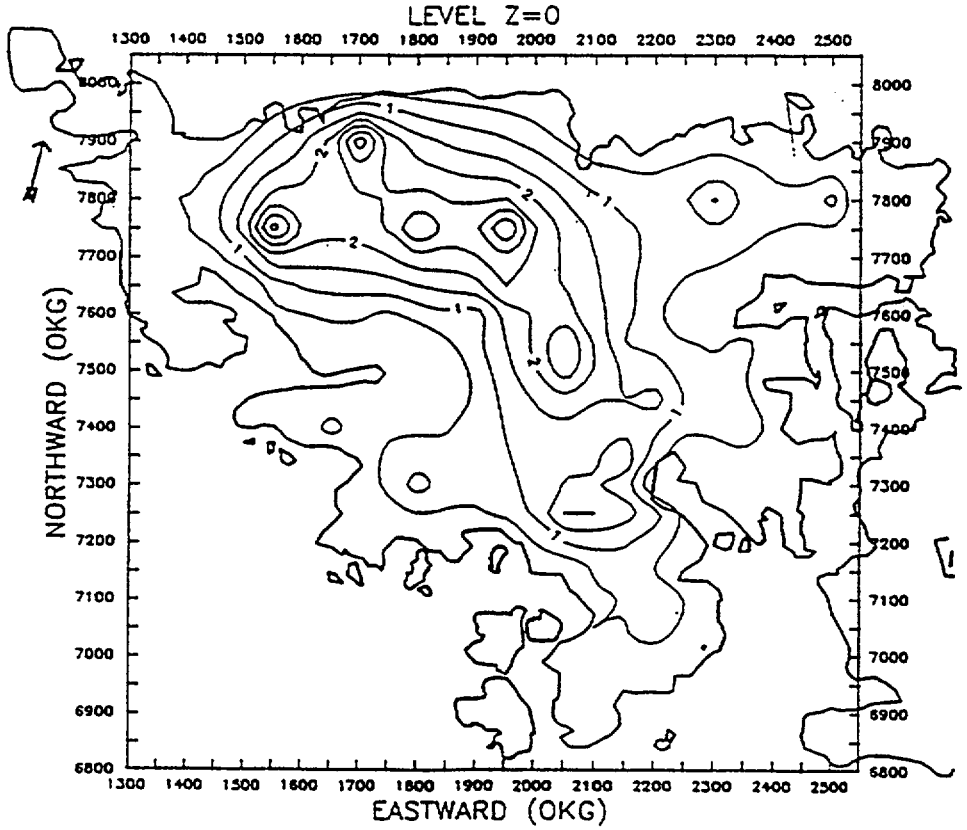

Figure 3-7. *Water table on the Äspö island under hydraulically undisturbed conditions (Wikberg et al., 1991).*

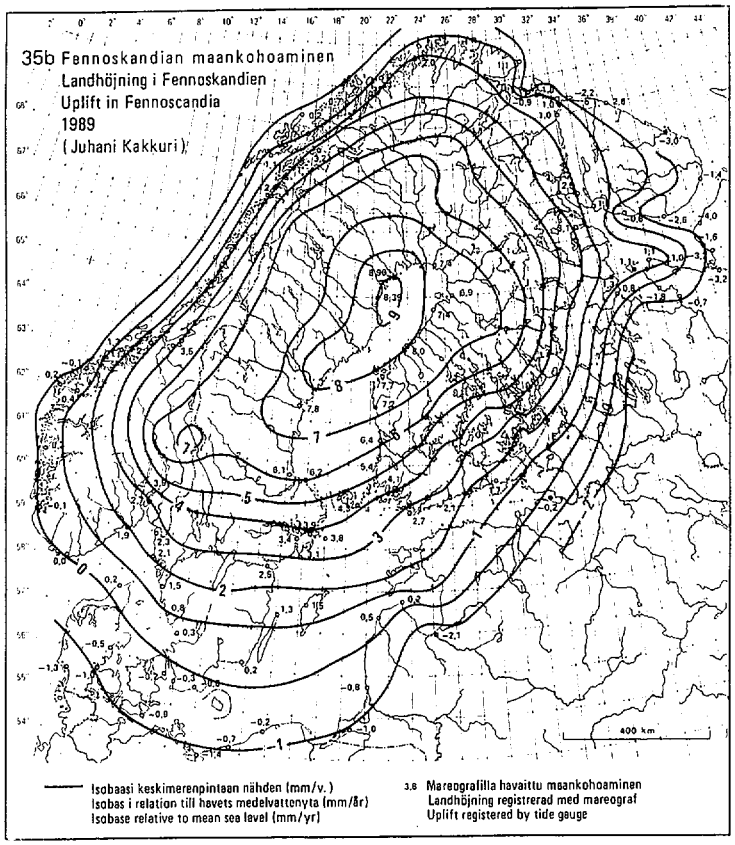

Figure 3-8. Land uplift in Fennoscandia (Alalammi, 1992).

3.3.2 Salinity

The initial and boundary conditions associated with the salt distribution are poorly known. Consequently, the effects of the uncertainties in the salinity field were studied by applying various salinity models. Three salinity models were used in transient simulations for the initial state for the whole model domain. The salinity models studied are defined in Table 3-5.

Table 3-5. Three salinity models applied in the simulations.

Salinity model	Description
(i)	Constant salinity of 10 g/l
(ii)	Constant salinity of 15 g/l
(iii)	Salinity increases linearly from 10 g/l to 17 g/l with depth

The constant-salinity models show the effects of a salt distribution, which is very simple but still justifiable on the basis of the field data. A constant salinity value of 10 g/l (model (i)) is in a good agreement with the experimental salt concentrations in some boreholes (e.g., KAS09, KAS11 and KAS14) although it contradicts the high salt concentrations observed deep in borehole KAS02. On the other hand, because the measured salinity values highly exceeding the constant value occur only at great depths, the simple salinity model can be used to represent salt concentrations at the depths of interest, say, for a depth interval from 0 to 500 m. A constant salinity value of 15 g/l (model (ii)) representing the concentration estimated for the Litorina Sea was used in simulations by Voss and Andersson (1991) and it was also examined in this study. The third salinity model is based on Wikberg et al. (1991), according to which the measured salinity at Äspö increases with depth approximately by 1 g/l per 100 m.

Land uplift is taken into account in the boundary condition for the upper boundary. The salt concentration was defined so that on the upper boundary of the model, a value of 0 g/l was used for the area that at each time step represents the water table at Äspö. The area enlarges as a function of time according to the rate of the uplift of the water table (Figure 3-7). The influence of land uplift on the boundary conditions of the concentration on the upper boundary is presented in Figure 3-9. Because the salt concentration in the Baltic Sea has changed since the Litorina Sea, the salinity value for the area representing the bottom of the Baltic Sea changed linearly as a function of time from the initial value to the final value of 7 g/l at the end of the simulation. In the salinity models (i) and (iii) (Table 3-5), the initial value at the surface was 10 g/l and in the model (ii) 15 g/l. In the steady state simulations, a value of 7 g/l was used for the sea bottom.

In transient simulations, the salt concentration on the vertical and bottom boundaries was maintained as fixed in the initial state. In the steady-state simulations, the concentration values related to each salinity model were assigned to the vertical boundaries. In the salinity model (iii) the values were assumed to increase linearly with depth from a value at the surface level of 7 g/l to 17 g/l at the bottom of the model. The boundary conditions for model (i) at the end of the simulation (the present time) are presented in Figure 3-10.

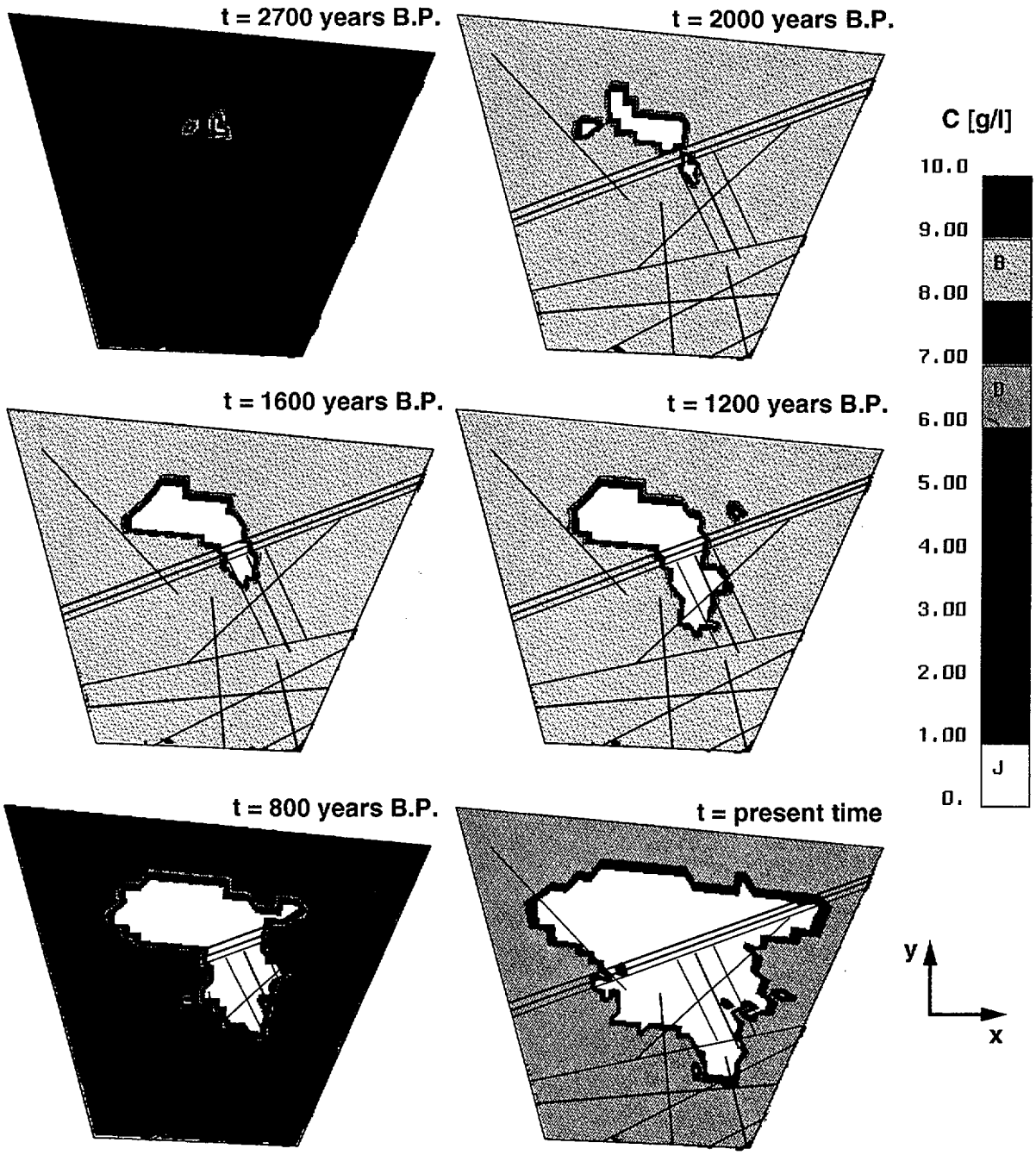

Figure 3-9. The effect of land uplift on the boundary conditions of the salt concentration on the upper model boundary.

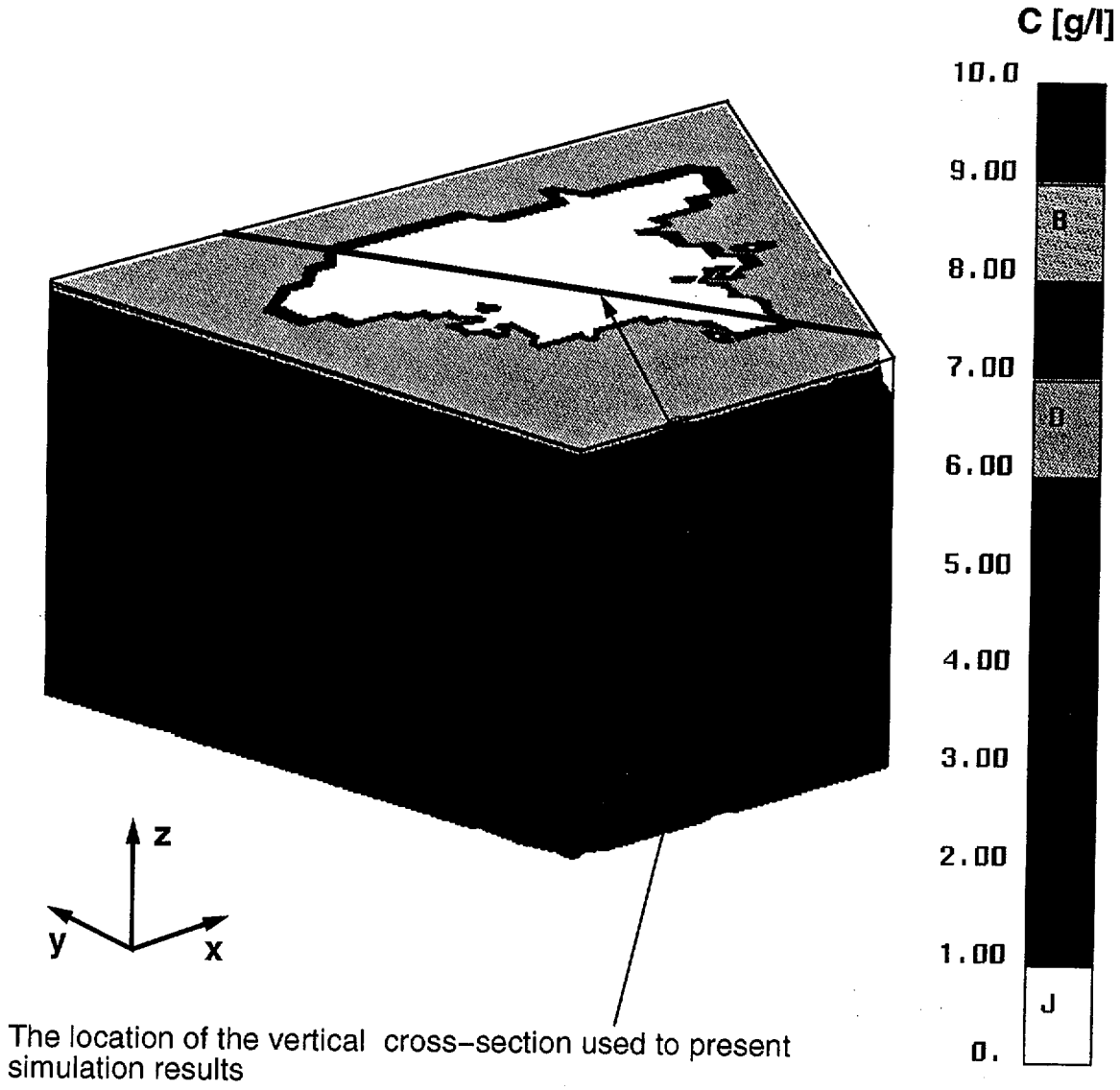

Figure 3-10. *Boundary conditions of the salt concentration for model (i) (constant 10 g/l, see Section 3.3.2 and Table 3-5) at the end of the simulation period (the present time).*

4 RESULTS AND DISCUSSION

Several steady-state and transient coupled simulations were performed for groundwater flow and salt transport at the Äspö site. The two conceptual models were applied to represent salt transport in the bedrock: the equivalent-continuum (EC) model (see Section 2.2) and the dual-porosity (DP) model (see Section 2.3). The simulations with the EC approximation were performed with one set of the properties of the bedrock whereas three values of the matrix porosity and four values of the matrix thickness were used with the DP approach (see Section 3.1.2 and Tables 3-2 - 3-4). Three different salinity models (see Section 3.3.2 and Table 3-5) were employed.

The simulation cases with the EC model consist of

- transient simulations with the salinity models (i), (ii) and (iii),
- transient simulation with the salinity model (i) and stochastic hydraulic conductivities, and
- steady-state simulation with the salinity model (i).

The simulations performed applying the DP model comprise

- transient simulation with a matrix block porosity of 10^{-2}, the matrix block thickness of 40 m and the salinity models (i), (ii) and (iii) (three cases),
- transient simulation with the salinity model (i), a matrix block thickness of 40 m and a matrix block porosity of 10^{-2}, $5 \cdot 10^{-3}$ and 10^{-3} (three cases), and
- transient simulation with the salinity model (i), a matrix block porosity of 10^{-2} and a matrix block thickness of 10, 20, 40 and 80 m (four cases).

In all the simulations the flow equation (2-1) and the transport equation (2-2) or (2-17) were taken as coupled. The results were compared to each other and against the experimental data along the cored boreholes. Several contour plots on the simulations results were produced, too.

4.1 PRESSURE

Experimental data

Rhén and Forsmark (1993) summarized the experimental data on the hydraulic pressure under the natural, hydraulically undisturbed flow conditions. The summary is based on the measurements performed in cored boreholes KAS01–KAS08 in 1990 and KAS09–KAS14 in 1991 (Figure 4-1).

The pressure was monitored in five or six packed-off sections in each of the observation boreholes except in four sections in KAS08 and in one section in both KAS01 and KAS10. Rhén and Forsmark (1993) report the minimum, maximum and average values over the measurement period for each packed-off section. The average values are also shown in all the figures where the simulation results are plotted along the cored boreholes, for example in Figures 4-2 and 4-3. Differences between the minimum and maximum values are typically 6000–8000 Pa, while the two highest differences, 22000 and 28000 Pa, are associated with KAS03.

Rhén and Forsmark (1993) state that the measured values of the pressure for KAS09–KAS14 are somewhat uncertain, mainly because at the southern part at Äspö the flow conditions were disturbed during the last six months in 1991. They estimate "the total error in groundwater level under hydraulically undisturbed conditions" in terms of the pressure to be ±1500–12000 Pa for the packed-off sections.

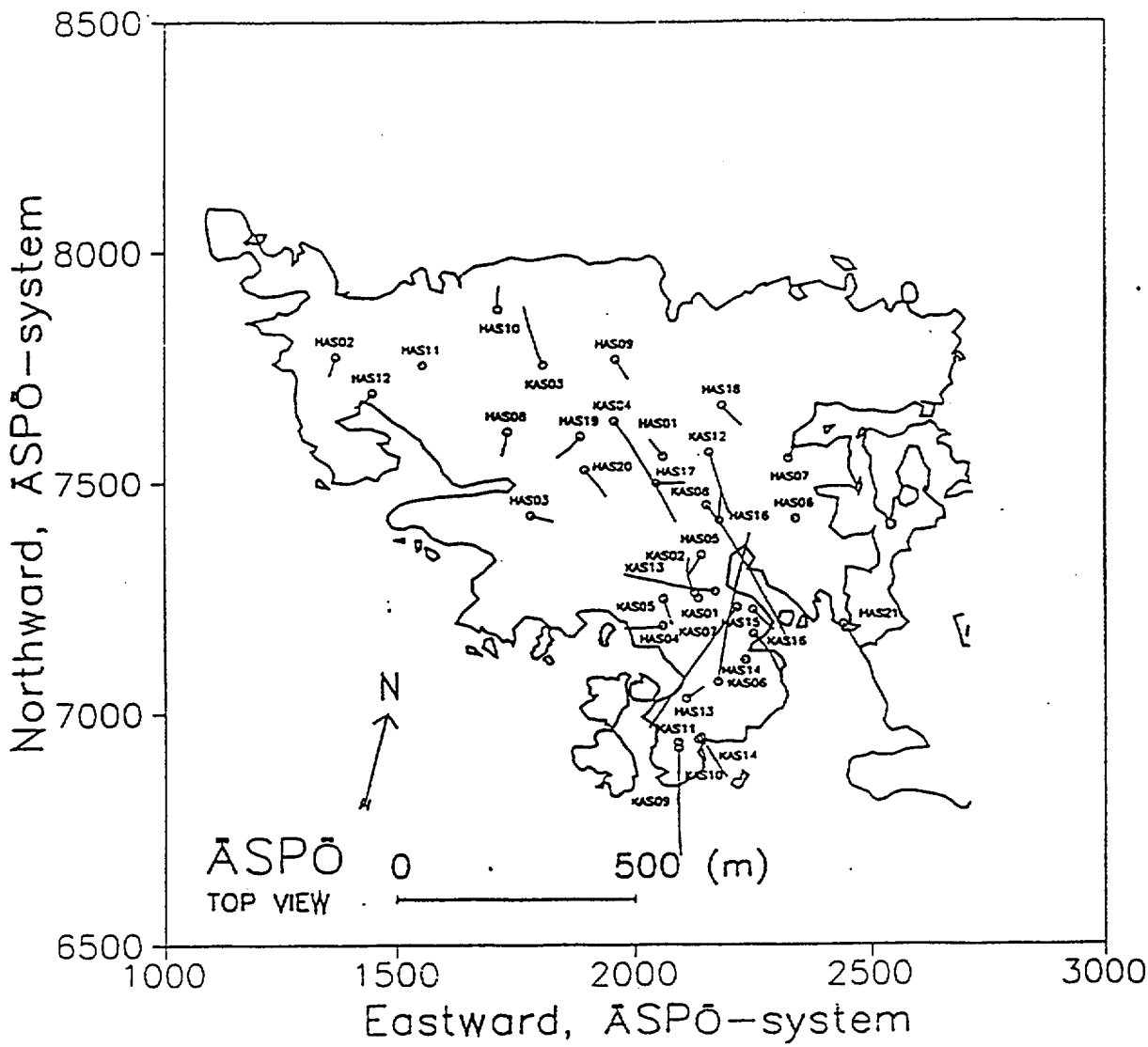

Figure 4-1. The location of the boreholes at Äspö (Forsmark, 1992).

Simulated pressure

The numerical simulations were thus carried out with three different initial and boundary conditions which were set according to the salinity models (i), (ii) and (iii) (see Section 3.3.2 and Table 3-5). The salinity models define the initial and boundary conditions for the pressure. The properties of the bedrock related closely to the pressure field such as hydraulic conductivities and transmissivities were not varied, except in one case in which stochastically distributed hydraulic conductivities and transmissivities were used.

The pressure simulated for the different salinity models applying the EC approach for transport together with the measured values along the cored boreholes is presented in Figure 4-2. The pressure field computed with the salinity models (i) (constant 10 g/l) and (iii) (linear 10-17 g/l) were almost the same up to a depth of 500 m in all boreholes. In both cases the simulation results compare successfully with the experimental values. Only in KAS03 below a depth of 600 m, in KAS05 below a depth of 450 m, in KAS12 and KAS14, the computed pressure was not close to the field data. The pressure simulated with the salinity model (ii) (constant 15 g/l) is clearly worse than those simulated with model (i) and (iii) in all boreholes, except in KAS12 and KAS14.

The simulations carried out with the salinity model (i) by varying the parameters relating to transport indicated that only the initial conditions (i.e. the salinity model) and the uplift of the water table have some influence on the pressure field. This can be seen in Appendix A, which shows the pressure fields computed with different salinity models (with the EC and DP models, with stochastic distributed hydraulic conductivities and for a steady state). The differences between the salinity fields (e.g., between those produced with the EC and DP models) were not large enough to cause any meaningful differences between the corresponding pressure fields.

The influence of land uplift on the pressure field is shown in Figure 4-3, in which the pressure computed for the salinity model (i) is presented at five different time steps. The earliest time presented is 600 years after the start of the simulation, i.e. 2400 years B.P. (before the present). That time step approximately corresponds to the initial state for all boreholes, except for KAS03 and KAS04 located in the highest part at Äspö. As time goes on, the pressure caused by land uplift increases. In KAS06, KAS09, KAS10, KAS11 and KAS14, the pressure does not change because those boreholes are located in the lowest part at Äspö, where the water table has not even today risen enough to cause any additional pressure.

In the simulations, the uplift rate of the water table was assumed to be 1 mm/year being about half of the rate of land uplift. Because only the present value of the rate was available, it was employed all through the simulations. In fact, the rate of land uplift has not been constant during the time that covered the simulations, but it has decreased slowly with time.

However, the water table was assumed to rise linearly from zero to the present day value.

The contours of the pressure for the transient simulation and for the salinity model (i) are presented in Figure 4-4.

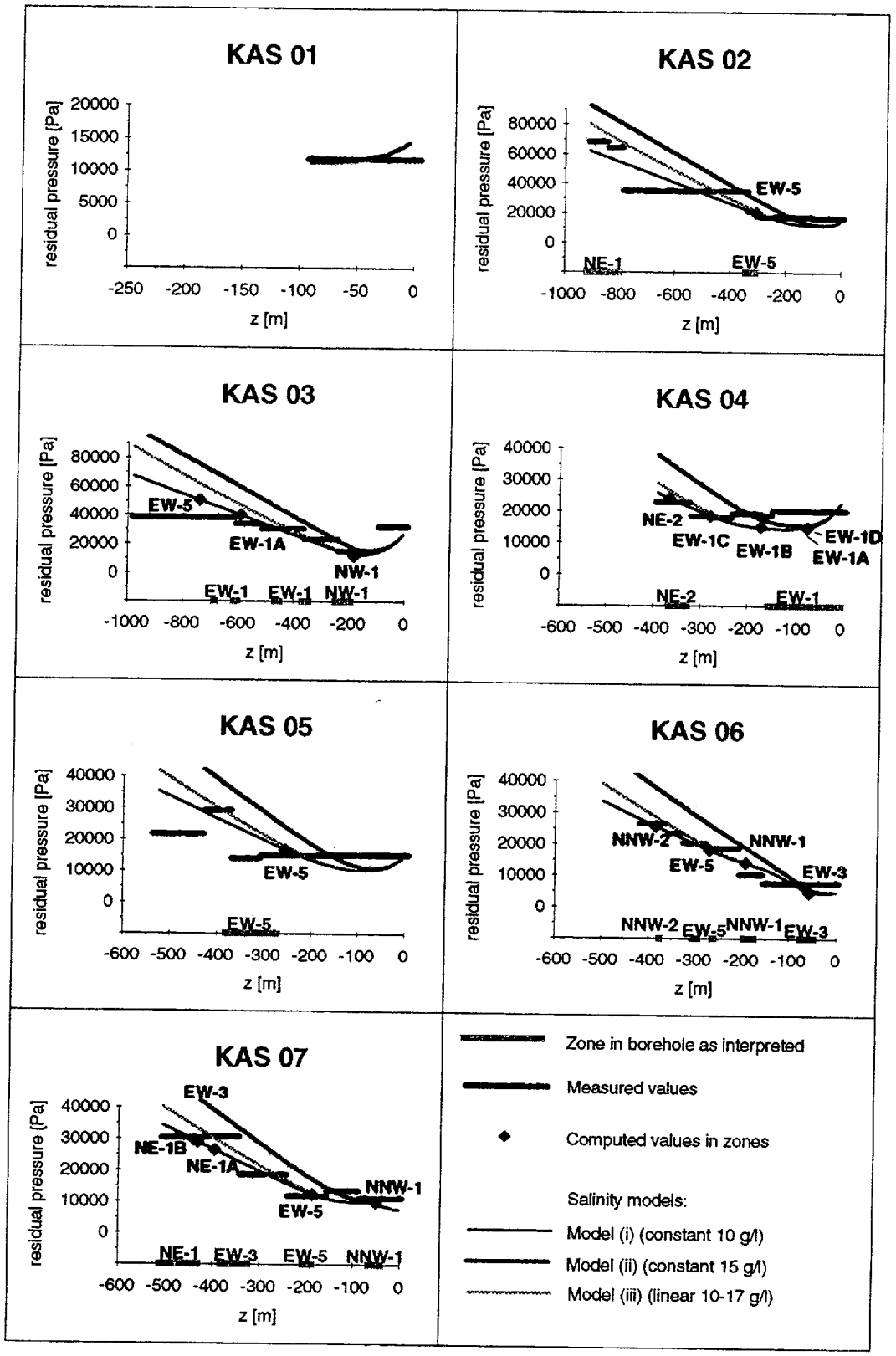

Figure 4-2. *Simulated and measured pressure along the cored boreholes as a function of depth. The transient simulations with three different salinity models (see Section 3.3.2 and Table 3-5). The simulation of salt transport performed with the equivalent-continuum approach. The experimental data from Rhén and Forsmark (1993).*

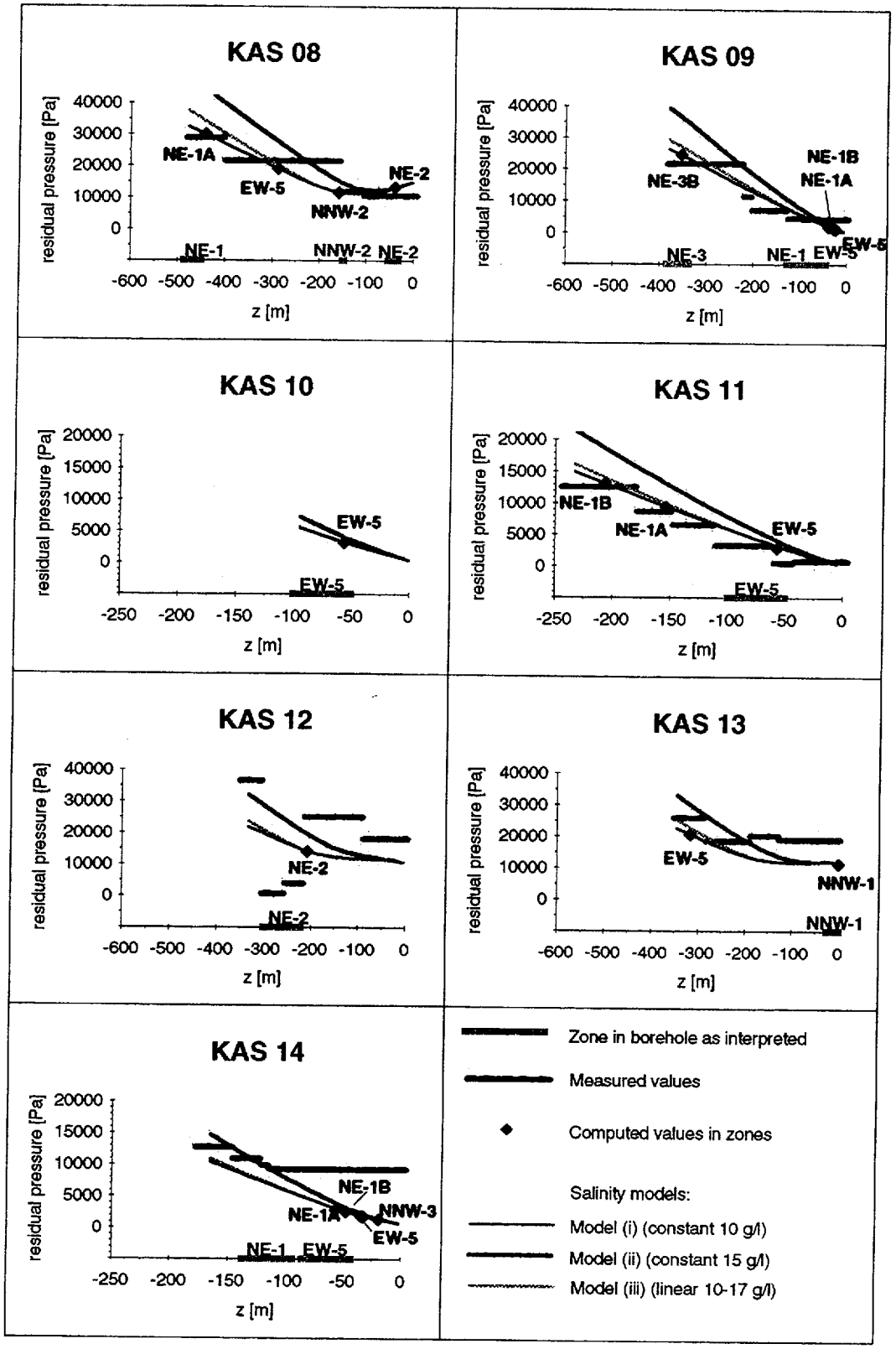

Figure 4-2. (Continued.)

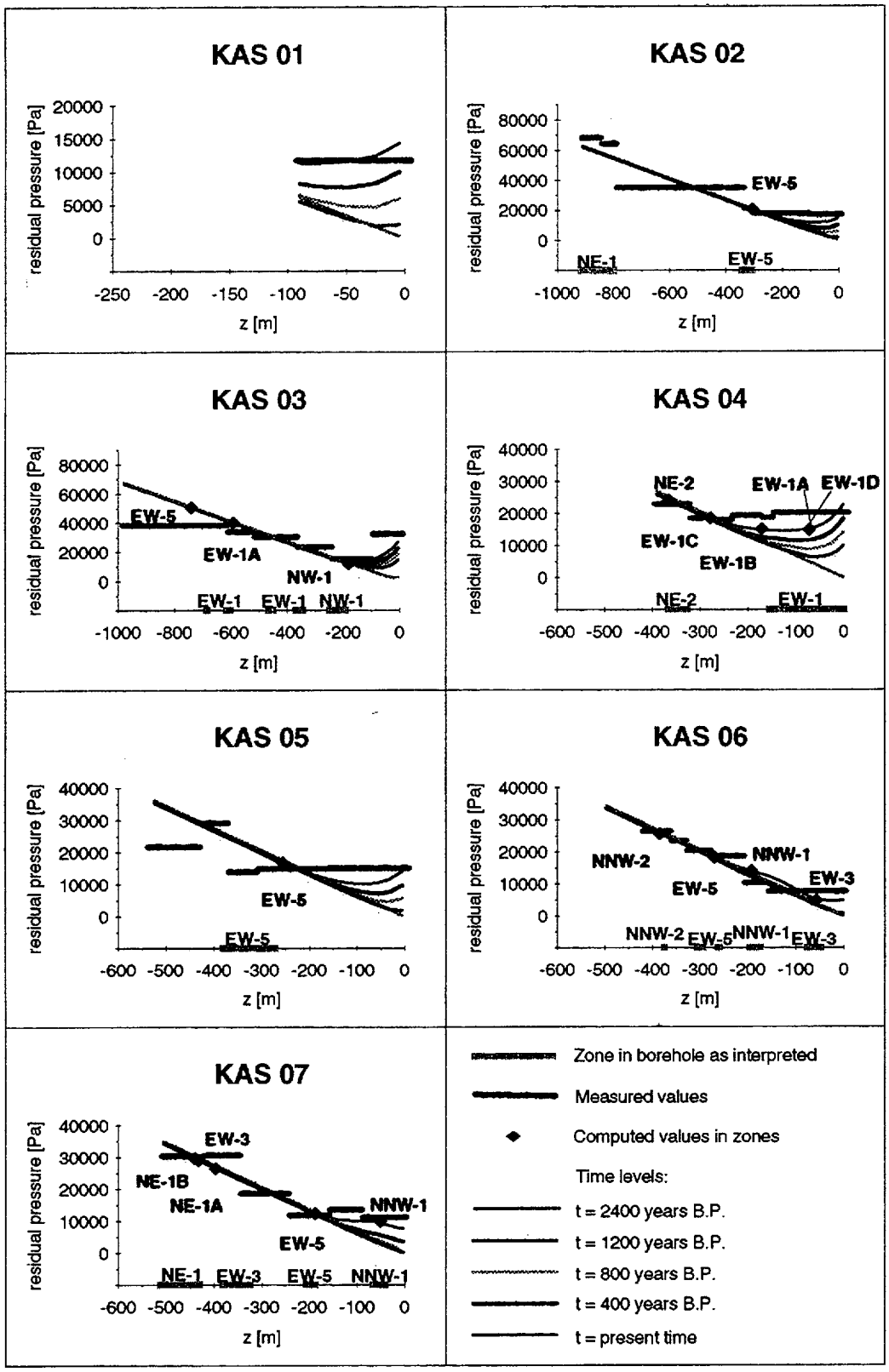

Figure 4-3. *Simulated and measured pressure along the cored boreholes as a function of depth at five different time steps. The simulation of transport performed with the equivalent-continuum approach and the salinity model (i) (constant 10 g/l, see Section 3.3.2 and Table 3-5). The experimental data from Rhén and Forsmark (1993).*

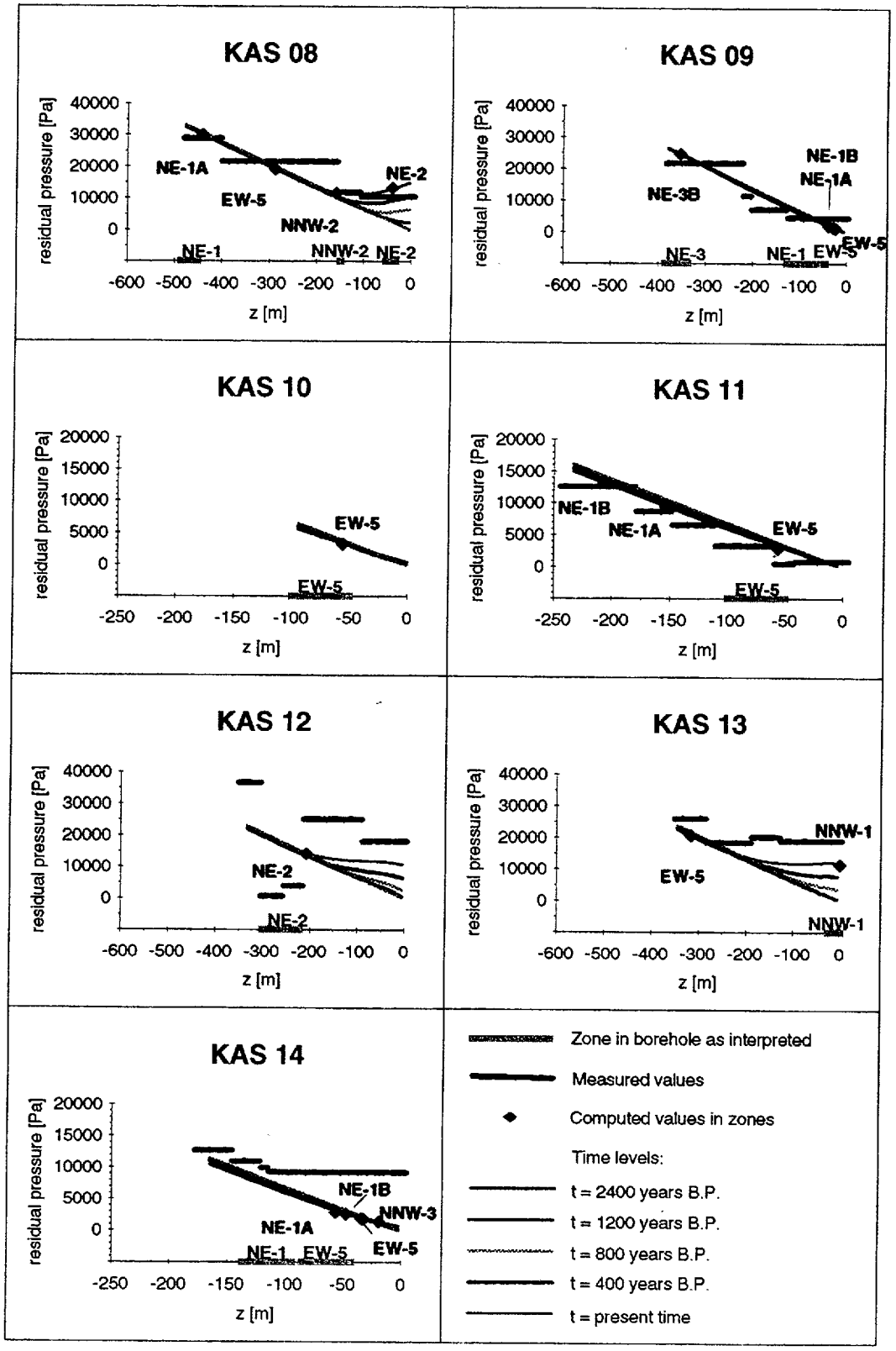

Figure 4-3. (Continued.)

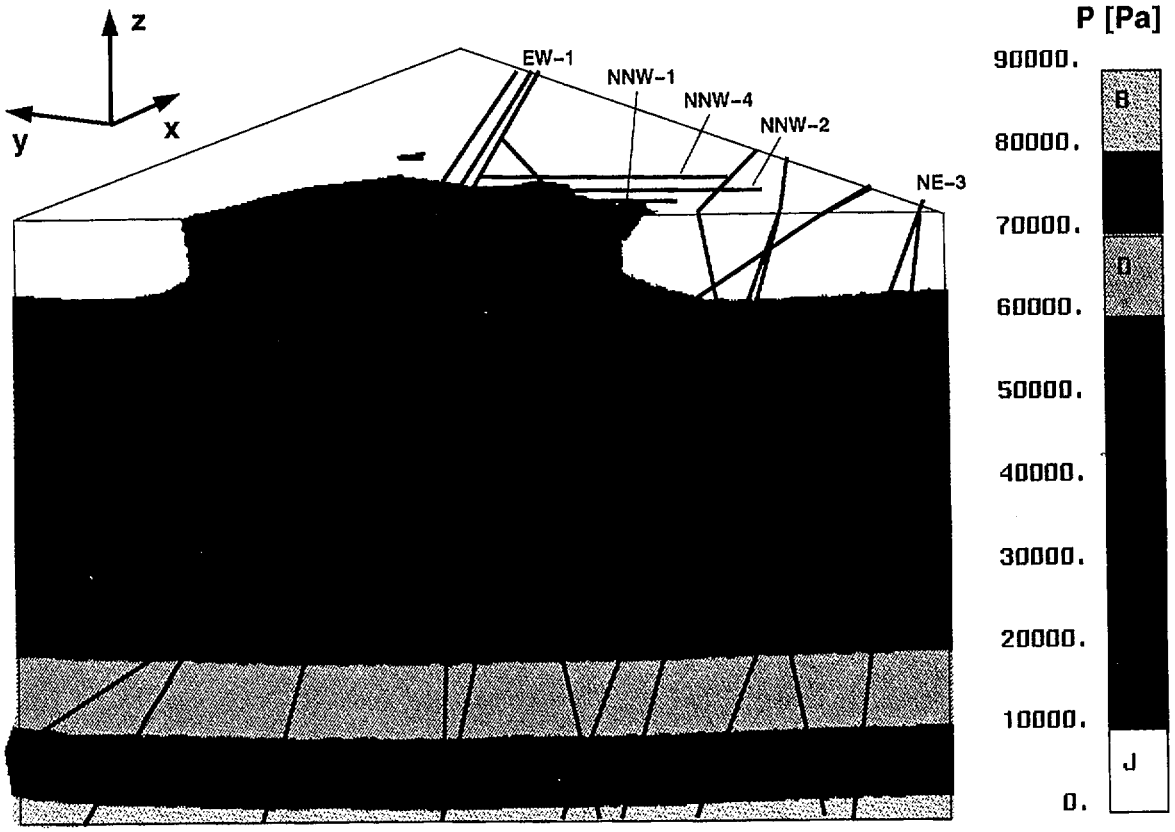

Figure 4-4. *Contours of the simulated pressure along a cross-section shown in Figure 3-10 for a transient simulation with the salinity model (i) (constant 10 g/l, see Section 3.3.2 and Table 3-5).*

4.2 SALINITY

Experimental data

The field data on the salt concentration of the groundwater at Äspö are based on the measured electric conductivity. Water samples were taken in 1988 from the packed-off sections of the boreholes (Figure 4-1) except boreholes KAS01 and KAS10, which were studied later (Rhén and Forsmark, 1993). A number of samples with the electric conductivity ranging from 60 to 3400 mS/m was analyzed and a linear dependence of the salt concentration on the electric conductivity was obtained by means of the least square fit. The salt concentration determined from the measured electric conductivity is included in all the figures where the simulation results are presented along the cored boreholes, for example in Figures 4-5 and 4-6.

Rhén and Forsmark (1993) do not directly address the uncertainty of the correlation between the measured electric conductivity and the salt concentration. However, they introduce linear fits for the dependence of the water density on both the temperature and electric conductivity. According to them, a single measurement differs from that straight correlation line no more than 1.5 kg/m^3 and usually less than 0.5 kg/m^3. They proceed that, taking into account the possibility of a water sample not being representative for the water in a packed-off section, the maximum error in the density is ±10 kg/m^3. Reliability of the field data varies. If the total uncertainty in the measured density is converted to the uncertainty in the salt concentration, the experimental error may be remarkable for an individual concentration value.

The experimental data for the salinity represent mainly the values in the water-bearing part of the system. Therefore, when employing the DP model, primarily the results for the water-bearing fracture domain can be compared with the field data. The salt concentration in the matrix blocks with stagnant water should not be compared to the salinity measured in water samples because they usually represent flowing water. The matrix concentrations should be compared the salt contents measured in stagnant water.

Effect of the initial and boundary conditions

The simulations were performed with three different initial and boundary conditions, i.e. salinity models (see Section 3.3.2 and Table 3-5). The simulated salinity for the different salinity models as well as the experimental salt concentrations along the cored boreholes are presented in Figure 4-5 (the EC model) and Figure 4-6 (the DP model).

The simplest salinity model (i) (constant 10 g/l) clearly gives the results which have the best over-all agreement with the experimental data in the cored boreholes. The results computed both with the EC and DP models agree well with measured values. Only at a depth interval of 800-900 m in

agree well with measured values. Only at a depth interval of 800-900 m in KAS02, at a depth up to 400 m in KAS05 and at a depth up to 150 m in KAS08, the computed salinity differs remarkably from the field data.

The salinity model (ii) (constant 15 g/l) is clearly not a good choice in the light of the field data. This salinity model overestimates the concentration field in all boreholes and it coincides with the measured values only deep in KAS02.

The salinity model (iii) (linear 10-17 g/l) was included in the study in order to combine the good results given by the salinity model (i) and still to reach the high salinity values measured deep in KAS02. The high salinity values deep in KAS02 was reached and the results compared well with the field data up to a depth of 200 m as in the case of the model salinity (i). However, below a depth of 200 m the model (iii) clearly overestimates the salt concentration.

Because of the best agreement with the experimental data, the salinity model (i) was selected as a "base salinity model" with which most of the simulations with varying parameter values were performed. Furthermore, all the contours for the salt concentration presented in the following figures are for the salinity model (i). Figure 3-10 shows the contours of the salinity on the boundaries of the finite element mesh for the time step representing the present time. The location of the vertical cross-section used in the other contour plots has been marked in the figure.

Effect of the conceptual model

The salt concentration along the cored boreholes (Figures 4-5 and 4-7 and Appendix B) at the intersections with the fracture zones and the contours of the salt concentration (Figure 4-9) indicate that the fractures zones do not have much influence on the salinity field when applying the EC model. The reason is that the EC model can not take into account the retardation effects caused by matrix diffusion. One reason could be also the dispersion lengths which are too large for many areas. They are at least the source of the wide interface of the saline and fresh water zones. Because of the low hydraulic conductivity, dispersion is a major transport mechanism in the intact rock, while convection is the main mechanism in the fracture zones.

On the other hand, the fracture zones can readily be identified in the simulation results (Figures 4-6 and 4-8 and Appendices C, D, E, F, G and H) that were computed with the DP model. The salt concentration is smaller at the intersections of the boreholes and the fracture zones than in the intact rock. Especially in KAS04 the influence of the matrix diffusion is very clear.

The matrix diffusion effects mainly the results in the intact rock. The salinity in the fracture zones is approximately the same regardless of the parameter values and conceptual model applied. This can be seen from the concentration plotted along the boreholes (Appendices C and D) and the

salinity contours (Figures 4-9 and 4-10). In the intact rock the difference of the salinity fields computed with the EC and the DP model is obvious as seen from the results for the boreholes. The interface between the fresh and saline water systems is also closer to the surface when applying the DP model than for the EC model as the plots in Figures 4-9 and 4-10 show. Generally the effect of retardation caused by the matrix diffusion can be seen in all boreholes (except in KAS10 and KAS14) up a depth of 300 m when using the DP model (Figures 4-6 and 4-8 and Appendices C, D and E).

For the EC model the salt concentration along the boreholes at all time steps is approximately the same below a depth of 400 m (Figures 4-5, 4-7 and 4-9 and Appendix B). Furthermore, when using the DP model the concentration in the boreholes below a depth of 300 m is insensitive to the values of the matrix porosity and matrix block thickness (Appendices C and D). Below a depth of 300 m (the DP model) or 400 m (the EC model), the flow produced by pressure differences is already too small to cause any significant convective transport of solute particles.

Although the DP representation is a more realistic way to model a fractured medium than the EC approach, the situation is not that simple when comparing the simulated values to the measured values in the boreholes. As mentioned above, matrix diffusion has a significant effect on the results simulated with the DP model. However, when the EC model is used and matrix diffusion is ignored, in some boreholes, the agreement of the simulation results with the field data is even better than of those computed with the DP model. For example, in KAS03, KAS04, KAS05, KAS06, KAS07, KAS12 and KAS13, with the parameters applied in the simulations the EC model gives results which compare better with the measured values (Appendices C and D). Moreover, the general behavior of the experimental values along the boreholes resembles more the results predicted by the EC model than those of the DP model. On the other hand, in KAS02, KAS09, KAS11 and KAS14, the salinity field computed with DP model is closer to the field data than the EC results.

When evaluating the performance of the two modelling approaches, we must take into account that the simulation results depend on the values of the parameters related to the conceptual model applied. Some of the properties do not have much influence on the results, while some of them do. Considering the DP model, the most important properties are the matrix block properties, the porosity and thickness. Those input parameters have the largest influence on the results as can be seen in Appendices C and D. The larger the matrix porosity or the smaller the matrix block thickness is, the larger the retardation effect of matrix diffusion in the fracture system is. The problem is how to choose the values of these input parameters. In this study, the matrix block thicknesses of 10-80 m and the porosities of 10^{-3}-10^{-2} were used. The simulation case with a matrix block porosity of 10^{-2} and a matrix block thickness of 40 m was selected as a base case for the simulations with DP model and all the contours of the salt concentration presented in the figures are for the base case.

Compatible with the experimental data in some boreholes, the results computed with the DP model also indicate that the matrix blocks (even close to the surface) still contain water of almost as a high salt concentration as 3000 years ago (Appendix E). The salinity field in the matrix blocks, however, depends on the input parameters. The salt concentration in Figure 4-11 and Appendices E and F shows that the salt content increases with distance from a water-bearing fracture being the largest at the center of a block. The salinity field in the matrix blocks depends on the size of the block. The larger the blocks are, the larger the difference of the salt concentrations in the center of the block and the fracture system is. The difference in the salt concentrations computed with a block thickness of 10 m is already quite small (Appendix F). Appendix G shows the effect of the matrix blocks thickness on the salt concentration in the center of the block. The larger the matrix blocks are, the larger the concentrations in the matrix blocks are. On the other hand, the influence of the matrix block porosity on the salinity field in the matrix blocks is small (Appendix H) whereas the effect is obvious in the water-bearing fractures (Appendix C).

Transient behavior

Land uplift causes the rise of the water table and the enlargement of the area at the Äspö island. The pressure gradient due to the water table of the island makes the fresh water flow into the groundwater system. The higher the water table is, the larger the pressure gradient is and the deeper the fresh water flows pushing the saline water deeper, too. The flow depends on the hydraulic conductivity. Since the hydraulic conductivity is much larger in the fracture zones than in the intact rock, the fresh water flows faster in the fracture zones. This behavior can clearly be identified in Figure 4-10, in which the contours of the salt concentration computed with the DP model are presented at four different time steps. Figure 4-8 shows the corresponding values along the cored boreholes.

The results of the steady-state and transient simulations with the EC model for the present time are nearly identical (Figure 4-9 and Appendix B). A transient simulation with the EC model was also performed with the stochastically determined hydraulic conductivities and transmissivities of the finite elements. The results do not differ much from those for deterministic hydraulic properties as can be recognized by comparing Figure 4-9 and Appendix B.

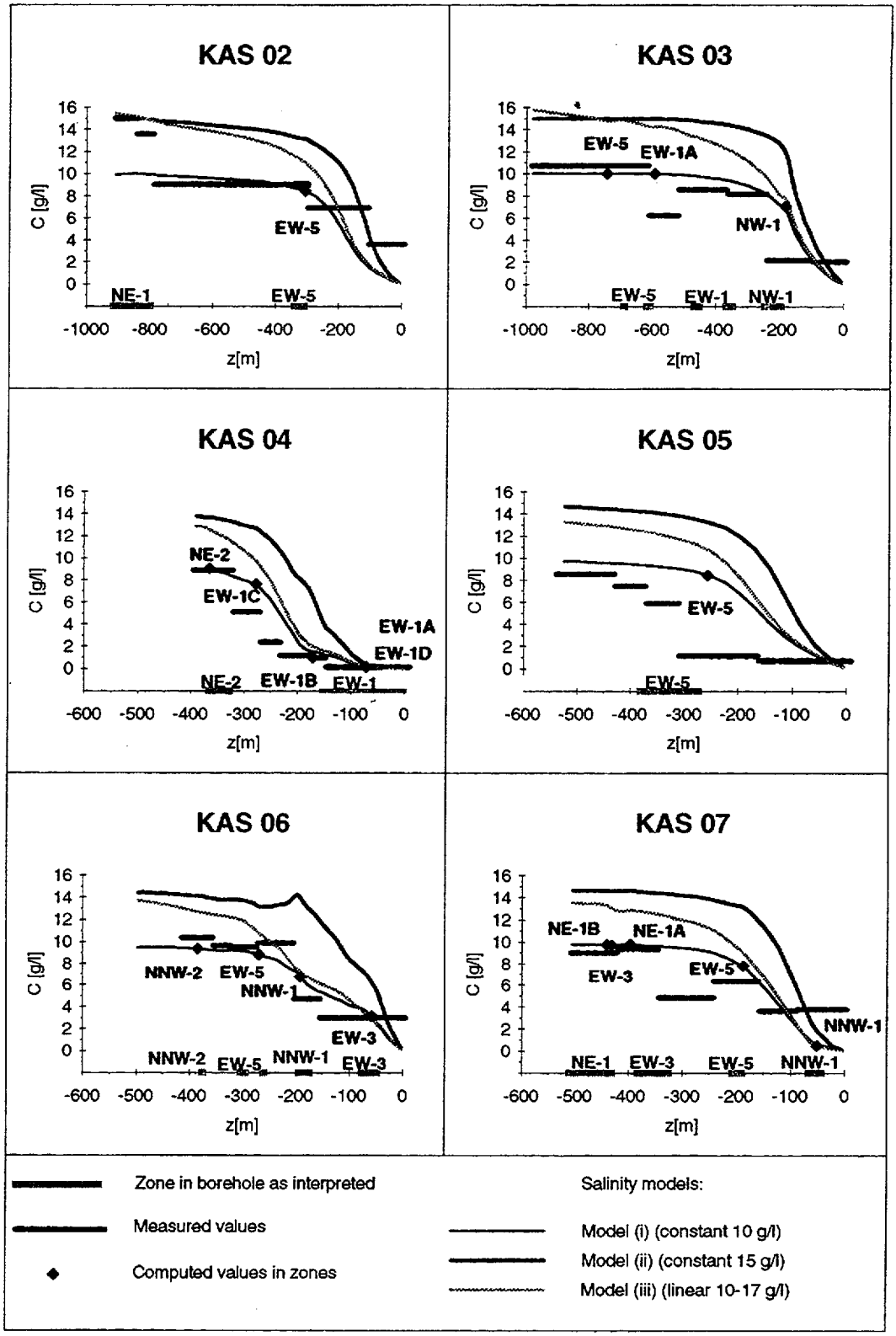

Figure 4-5. Simulated and measured salt concentration along the cored boreholes as a function of depth. The simulations were performed as transient with the equivalent-continuum model and the three different salinity models (see Section 3.3.2 and Table 3-5). The experimental data from Rhén and Forsmark (1993).

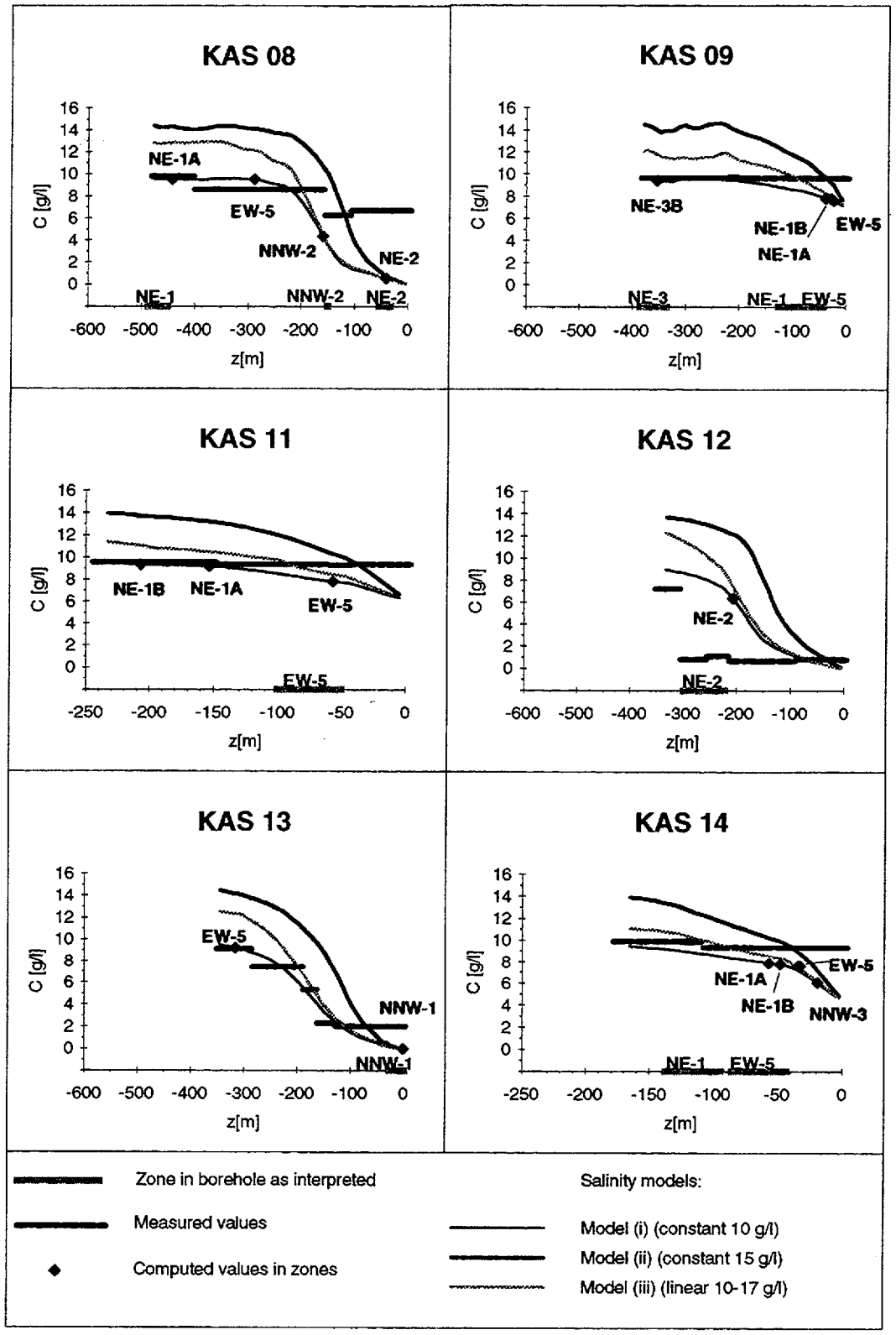

Figure 4-5. (Continued.)

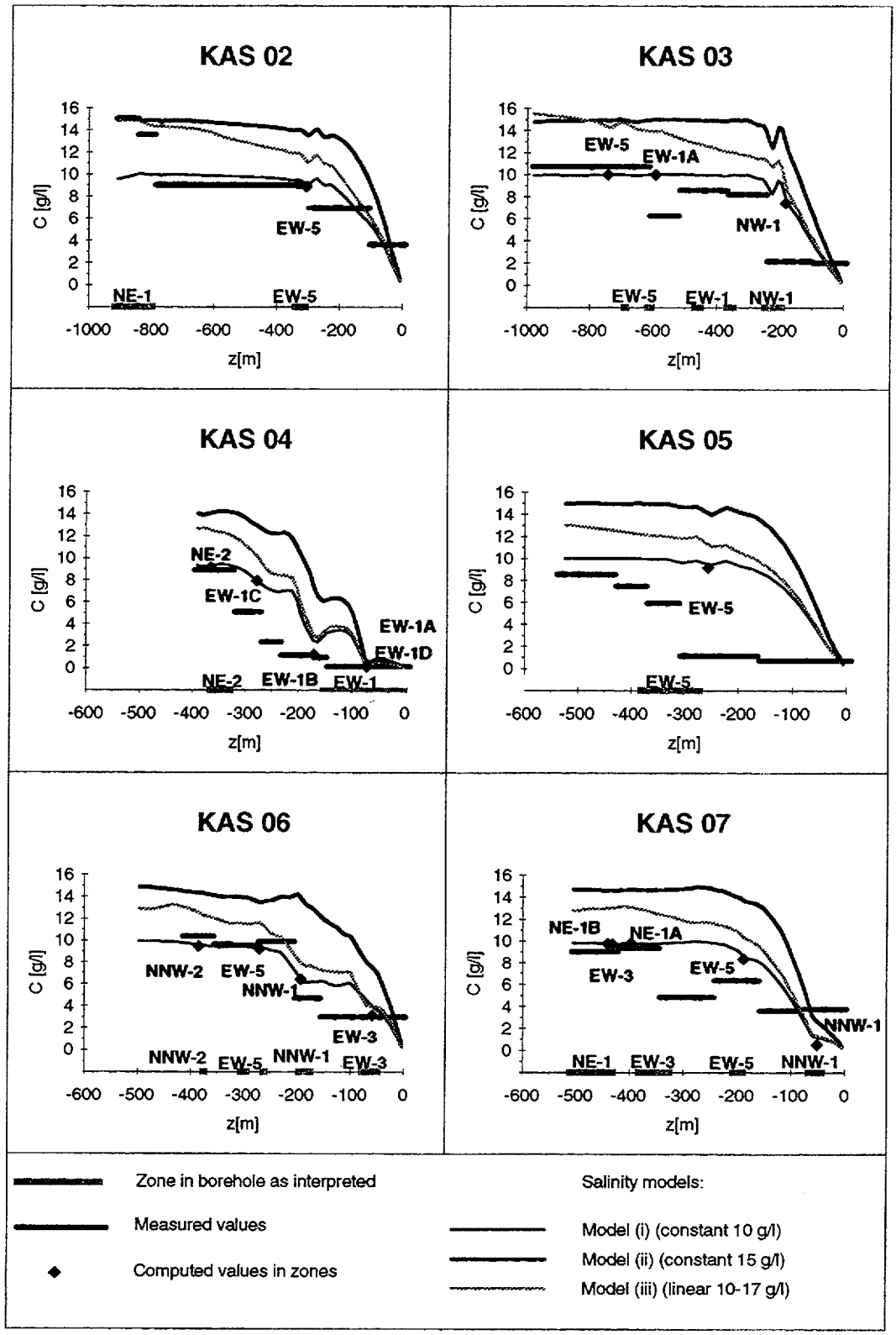

***Figure 4-6**. Simulated and measured salt concentration along the cored boreholes as a function of depth. The simulations were performed as transient with the dual-porosity model, the three different salinity models (see Section 3.3.2 and Table 3-5), a matrix porosity of 0.01 and a thickness of 40 m. The experimental data from Rhén and Forsmark (1993).*

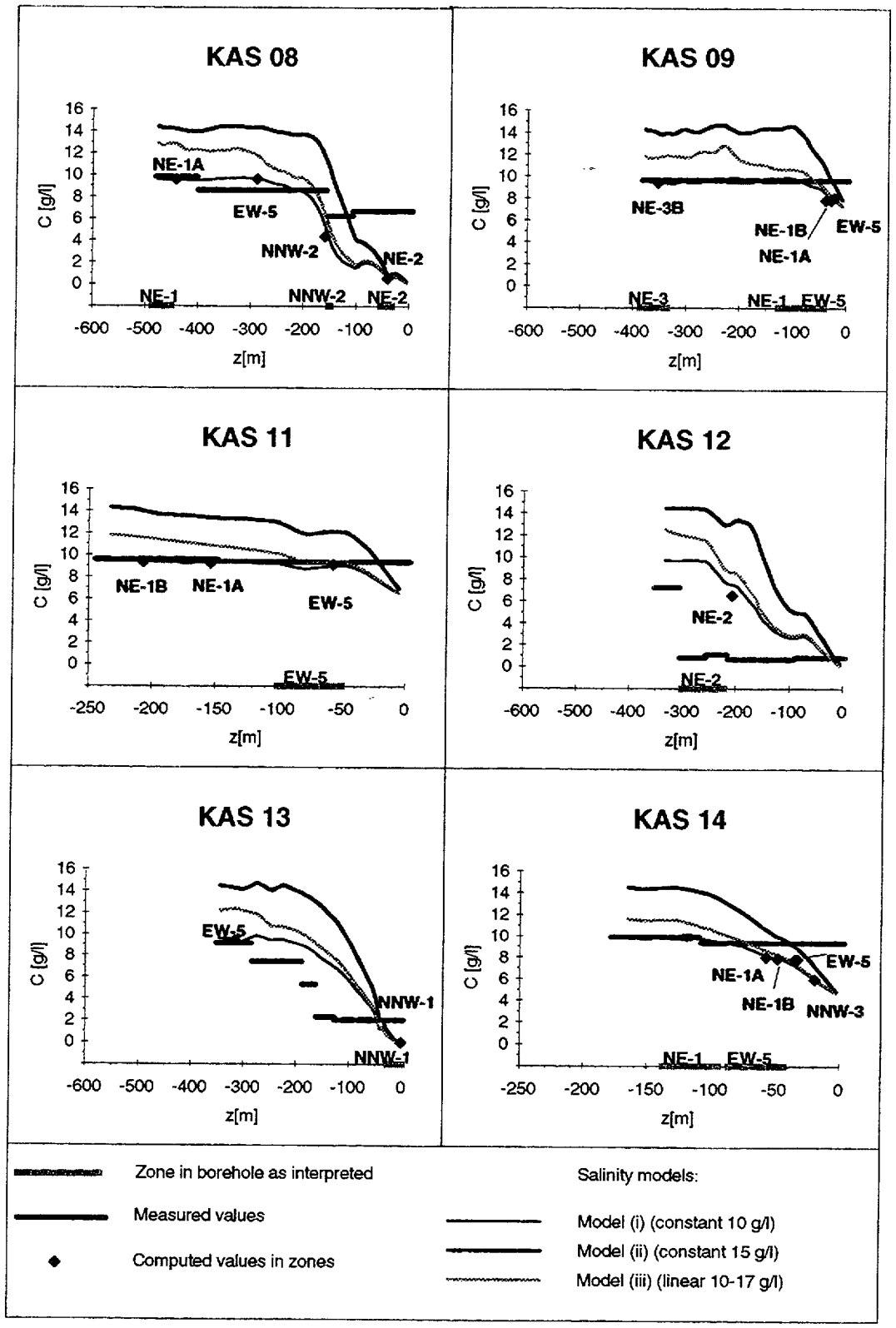

Figure 4-6. (Continued.)

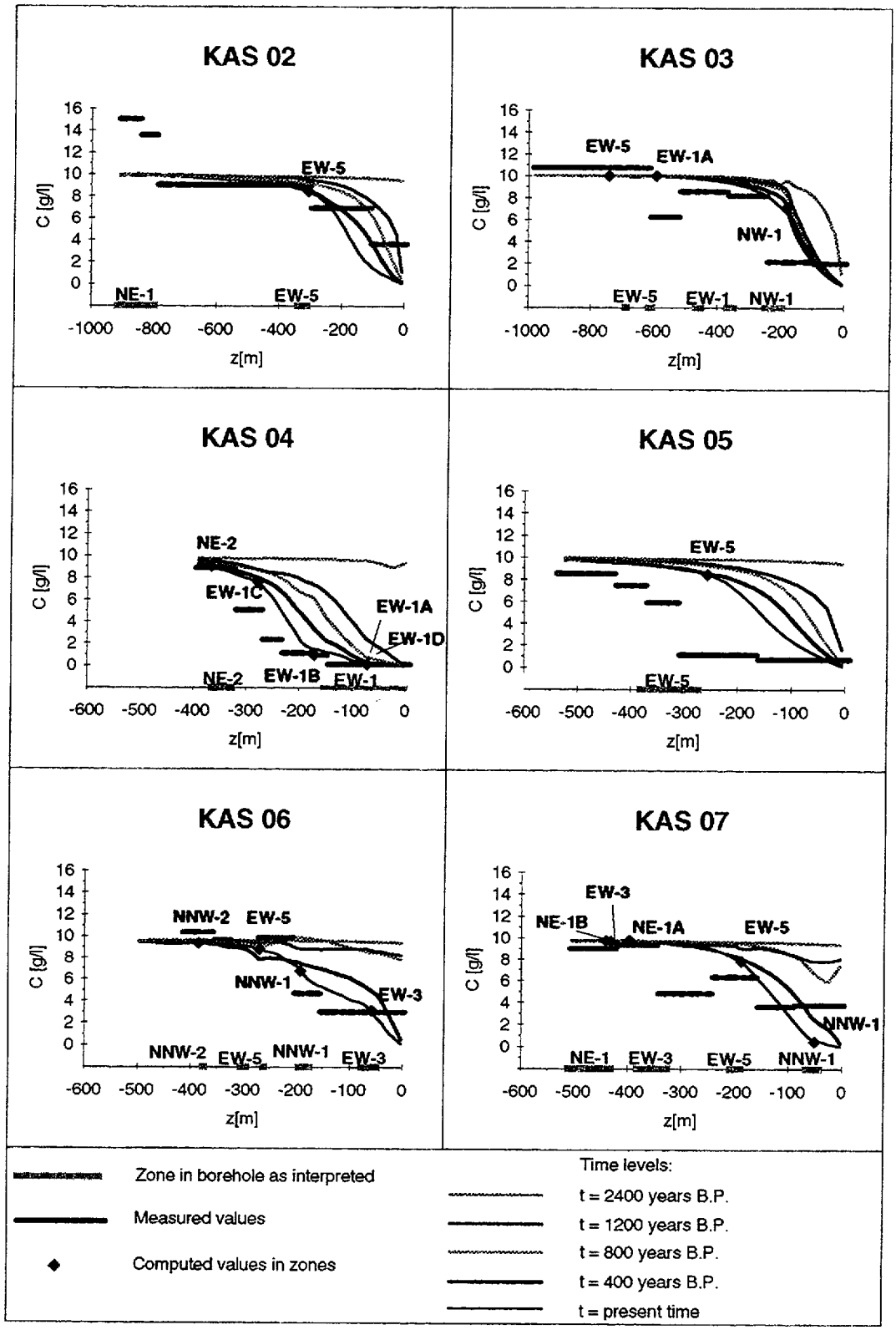

Figure 4-7. *Simulated and measured salt concentration along the cored boreholes as a function of depth at five different time steps. The simulation was performed with the equivalent-continuum model and the salinity model (i) (constant 10 g/l, see Section 3.3.2 and Table 3-5). The experimental data from Rhén and Forsmark (1993).*

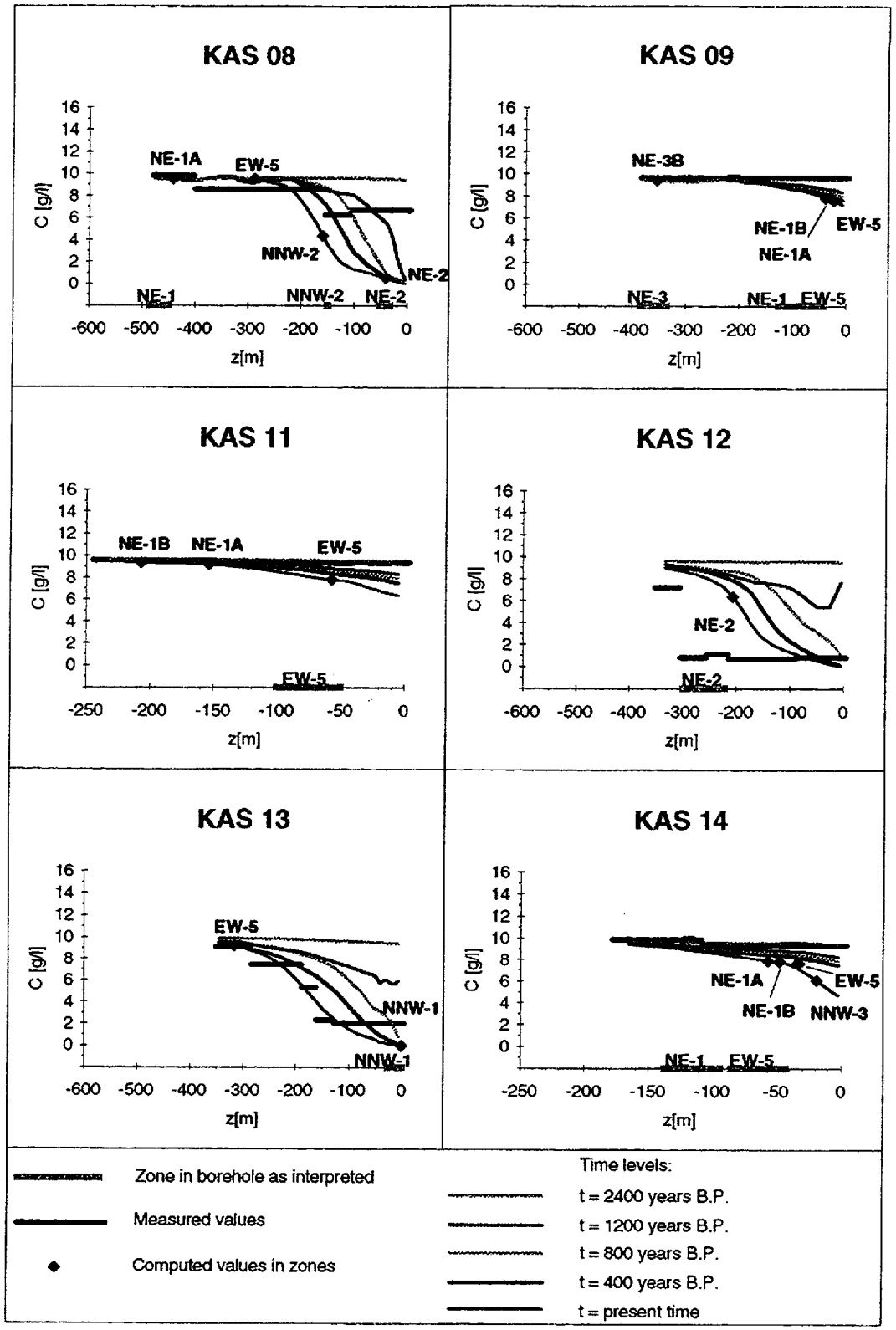

Figure 4-7. (Continued.)

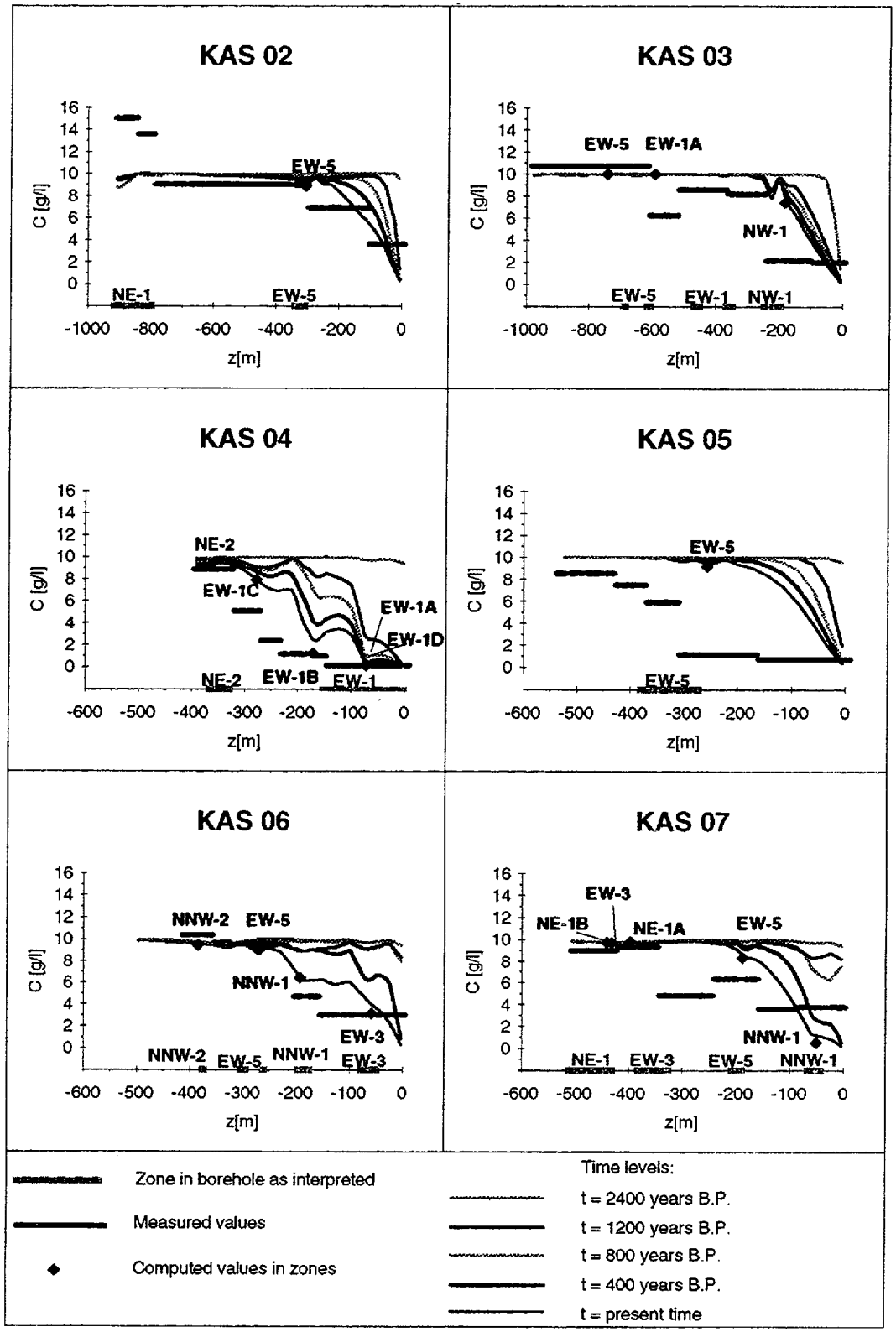

Figure 4-8. *Simulated and measured salt concentration along the cored boreholes as a function of depth at five different time steps. The simulation performed with the dual-porosity model, the salinity model (i) (constant 10 g/l, see Section 3.3.2 and Table 3-5), a matrix porosity of 0.01 and a thickness of 40 m. The experimental data from Rhén and Forsmark (1993). Compare with Figure 4-10.*

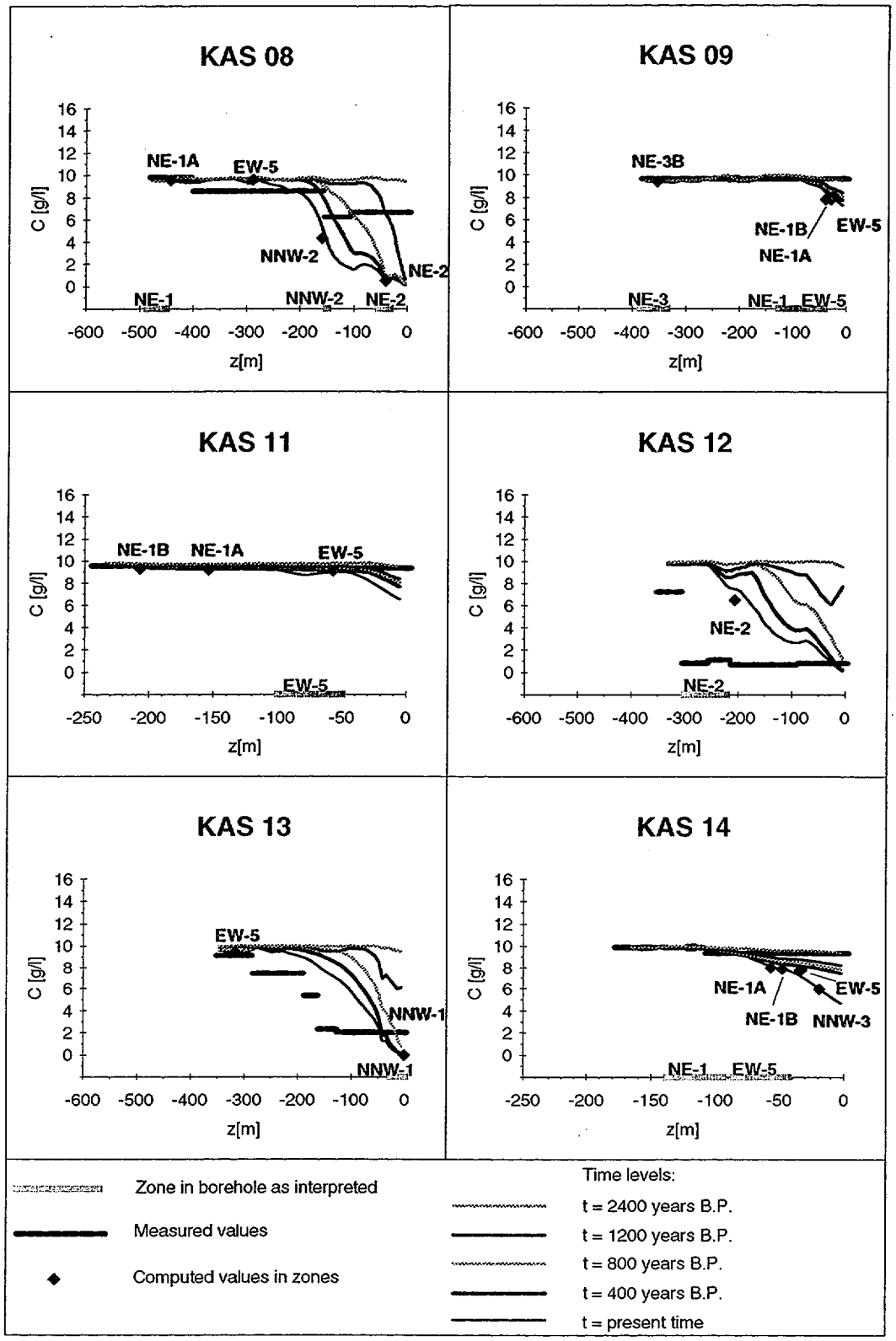

Figure 4-8. (Continued.)

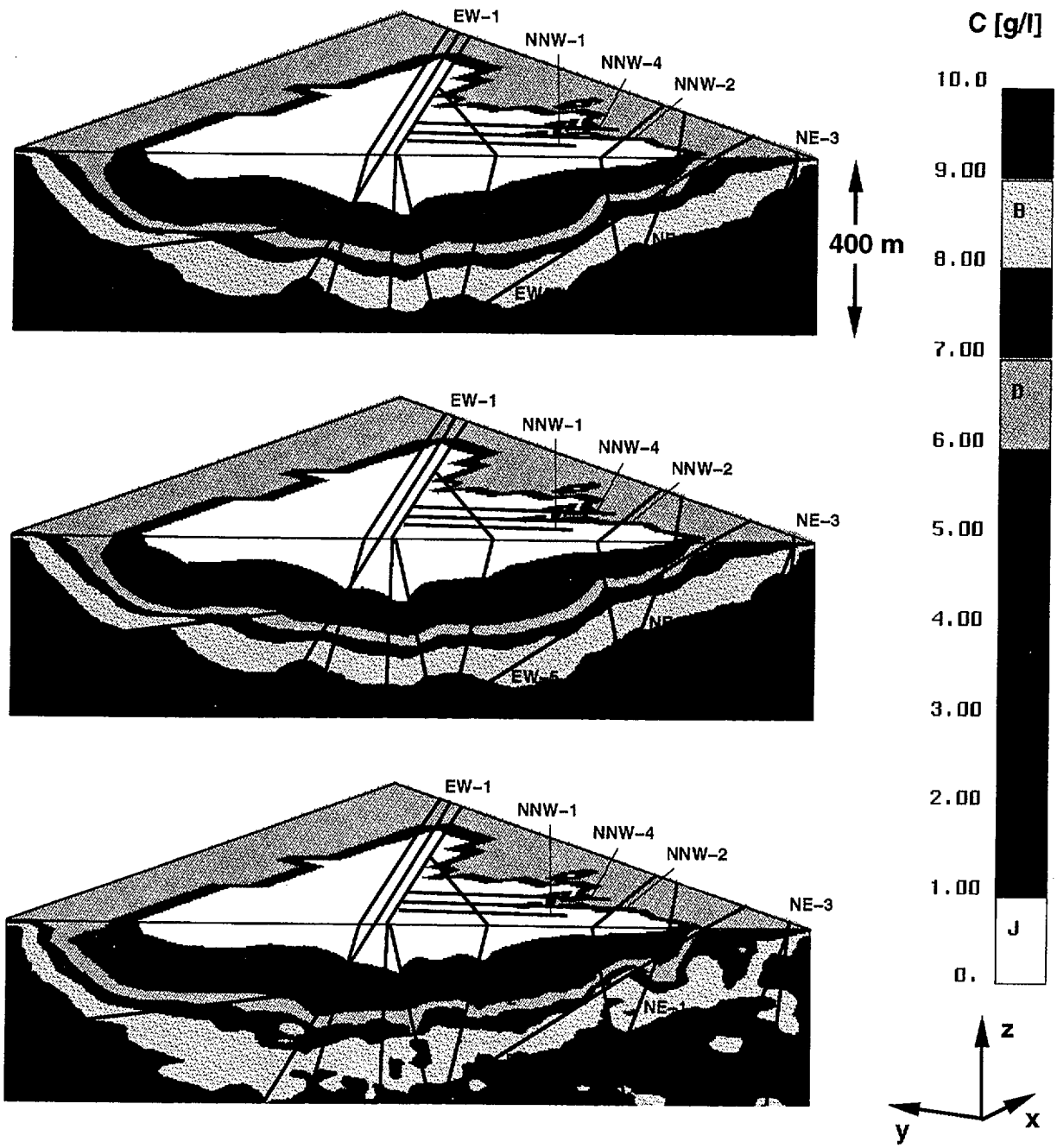

Figure 4-9. Contours of the simulated salt concentration along a cross-section shown in Figure 3-10 with the salinity model (i) (constant 10 g/l, see Section 3.3.2 and Table 3-5). Results for the steady-state and transient simulations with deterministic hydraulic conductivities in the top and middle parts, respectively. Results for the transient simulation with stochastically determined hydraulic conductivity in the bottom part. The results for the transient simulation computed with the equivalent-continuum model and plotted for the time step representing the present time.

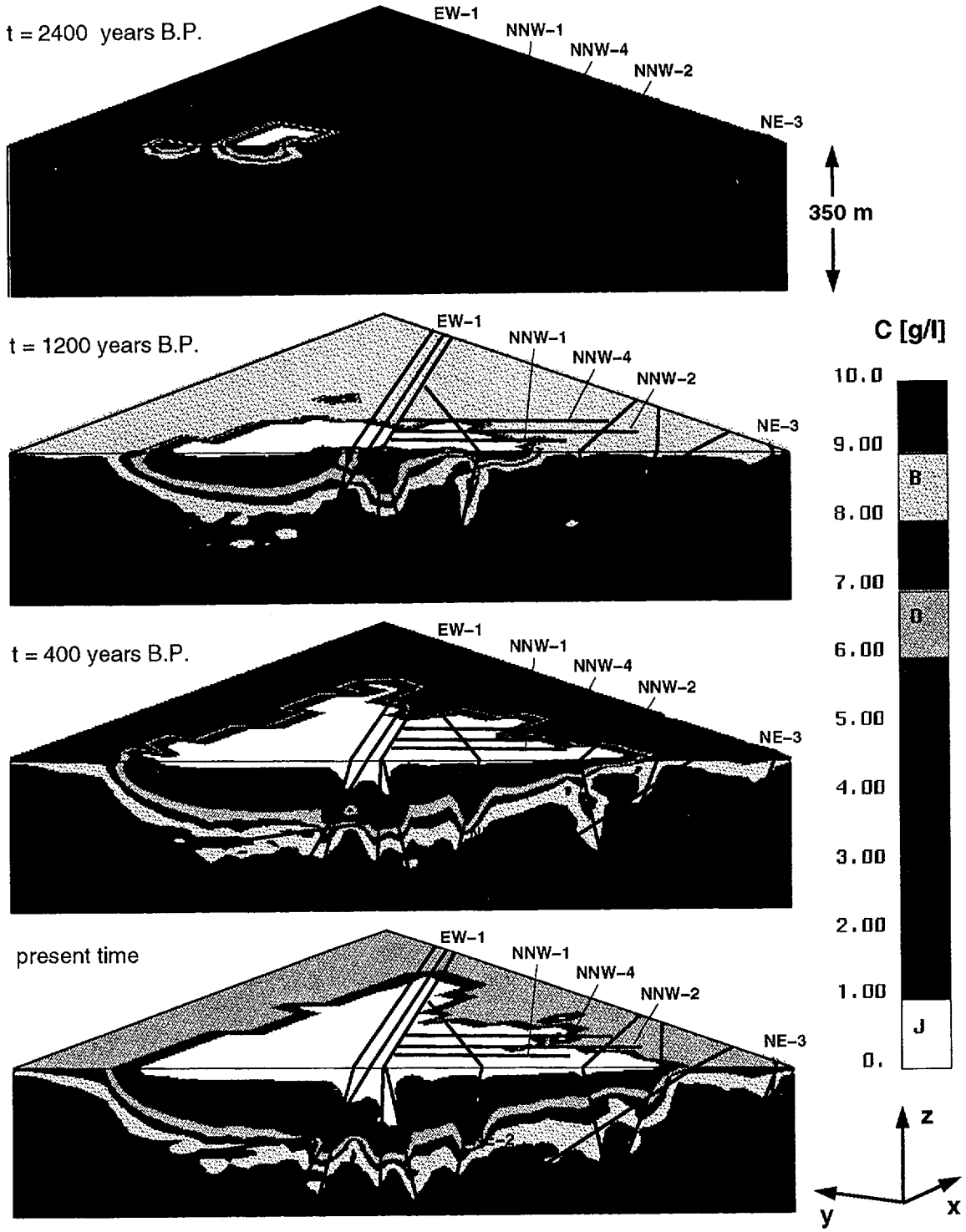

Figure 4-10. Contours of the simulated salt concentration along a cross-section shown in Figure 3-10 with the salinity model (i) (constant 10 g/l, see Section 3.3.2 and Table 3-5). The simulation was carried out as transient with the dual-porosity model and a matrix porosity of 0.01 and a thickness of 40 m. The results are plotted for four different time steps. Compare with Figure 4-8.

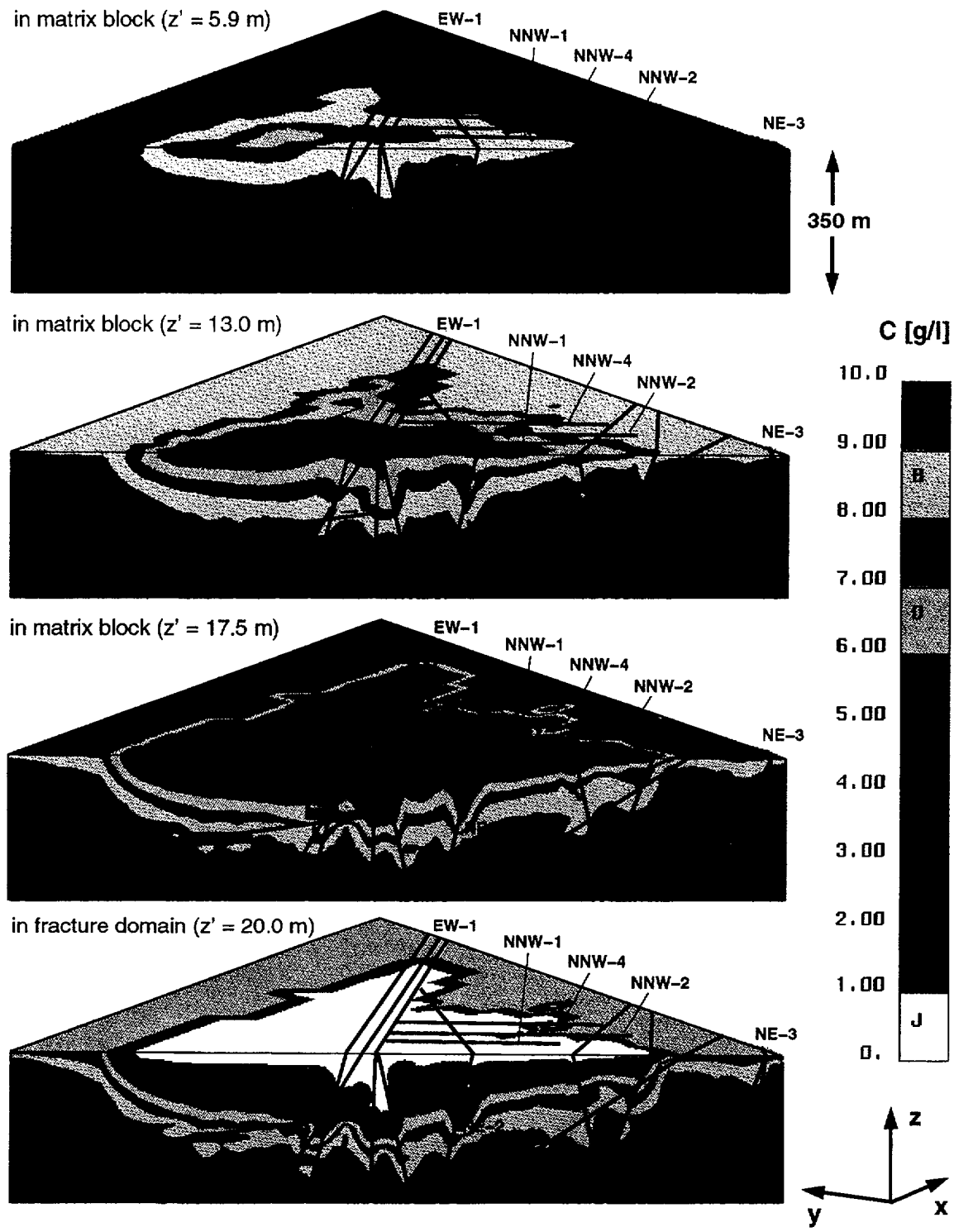

Figure 4-11. Contours of the simulated salt concentration along a cross-section shown in Figure 3-10 with the salinity model (i) (constant 10 g/l, see Section 3.3.2 and Table 3-5). The simulation was carried out as transient with the dual-porosity model and a matrix porosity of 0.01 and a thickness of 40 m. The results are plotted in different distances from the center of a matrix block to a water-bearing fracture for the present time. Compare with the figure presented in Appendix G.

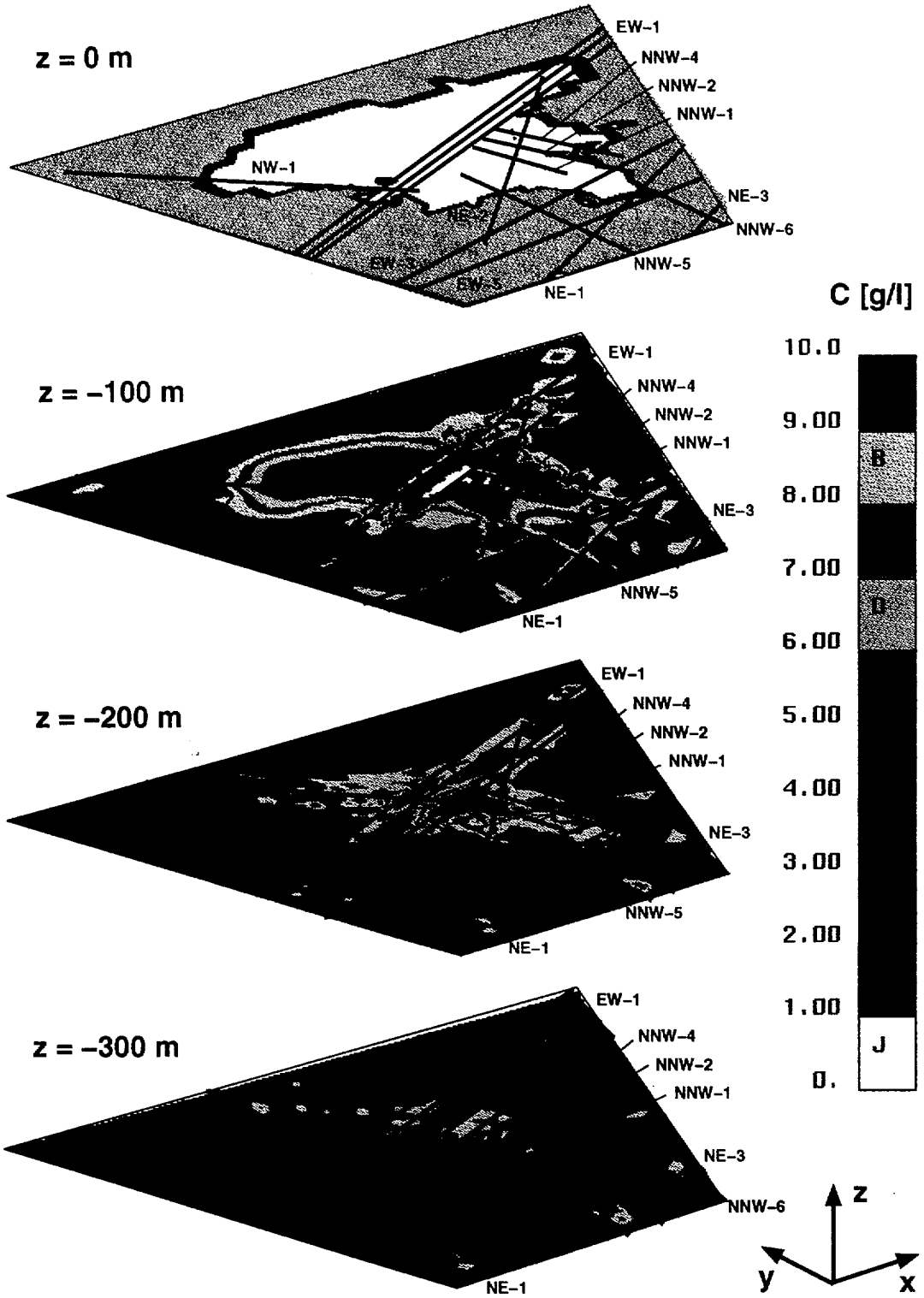

Figure 4-12. Contours of the simulated salt concentration along horizontal cross-sections with the salinity model (i) (constant 10 g/l, see Section 3.3.2 and Table 3-5). The simulation was carried out as transient with the dual-porosity model and a matrix porosity of 0.01 and a thickness of 40 m. The results are plotted at different depths for the present time.

5 CONCLUSIONS

The primary objective of this study was to examine whether the geochemical field data from the Äspö site can be interpreted and understood by means of numerical simulations for flow and transport. The coupled system of groundwater flow and salt transport was analyzed with a computer model. The simulation model is based on the results of the field investigations. The computational results were evaluated against the field data. Experimental values for the pressure and salt concentration are available for almost all of the cored boreholes. Computer simulations were performed for various conceptual models, boundary conditions and properties of the bedrock. Both steady-state and transient analyses were carried out. In the transient simulations, land uplift was taken into account. The influence of the rock blocks with stagnant water on salt transport with flowing water, as well as on the salt distribution in the matrix blocks, was also considered.

Modelling approach

In order to simulate the flow of water with a varying salt concentration realistically, coupled modelling of flow and salt transport is required. The mathematical model consists of two coupled and non-linear partial differential equations written for the pressure and solute concentration.

The highest hills at the Äspö island rose above sea level 3000 years ago. During the last 3000 years, the effect of diffusion on salt transport cannot be assumed to have yet reached a steady state. Because of salt diffusion from blocks with stagnant water and the transient flow field caused by land uplift, transient simulations were used in order to explain the sharp spatial variations of the experimental salinity values.

Solute transport is obviously faster with flowing water, e.g., in water-bearing fractures, than in rock blocks with stagnant water, e.g., in the matrix. A realistic simulation of transport calls for taking into account both the water-bearing and non-bearing subsystems of the bedrock. Conventional methods for transport simulations, e.g., the equivalent-continuum (EC) approximation, cannot consider the features discussed above. Therefore, the dual-porosity (DP) representation was employed in this study. In the DP concept, a rock mass is assumed to consist of two subsystems: the fractures with moving water and the matrix blocks with stagnant water. The DP model is a more realistic and more complex approach than the EC model. It improves our flexibility in representing the real bedrock but, on the other hand, increases the number of input parameters. Experimental data for the additional parameters are rarely available.

Implementation and verification of the dual-porosity model

The efficient DP algorithm developed by Huyakorn et al. (1983) for solute transport in a fractured medium was implemented in the FEFLOW code. The DP approach for transport is applied as coupled with flow simulations. The water in the matrix is assumed to be stagnant and to have no influence on flow. The matrix blocks applied in this study were prismatic rectangulars with parallel fractures (Figure 2-2). It would also have been possible simulate transport in a blocky-fracture system via a spherical approximation of the matrix blocks. The effects of retardation and tortuosity on solute transport in the matrix blocks were assumed to be negligible.

The algorithm implemented was verified with two cases. The first test problem considers a one-dimensional transport situation with an analytical solution (Figures 2-7 and 2-8). As no verification cases for the coupled system of flow and transport are available in the literature, a two-dimensional problem was developed in the second test case. The results computed with the DP algorithm were compared with those of the method used by Grisak and Pickens (1980). They applied the standard finite element method with the EC model to simulate mass transport in a DP medium. The third dimension represents the rock matrix. The results of the two approaches compare well with each other (Figures 2-12 and 2-13).

Salinity models for Äspö

In the coupled simulations of flow and salt transport for the Äspö site, three different and quite simple sets of initial and boundary conditions, i.e. salinity models, were employed (see Section 3.3.2 and Table 3-5). Comparing the computational results of the different models against the experimental data along the cored boreholes shows that the simplest salinity model (in which the whole modelling domain was initially assumed to be saturated with water with a constant salinity of 10 g/l) was clearly the best for both the pressure (Figure 4-2) and the concentration (Figures 4-5 and 4-6).

The simulations for the different salinity models proved that the initial and boundary conditions comprise a major source of uncertainty in the simulations. They clearly have a large impact on the simulation results. The simulations carried out by varying the input parameters relating to transport indicated that only the initial state (i.e. the salinity model) and the uplifting of the water table have any influence on the final pressure field. Because the elevation of the water table is known, the main factor which affects the pressure field and can be varied in the simulations is the salt distribution.

The results of the coupled simulations for flow and salt transport thus depend strongly on the poorly known initial salinity field in the modelling domain. For this study, there was not much information about the initial state of the salinity field below the Äspö island 3000 years ago at the end of the Litorina stage. The high salt concentrations observed deep in the boreholes were assumed to originate from the Litorina stage. The use of a

simple salinity model was based on the fact that Äspö had not yet risen above sea level at the beginning of the simulation period and that the whole solution domain can be assumed to have been saturated with the sea water. The initial and boundary conditions for pressure were also mainly set according to the salinity field, which made the role of the initial salinity field even more important.

Conceptual models

The salt concentrations computed both with the EC and DP models compare equally well with the field data. The difference between the two approaches can be recognized in the salt concentration plotted along the cored boreholes. The salt concentration in the boreholes at the intersections with the fracture zones (Figures 4-5 and 4-7) and the contours of the concentration (Figure 4-9) show that the fracture zones do not seem to have much effect on the salinity field of the EC model. The reason is that the EC approximation cannot take into account the retardation effects caused by the diffusion of salt from the matrix blocks with stagnant water. Another reason could be the large values of the dispersion lengths, which are at least the source of the wide interface between the saline and fresh water systems. On the other hand, the fracture zones can be identified clearly in the results computed with the DP model (Figures 4-6, 4-8 and 4-10).

Salt diffusion from blocks with stagnant water mainly affects the salt distribution in the intact rock. The computed salt concentration in the fracture zones is approximately the same regardless of the input parameter values and conceptual model applied, while in the intact rock the difference between the salinity fields computed with the EC and DP models is obvious (Appendices C and D). The interface between the fresh and salt water systems is also located closer to the surface when using the DP model (Figure 4-10) than with the EC model (4-9).

Although the DP representation is a more realistic approach of modelling transport in a fractured rock mass than the EC approach, the situation is not that simple when comparing the simulated values to the values measured along the boreholes. As mentioned above, diffusion from the matrix significantly affects the results simulated with the DP model. However, when the EC model is applied and salt diffusion from blocks with stagnant water is ignored, the results in some boreholes agree better with the experimental data than those computed with the DP model (Appendices C and D). The general behavior of the values measured in the boreholes is actually more like the behavior of the EC results than that of the DP results.

The computational results are sensitive to some parameters related to the conceptual model employed. Some of the medium properties do not influence the results, while some of them have major impacts on predictions. The DP model contains input parameters relating to the properties of the bedrock, that are rarely available in the field data. The simulations with various parameter values proved that the most important parameters in the

case of the DP model were the matrix block properties, the matrix block porosity and block thickness (Appendices C and D). The problem is how to choose the values of these parameters. Matrix block thicknesses of 10-80 m and matrix porosities of 10^{-3}-10^{-2} were employed in the simulations. The distance between the water-bearing fractures in the bedrock varies and, at some parts at Äspö, is probably just a few meters. The DP model, however, assumes a constant matrix block thickness. The values for the matrix block thickness and porosity could have also been more realistic, i.e. smaller, than the values employed here. DP results which would agree better with the field data would obviously be obtained by varying the salinity models and the input parameters more than was possible in this study, in which the application of the DP model was of preliminary nature. In addition, retardation and tortuosity may affect solute transport (at least with small matrix porosities) but these phenomena were considered insignificant in this study. Varying the input parameters and taking into account the phenomena neglected in this work, for example, would be suitable topics for future studies.

The results computed with the DP approach indicated that the matrix blocks could still contain water of as high a salt concentration as 3000 years ago (Figure 4-11 and Appendix E). The salt distribution in the matrix blocks depends, however, on the input parameters. For example, the larger the matrix blocks are, the larger the difference between the salt concentrations in the center of the matrix blocks and in the fracture domain is (Appendices E, F and G). On the other hand, the effect of the matrix block porosity on the salt distribution in the matrix blocks is small (Appendix H). Unfortunately, the results for the matrix cannot be compared with the field data available, because the experimental results mainly represent the salt concentration in flowing water, i.e. in the water-bearing fractures. Some of the (early) water samples represent water from dead-end paths and they could be compared with the values computed for the matrix.

Despite the scarcity of prior information about the input parameters, the DP representation is a useful approach when examining salt transport in a fractured rock mass. Transport both in the water-bearing and non-bearing subsystems of the rock mass can be simulated, whereas the EC approximation can be applied in simulating transport only in the water-bearing fractures.

ACKNOWLEDGEMENTS

The authors wish to thank their colleague Mr Lasse Koskinen for constructive discussions and comments, which led considerable improvements in the contents of this study. We are also grateful to Dr Seppo Vuori for his critical review.

REFERENCES

Alalammi (ed.), 1992. Atlas of Finland - Geology. National Board of Survey, Geographical Society of Finland, Helsinki.

Bear J, 1979. Hydraulics of Groundwater. McGraw-Hill, Israel.

Bibby R, 1981. Mass Transport of Solutes in Dual-Porosity Media. Water Resources Research, vol. 17, no. 4, pp. 1075 - 1081.

Carlsson L, Grundfelt B, Winberg A, 1987. Hydraulic modelling of the final repository for reactor waste (SFR) - Evaluation of the groundwater modelling of groundwater flow situation at SFR. Stockholm, SKB - PR SFR 86-07.

Dykhuizen R C, 1990. A New Coupling Term for Dual-Porosity Models. Water Resources Research, vol. 26, no. 2, pp. 351 - 356.

Forsmark T, 1992. Hydraulic tests at Äspö in KAS16. Evaluation. SKB PR 25-92-15.

FTRANS, 1983. A Two-Dimensional Code for Simulating Fluid Flow and Transport of Radioactive Nuclides in Fractured Rock for Repository Performance Assessment - Technical Report. INTERA Environmental Consultants, Inc., Houston.

Grisak G E, Pickens J F, 1980. Solute Transport Through Fractured Media, 1, The Effect of Matrix Diffusion. Water Resources Research, vol. 16, no. 4, pp. 719 - 730.

Grundfelt B, Lindbom B, Liedholm M, Rhén I, 1990. Predictive Groundwater Flow Modelling of a Long Time Pumping Test (LPT1) at Äspö. SKB PR 25-90-04.

Herbert A W, Gale J E, 1989. Fracture flow modelling of the site characterization and validation area in the Stripa mine. NEA/SKB International Symposium on the Stripa Project, Stockholm, Sweden.

HYDROCOIN, 1988. The international HYDROCOIN project - Level 1: Code verification. Paris, Organization for Economic Co-operation and Development (OECD).

HYDROCOIN, 1990. The international HYDROCOIN project - Level 2: Code validation, Paris, Organization for Economic Co-operation and Development (OECD).

HYDROCOIN, 1991. The international HYDROCOIN project - Level 3: Sensitivity and uncertainty analysis, Paris, Organization for Economic Co-operation and Development (OECD).

HYDROCOIN, 1992. The international HYDROCOIN project - Summary report. Paris, Organization for Economic Co-operation and Development (OECD).

Huyakorn P S, Lester B H, Mercer J W, 1983. An Efficient Finite Element Technique for Modelling Transport in Fractured Porous Media, 1, Single Species Transport. Water Resources Research, vol. 19, no. 3, pp. 841 - 854.

Huyakorn P S, Pinder G F, 1983. Computational Methods in Subsurface Flow. Academic Press INC, Orlando.

Kakkuri J, 1986. Newest results obtained in studying the Fennoscandian land uplift phenomenon. In: Hennenerg H G (ed.), Recent Crustal Movements, 1985. Tectonophysics, 130, pp. 327-331.

Laitinen M, 1995. Modelling convection dominated transport problems with improved Galerkin finite element formulations. Technical Research Centre of Finland, Espoo. VTT julkaisuja - Publikationer 804 (in Finnish).

Lide D R (ed.), 1990. CRC Handbook of Chemistry and Physics. 71st edition 1990-1991. CRC Press, Inc., Boston.

Liedholm M, 1987. Regional Well Water Chemistry. SKB PR 25-87-08.

Löfman J, Taivassalo V, 1993. FEFLOW 1.10 - Solving of Coupled Equations for Flow, Heat and Solute Transport. Nuclear Waste Commission of Finnish Power Companies, Helsinki. YJT-93-30 (in Finnish).

Marsily G de, 1986. Quantitative Hydrogeology - Groundwater Hydrology for Engineers. Academic Press INC, Orlando.

Narasimhan T N, 1982. Multidimensional Numerical Simulation of Fluid Flow in Fractured Porous Media, Water Resources Research, vol. 18, no. 4, pp. 1235 - 1247.

Neretnieks I, Abelin H, Birgersson L, 1987. Some recent observations of channeling in fractured rock - Its potential impact on radionuclide migration. In: Buxton, B.E. (ed.) Proc. DOE/AECL Conf. on Geostatistical, Sensitivity, and Uncertainty methods for Groundwater flow and Radionuclide Transport Modeling, 387-410. Battelle Press, San Francisco.

PATRAN, 1989. Patran Plus User Manual, Release 2.4. Costa Mesa, PDA Engineering, California.

Press W H, Flannery B P, Teukolsky S A, Vetterling W T, 1986. Numerical Recipes - The Art of Scientific Computing. Cambridge University Press, Cambridge.

Rhén I, Forsmark T, 1993. Information for numerical modelling, undisturbed pietzometric levels and uncertainty of pietzometric levels. Äspö Hard Rock Laboratory, Technical note 25-92-63G.

SKB, 1992. Treatment and final disposal of nuclear waste - Äspö Hard Rock Laboratory. Background report to RD&D-Programme 92. SKB.

Ström A, 1993. Äspö Hard Rock Laboratory, Task Force on modelling of groundwater flow and transport of solutes, Data delivery No. 4 for Task No. 1: Geometric data for hydraulically interpreted fracture zones at Äspö. Memorandum 15.2.1993.

Ström A, 1993a. Äspö Hard Rock Laboratory, Task Force on modelling of groundwater flow and transport of solutes, Data delivery No. 5 for Task No. 1: Complementary information regarding the LPT2 experiment. Memorandum 11.6.1993.

Sudicky E A, Frind E O, 1982. Contaminant Transport in Fractured Porous Media: Analytic Solutions for a System of Parallel Fractures. Water Resources Research, vol. 18, no. 6, pp. 1634 - 1642.

Svensson U, 1990. The island of Äspö - Numerical calculations of natural and forced groundwater circulation. SKB Progress Report 25-90-03.

Tang D H, Frind E O, Sudicky E A, 1981. Contaminant Transport in Fractured Porous Media: Analytical solution for A Single Fracture. Water Resources Research, vol. 17, no. 3, pp. 555 - 564.

Taivassalo V, Koskinen L, Laitinen M, Löfman J, Mészáros F, 1994. Modelling the LPT2 pumping and tracer test at Äspö - Pumping test. SKB ICR 94-12.

Taivassalo V, Koskinen L, Meling K, 1994. Groundwater flow modelling in the preliminary site investigations - Modelling strategy and computer codes. Nuclear Waste Commission of Finnish Power Companies, Helsinki. YJT-94-04.

Taivassalo V, Koskinen L, Mészáros F, 1991. Further development of the FEFLOW code for transient simulations. Teollisuuden Voima Oy, TVO/Safety and Technology, Helsinki. Work Report 91-14 (in Finnish).

Taivassalo V, Mészáros F, 1994. Simulation of the groundwater flow of the Kivetty area: (1) Flow model and finite element meshes, (2) Calibration of the flow model, (3) Results. Nuclear Waste Commission of Finnish Power Companies, Helsinki. YJT-94-03.

Taivassalo V, Saarenheimo A, 1991. Groundwater flow analysis for the VLJ repository. Nuclear Waste Commission of Finnish Power Companies, Helsinki. YJT-91-10.

Valkiainen, 1992. Diffusion in the rock matrix - A review of laboratory tests and field studies. Nuclear Waste Commission of Finnish Power Companies, Helsinki. YJT-92-04.

Vieno T, Hautojärvi A, Koskinen L, Nordman H, 1992. TVO-92 Safety analysis of spent fuel disposal. Nuclear Waste Commission of Finnish Power Companies, Helsinki. YJT-92-33E.

Voss C, Andersson J, 1991. Some Aspects of Regional Flow of Variable-Density Groundwater in Crystalline Basement Rock of Sweden. Swedish Nuclear Power Inspectorate, SKI Technical Report 91:9.

Wikberg P (ed.), Gustafson G, Rhén I, Stanfors R, 1991. Äspö Hard Rock Laboratory. Evaluation and conceptual modelling based on the pre-investigations 1986 - 1990. SKB TR 91-22.

Measured and computed pressures in boreholes

transient and steady state simulation with salinity model (i) (constant 10 g/l)

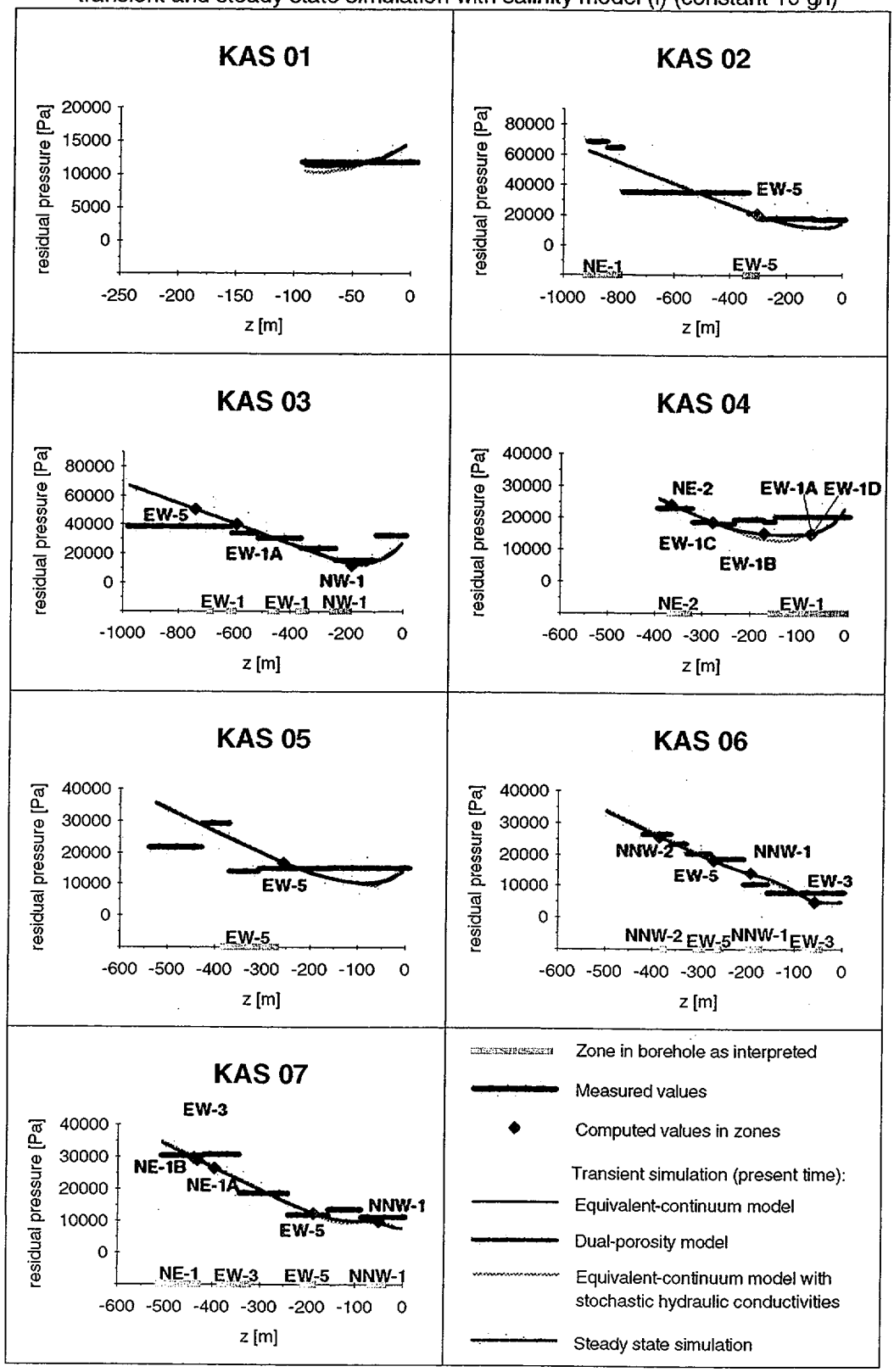

Measured and computed pressures in boreholes

transient and steady state simulation with salinity model (i) (constant 10 g/l)

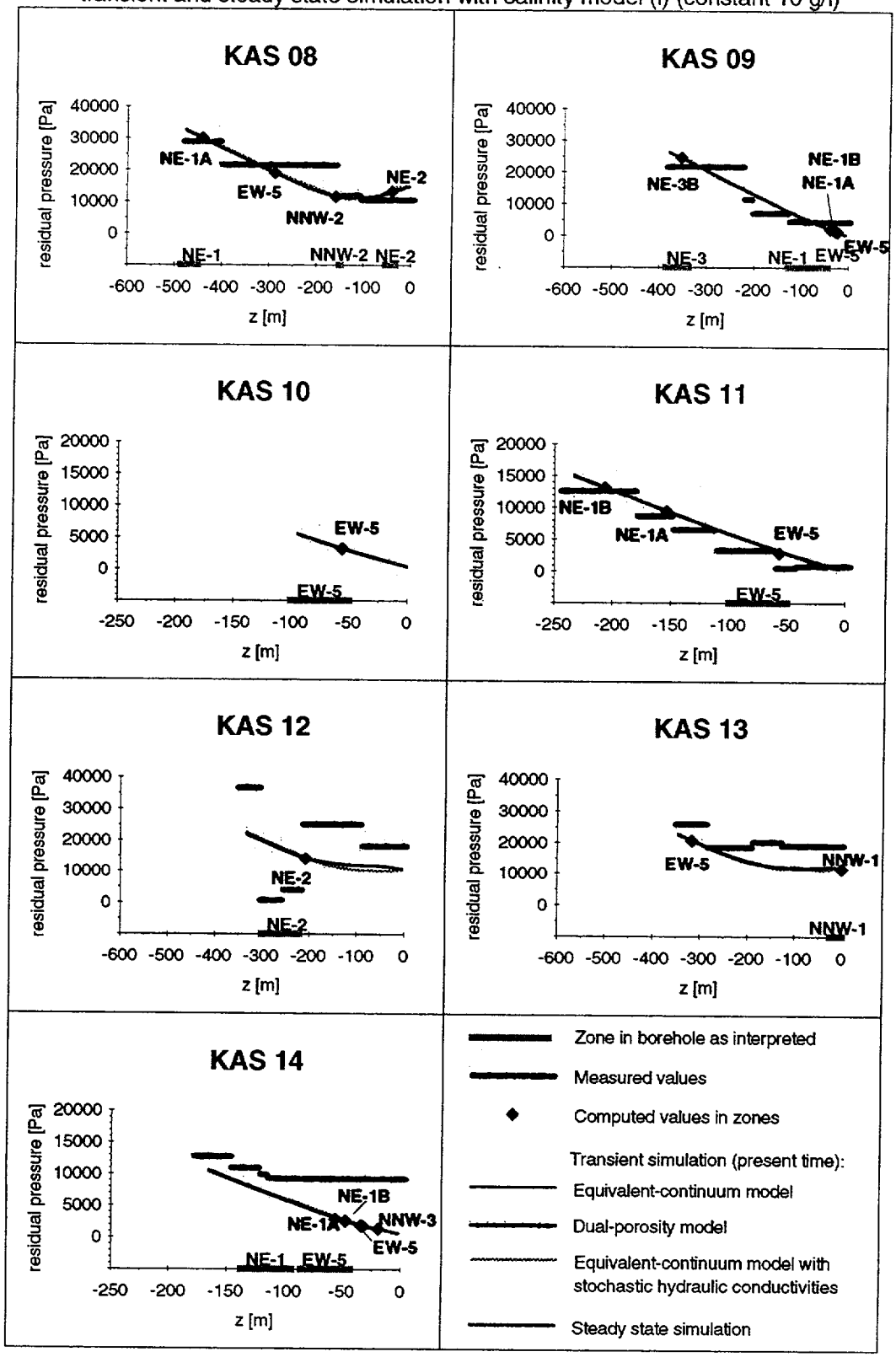

Measured and computed concentrations in boreholes at present time

transient simulation with equivalent-continuum model and salinity model (i)

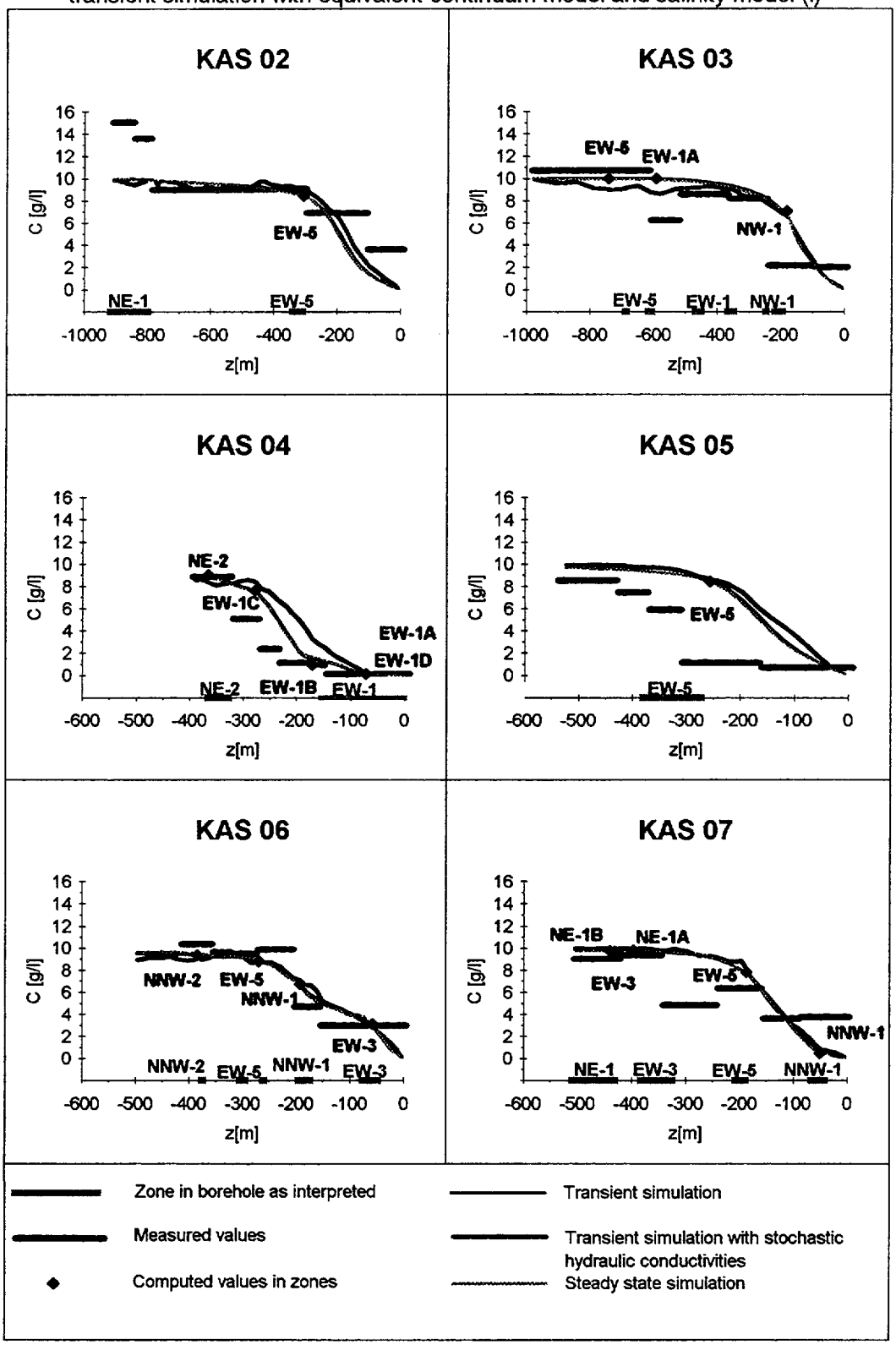

Measured and computed concentrations in boreholes at present time

transient simulation with equivalent-continuum model and salinity model (i)

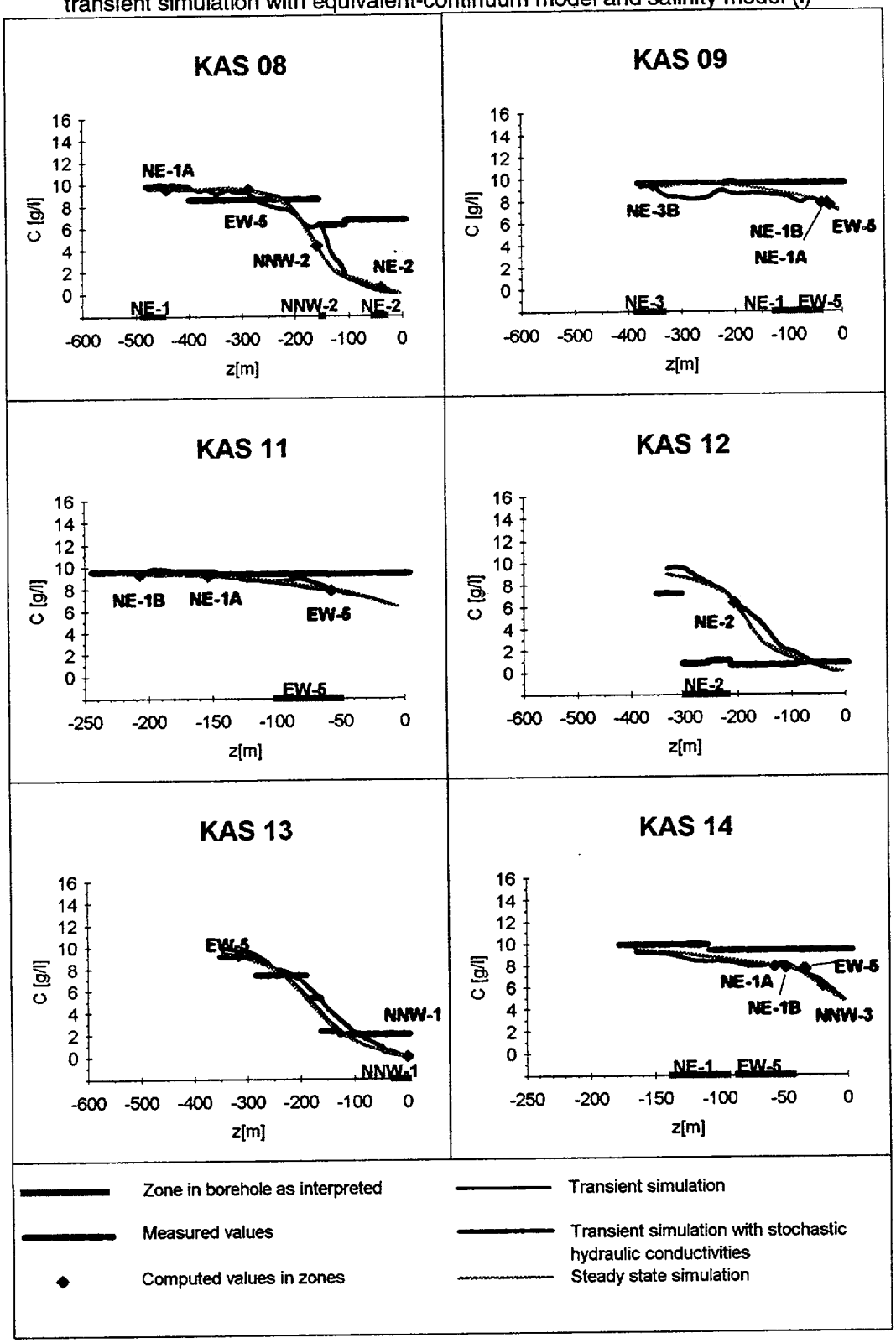

Measured and computed concentrations in the fracture domain in boreholes at present time

transient simulation with dual-porosity model and different matrix porosities

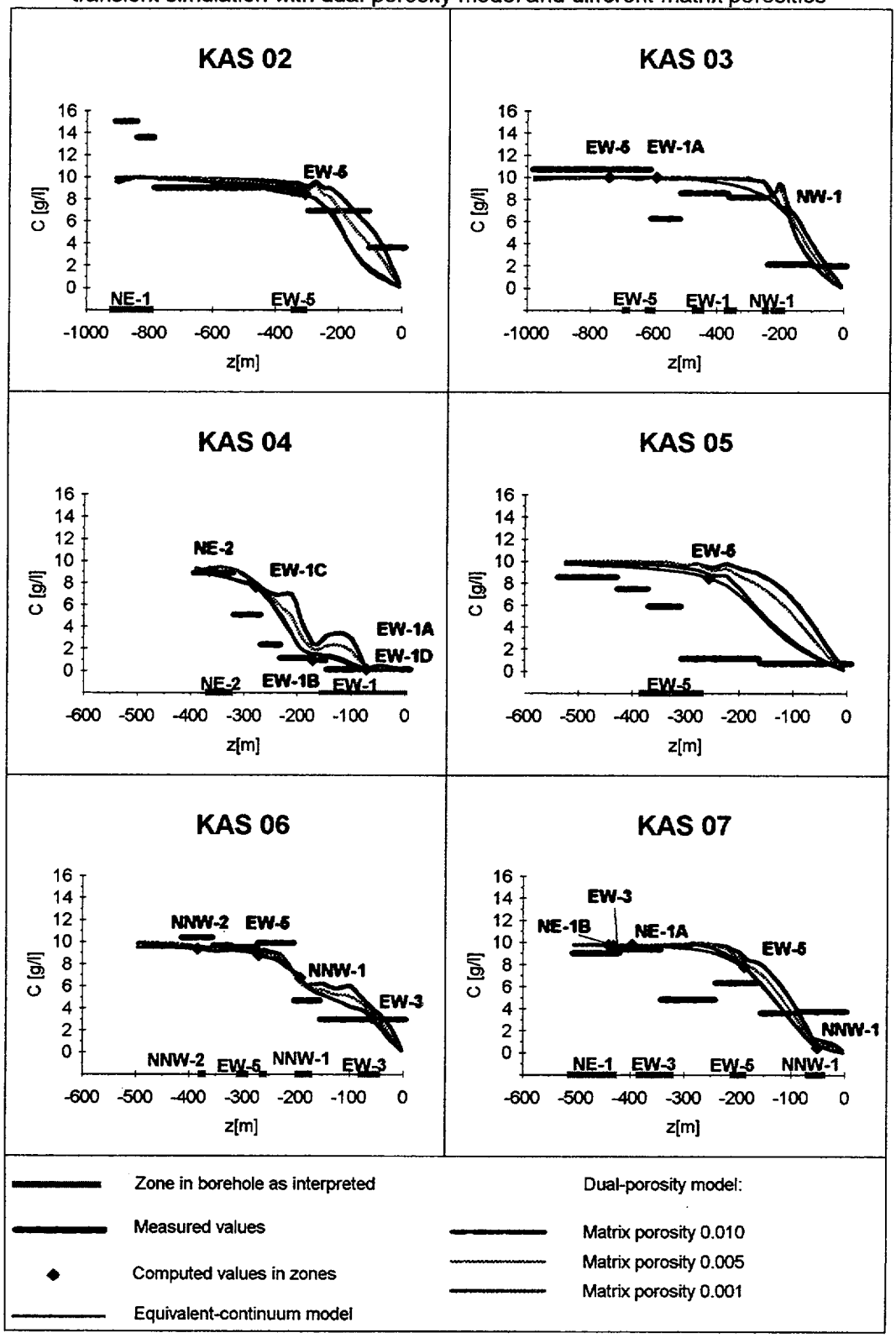

Measured and computed concentrations in the fracture domain in boreholes at present time

transient simulation with dual-porosity model and different matrix porosities

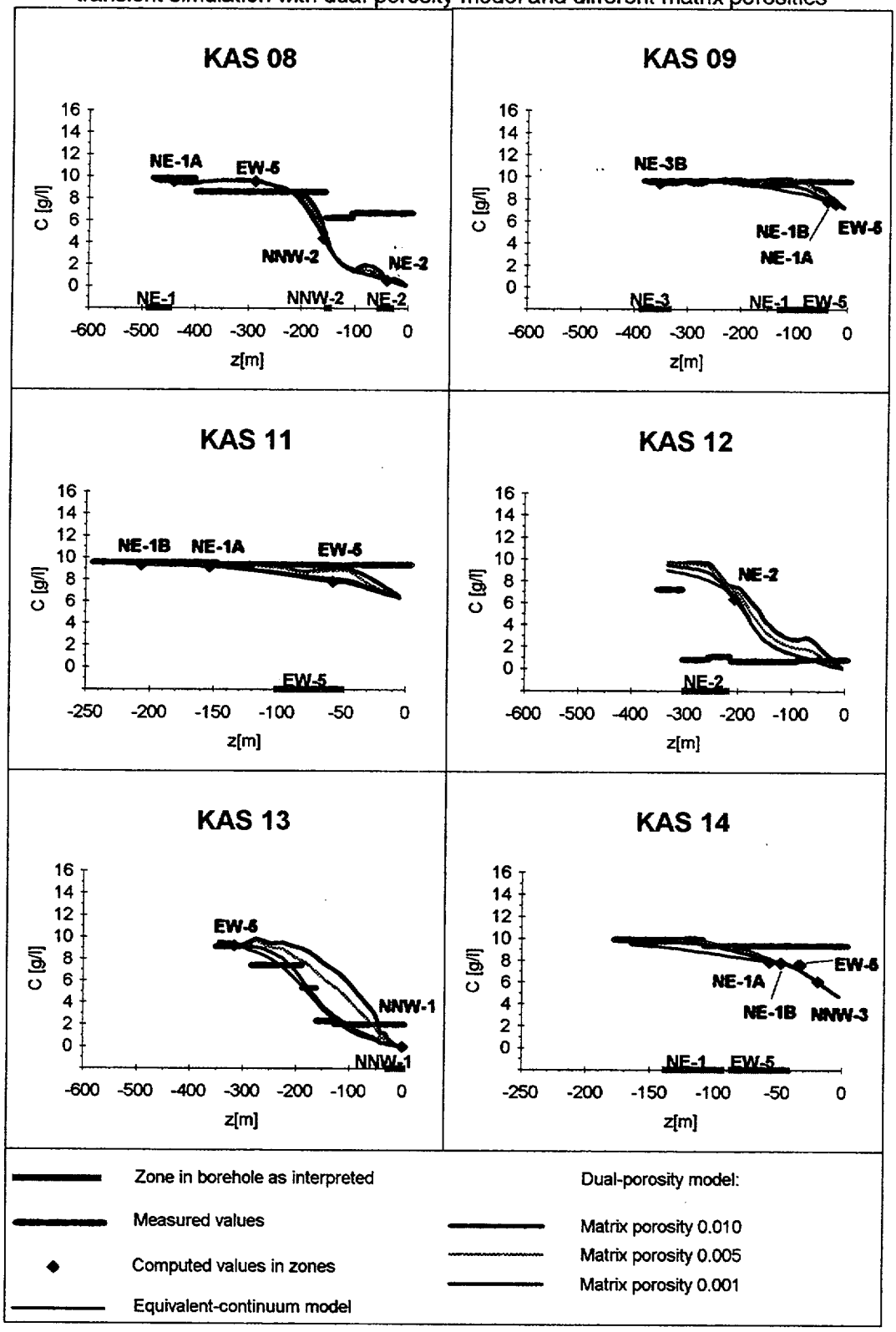

Measured and computed concentrations in the fracture domain in boreholes at present time

transient simulation with dual-porosity model and different matrix thicknesses

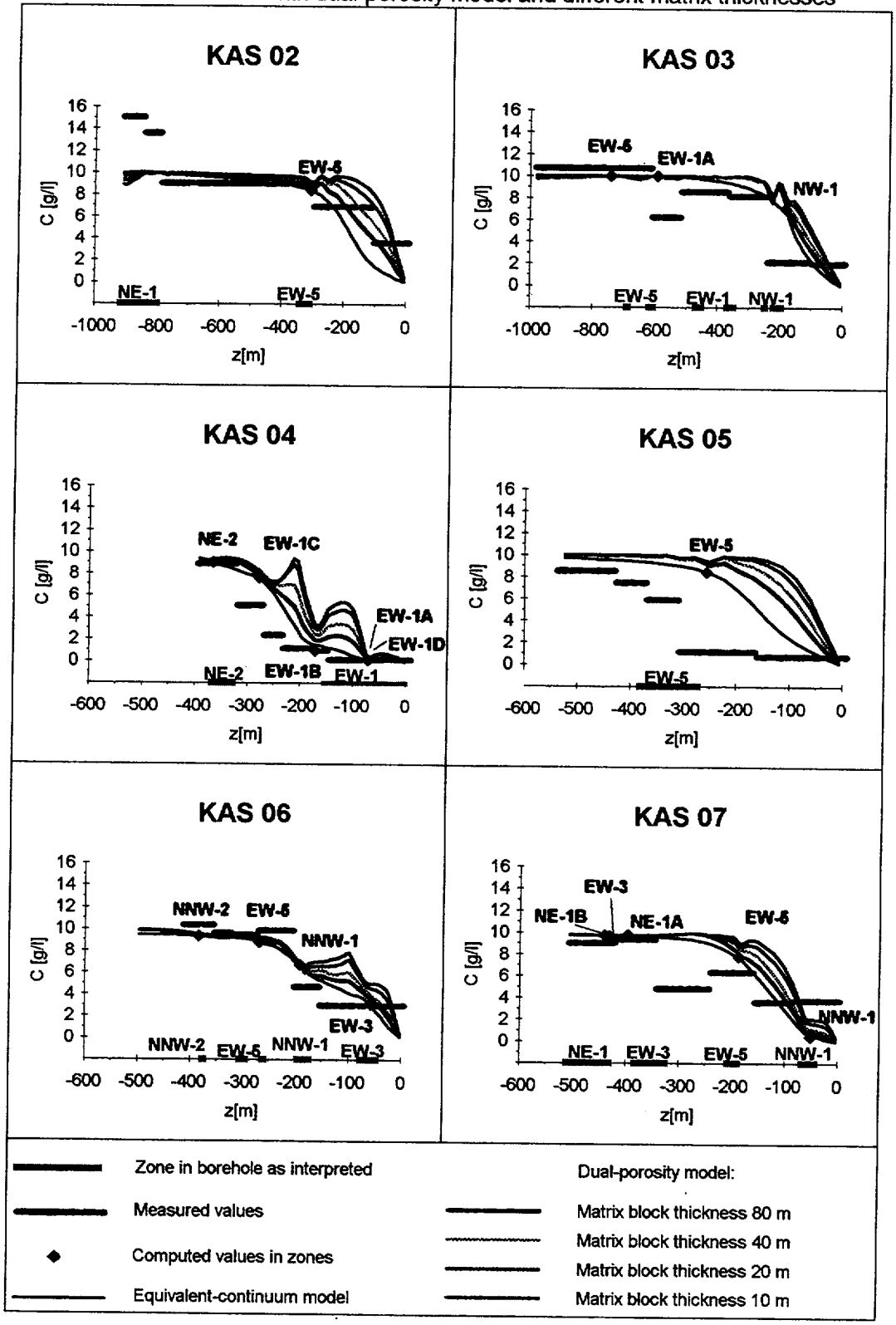

Measured and computed concentrations in the fracture domain in boreholes at present time

transient simulation with dual-porosity model and different matrix thicknesses

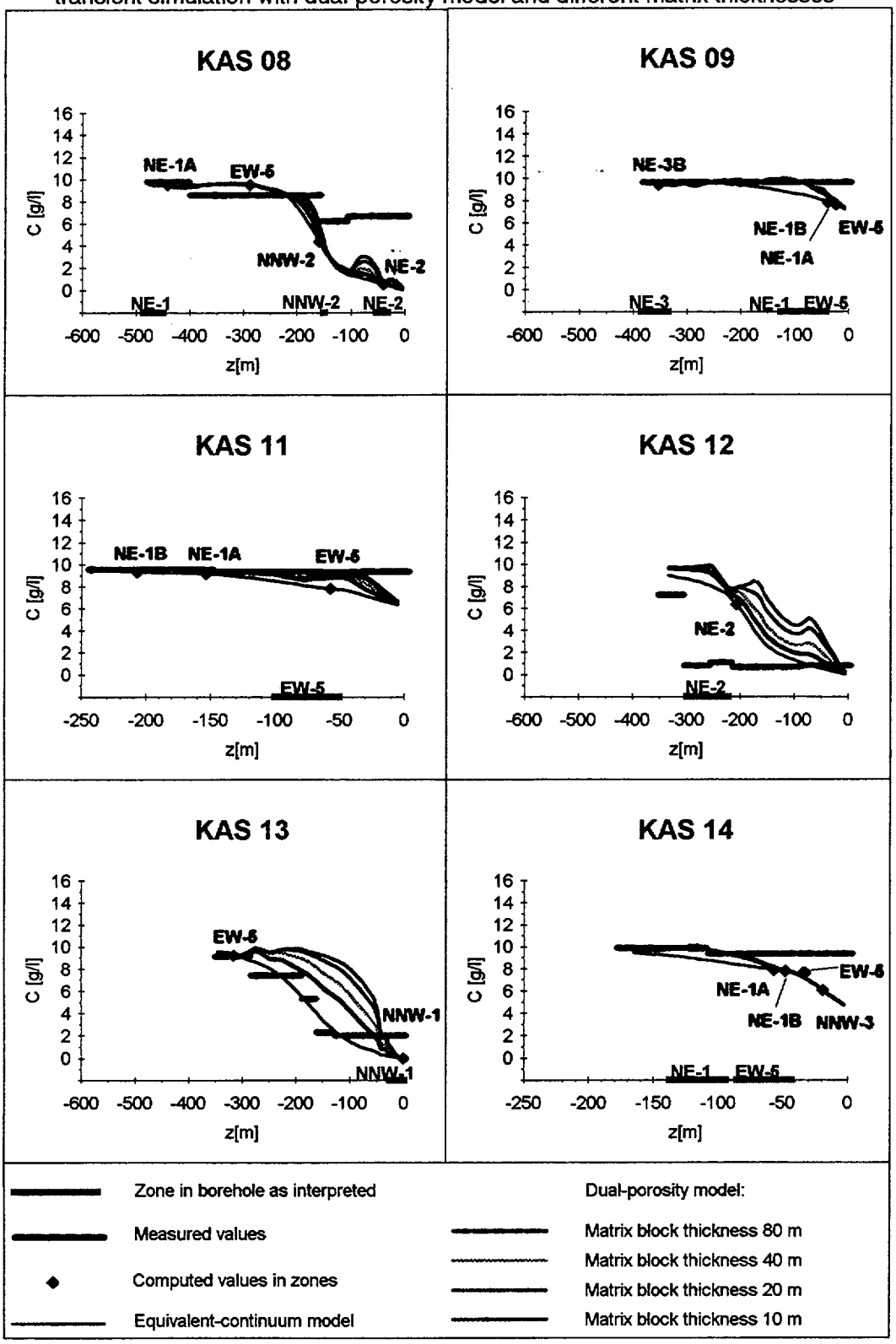

Computed concentrations in matrix blocks in boreholes at present time

dual-porosity model with matrix block thickness 40 m and porosity 0.01

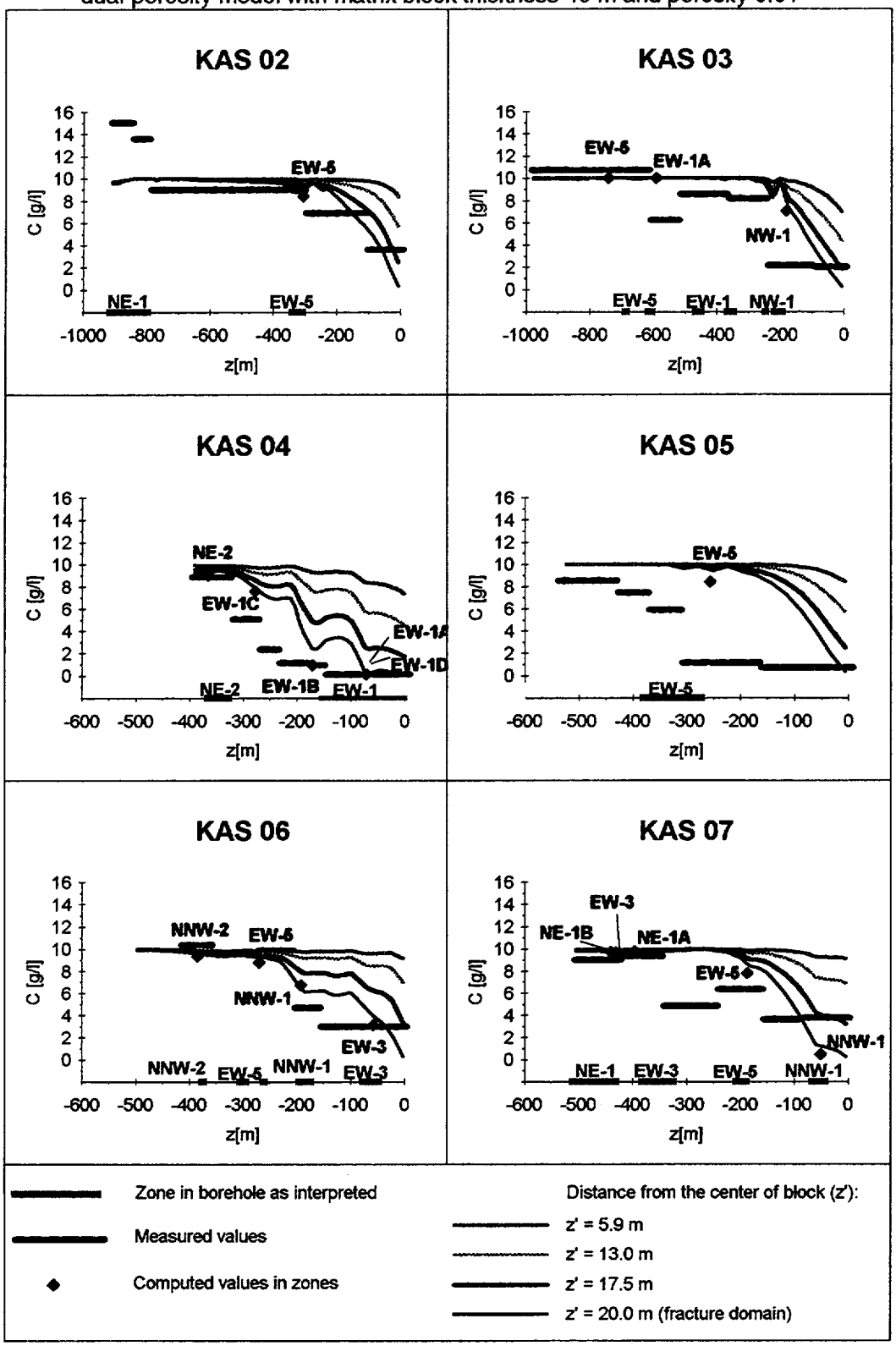

Computed concentrations in matrix blocks in boreholes at present time

dual-porosity model with matrix block thickness 40 m and porosity 0.01

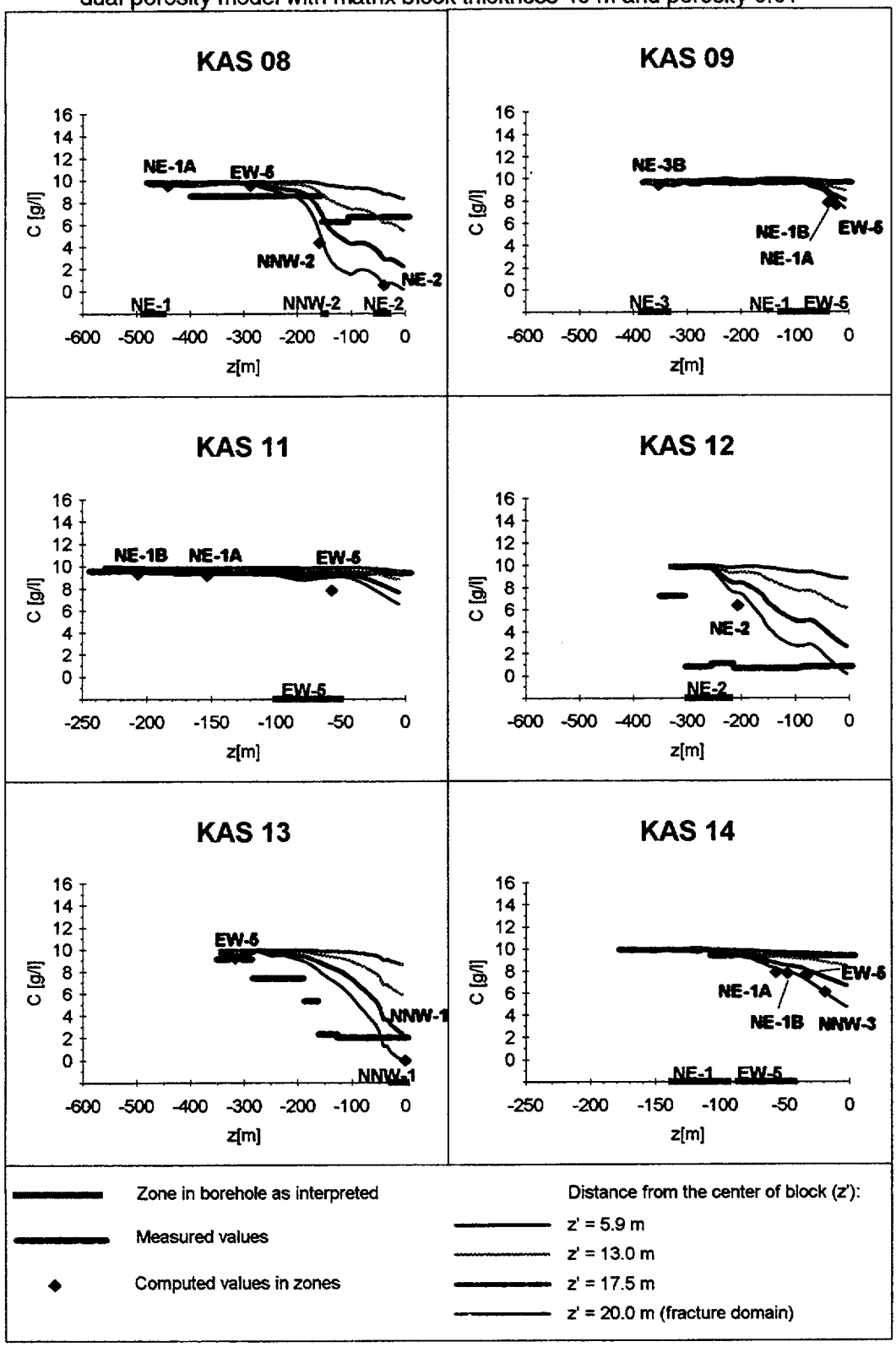

Computed concentrations in matrix blocks in boreholes at present time

dual-porosity model with matrix block thickness 10 m and porosity 0.01

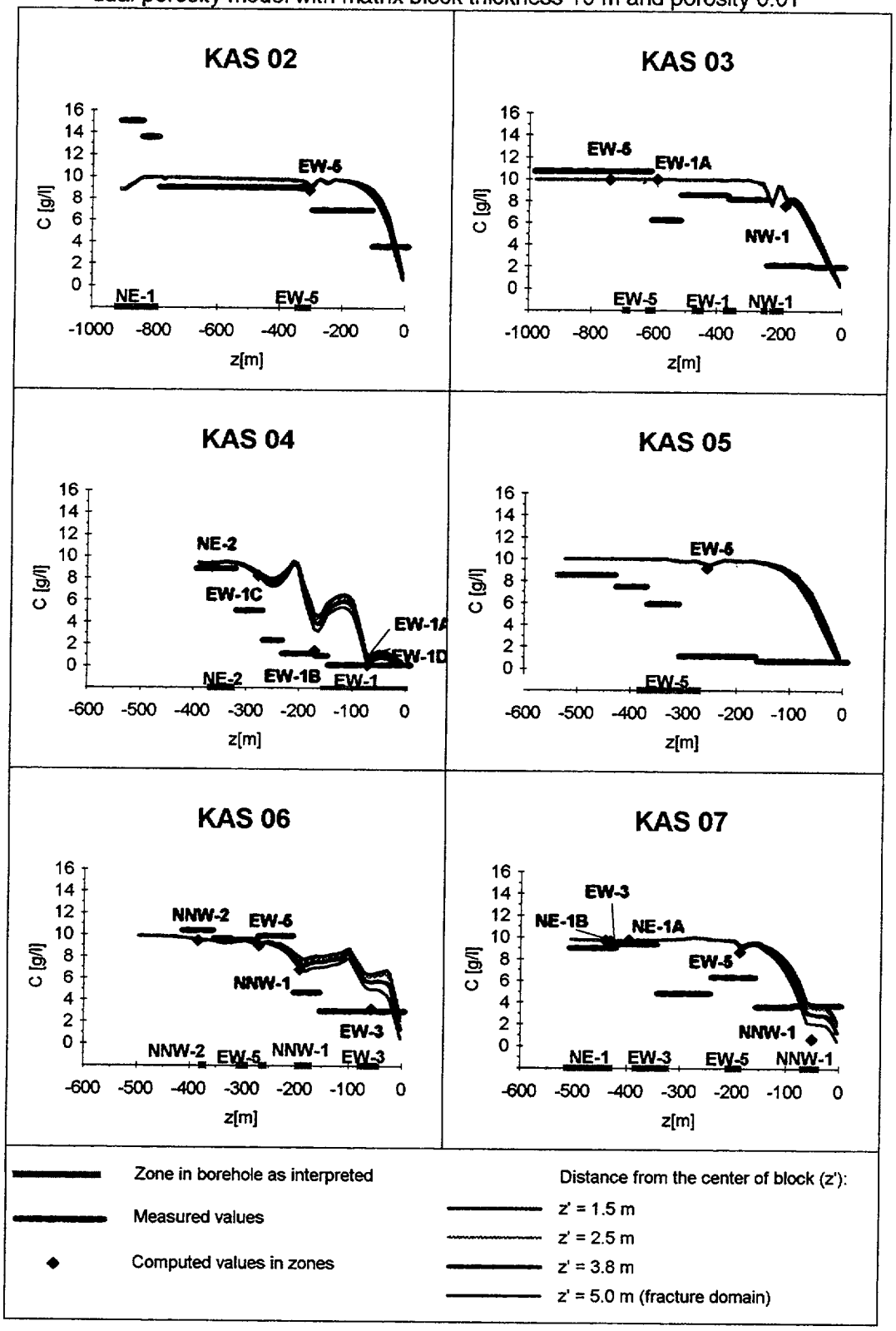

Computed concentrations in matrix blocks in boreholes at present time

dual-porosity model with matrix block thickness 10 m and porosity 0.01

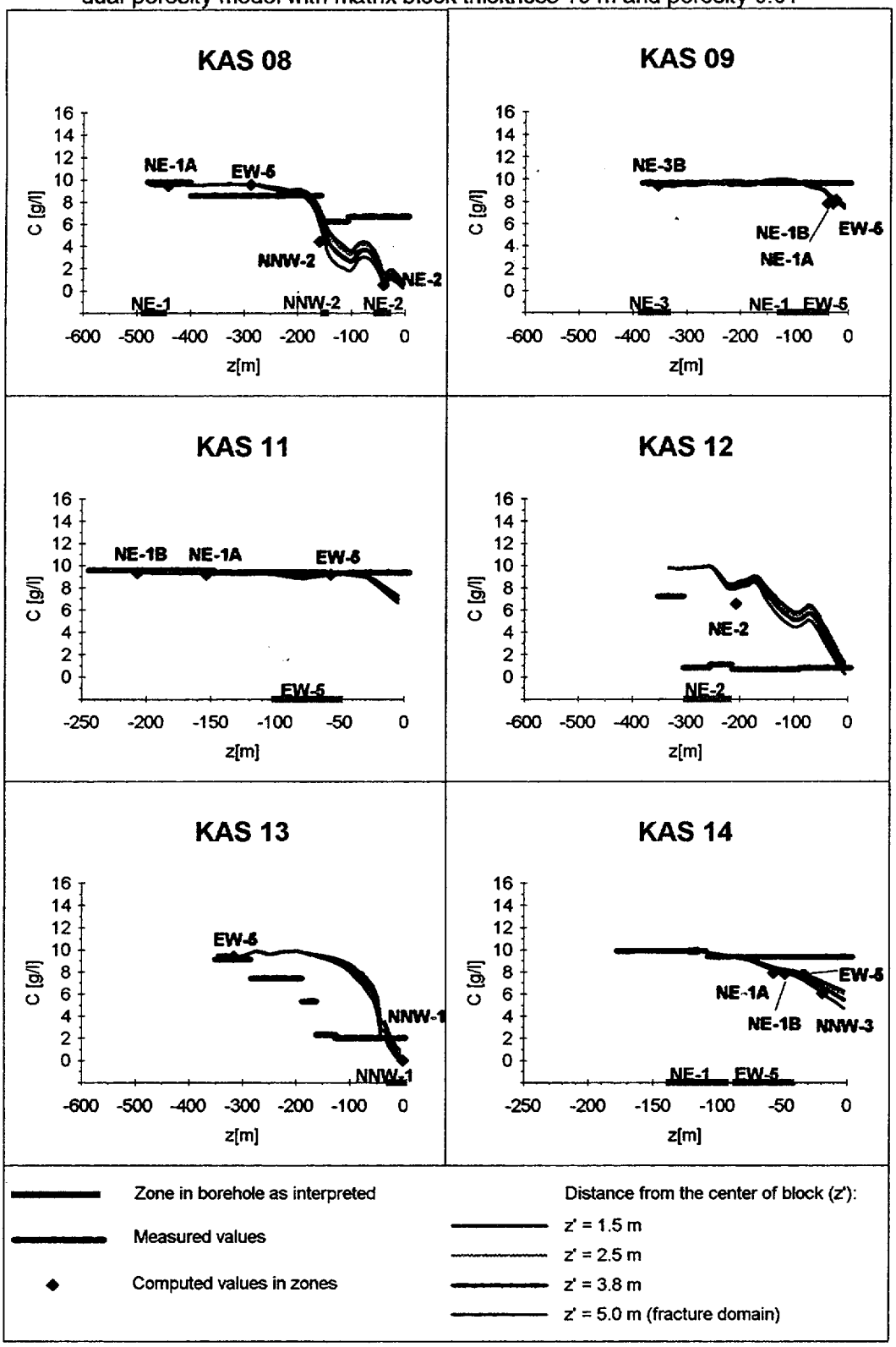

Computed concentrations at the center of the matrix blocks (z' = 0) in boreholes at present time

dual-porosity model with matrix block porosity 0.01

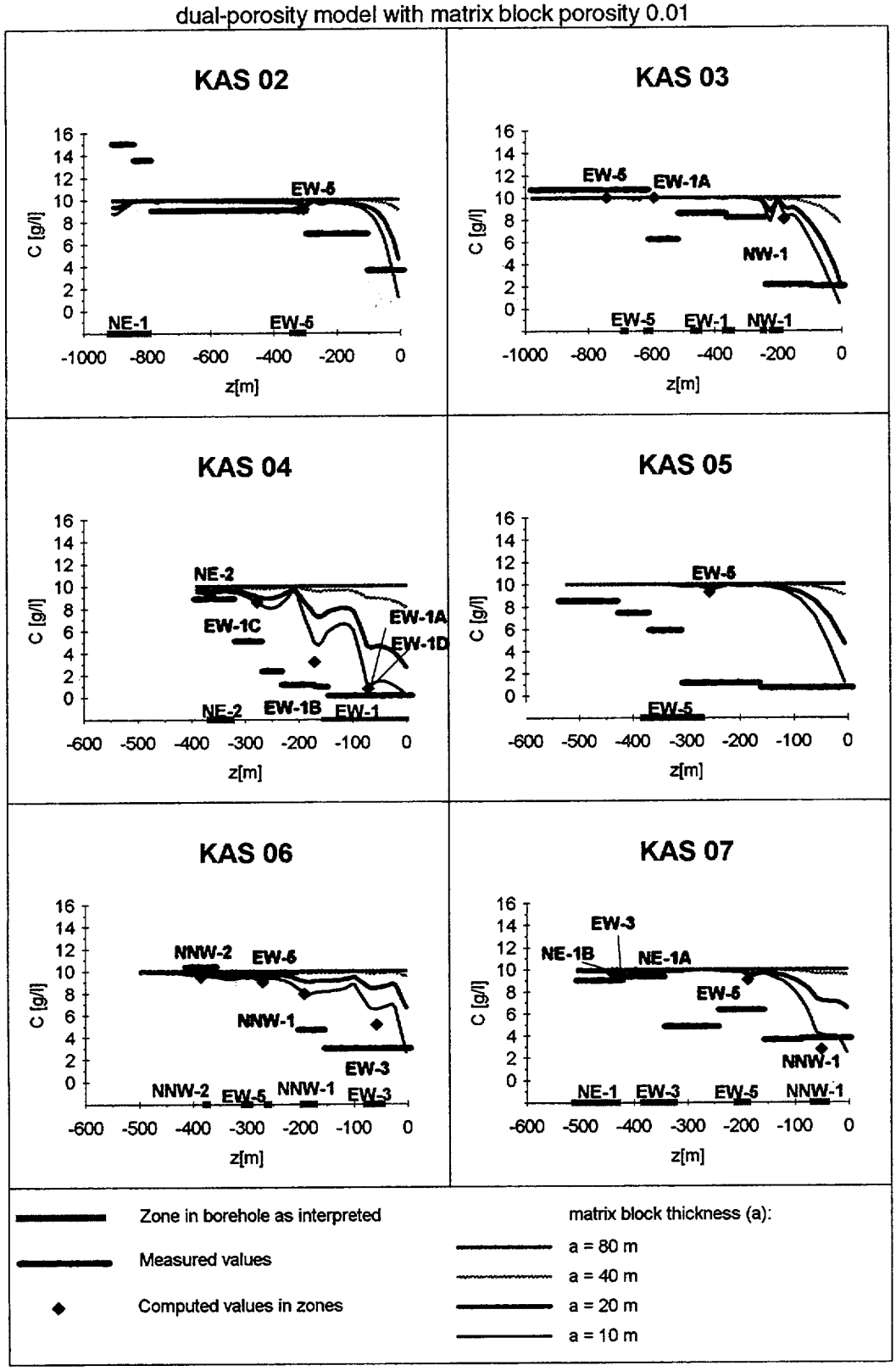

Computed concentrations at the center of the matrix blocks (z' = 0) in boreholes at present time

dual-porosity model with matrix block porosity 0.01

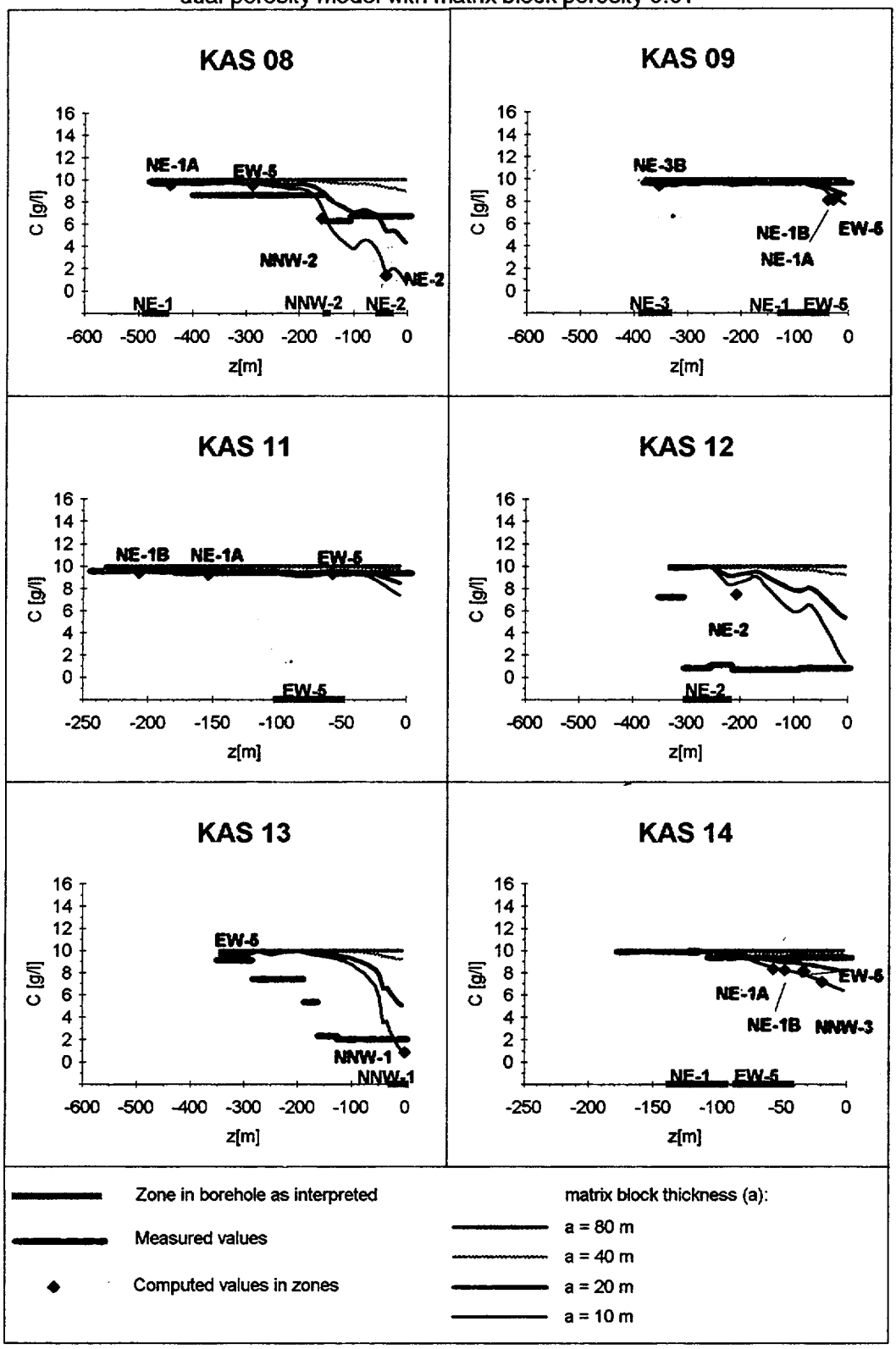

Computed concentrations at the center of the matrix blocks (z' = 0) in boreholes at present time

dual-porosity model with matrix block thickness 40 m

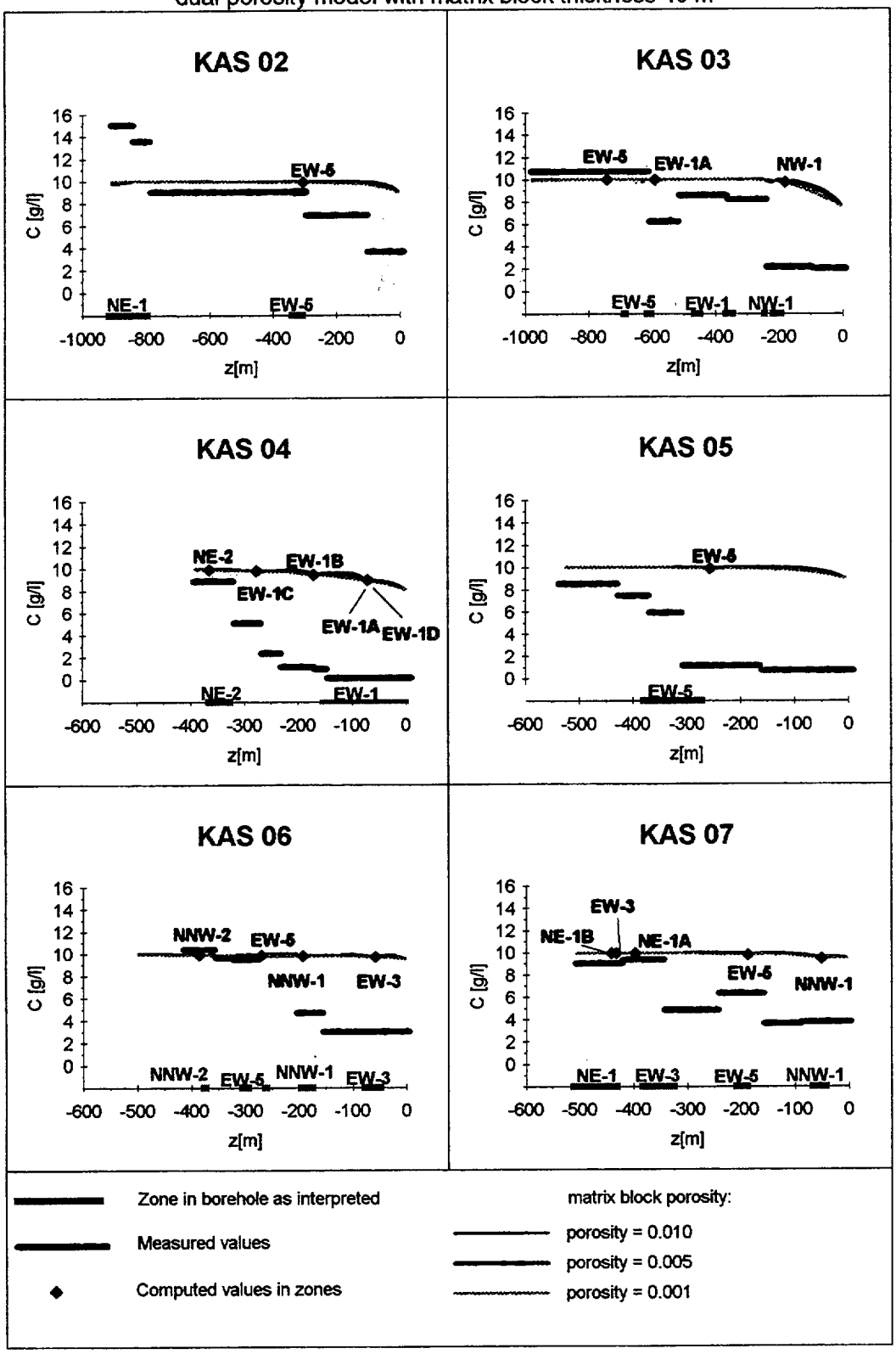

Computed concentrations at the center of the matrix blocks (z' = 0) in boreholes at present time

dual-porosity model with matrix block thickness 40 m

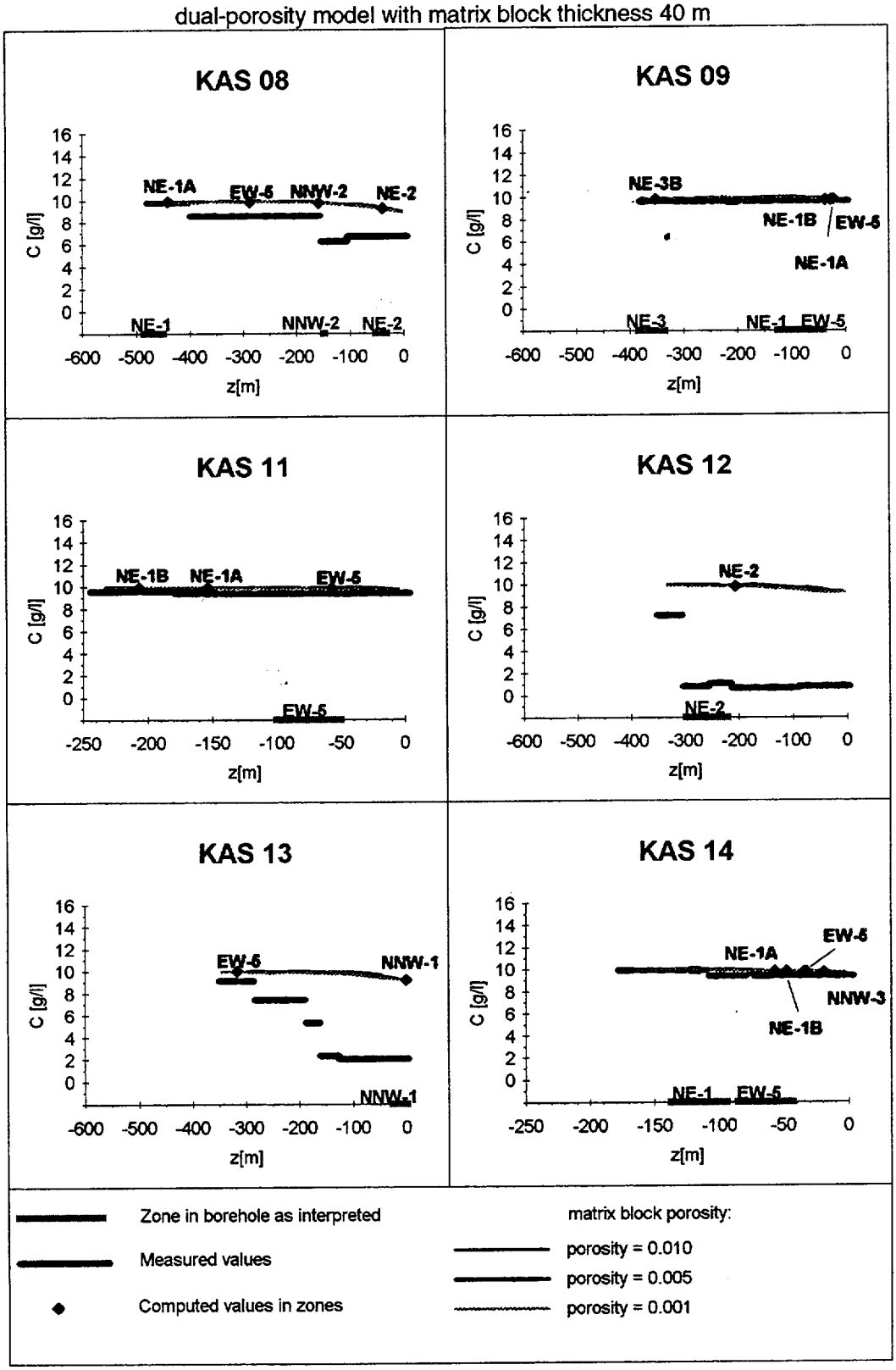

List of International Cooperation Reports

ICR 93-01
Flowmeter measurement in borehole KAS 16
P Rouhiainen
June 1993
Supported by TVO, Finland

ICR 93-02
Development of ROCK-CAD model for Äspö Hard Rock Laboratory site
Pauli Saksa, Juha Lindh,
Eero Heikkinen
Fintact KY, Helsinki, Finland
December 1993
Supported by TVO, Finland

ICR 93-03
Scoping calculations for the Matrix Diffusion Experiment
Lars Birgersson[1], Hans Widén[1],
Thomas Ågren[1], Ivars Neretnieks[2],
Luis Moreno[2]
1 Kemakta Konsult AB, Stockholm, Sweden
2 Royal Institute of Technology, Stockholm, Sweden
November 1993
Supported by SKB, Sweden

ICR 93-04
Scoping calculations for the Multiple Well Tracer Experiment - efficient design for identifying transport processes
Rune Nordqvist, Erik Gustafsson,
Peter Andersson
Geosigma AB, Uppsala, Sweden
December 1993
Supported by SKB, Sweden

ICR 94-01
Scoping calculations for the Multiple Well Tracer Experiment using a variable aperture model
Luis Moreno, Ivars Neretnieks
Dept. of Chemical Engineering and Technology,
Royal Institute of Technology, Stockholm, Sweden
January 1994
Supported by SKB, Sweden

ICR 94-02
Äspö Hard Rock Laboratory. Test plan for ZEDEX - Zone of Excavation Disturbance EXperiment. Release 1.0
February 1994
Supported by ANDRA, NIREX, SKB

ICR 94-03
The Multiple Well Tracer Experiment - Scoping calculations
Urban Svensson
Computer-Aided Fluid Engineering
March 1994
Supported by SKB, Sweden

ICR 94-04
Design constraints and process discrimination for the Detailed Scale Tracer Experiments at Äspö - Multiple Well Tracer Experiment and Matrix Diffusion Experiment
Jan-Olof Selroos[1], Anders Winberg[2], Vladimir Cvetkovic[2]
1 Water Resources Eng., KTH
2 Conterra AB
April 1994
Supported by SKB, Sweden

ICR 94-05
Analysis of LPT2 using the Channel Network model
Björn Gylling[1], Luis Moreno[1], Ivars Neretnieks[1], Lars Birgersson[2]
1 Department of Chemical Engineering and Technology, Royal Institute of Technology, Stockholm, Sweden
2 Kemakta Konsult AB, Stockholm, Sweden
April 1994
Supported by SKB, Sweden

ICR 94-06
SKB/DOE Hard Rock Laboratory Studies Task 3. Geochemical investigations using stable and radiogenic isotopic methods
Bill Wallin[1], Zell Peterman[2]
1 Geokema AB, Lidingö, Sweden
2 U.S. Geological Survey, Denver, Colorado, USA
January 1994
Supported by SKB and U.S.DOE

ICR 94-07
Analyses of LPT2 in the Äspö HRL with continuous anisotropic heterogeneous model
Akira Kobayashi[1], Ryo Yamashita[2], Masakazu Chijimatsu[2], Hiroyuki Nishiyama[3], Yuzo Ohnishi[3]
1 Iwate University, Iwate, Japan
2 Hazama Corporation, Ibaraki, Japan
3 Kyoto University, Kyoto, Japan
September 1994
Supported by PNC, Japan

ICR 94-08
Application of three-dimensional smeared fracture model to the groundwater flow and the solute migration of LPT-2 experiment
T Igarashi, Y Tanaka, M Kawanishi
Abiko Research Laboratory, Central Research Institute of Electric Power Industry, Abiko, Japan
October 1994
Supported by CRIEPI, Japan

ICR 94-09
Discrete-fracture modelling of the Äspö LPT-2, large-scale pumping and tracer test
Masahiro Uchida[1], Thomas Doe[2], William Dershowitz[2], Andrew Thomas[2], Peter Wallmann[2], Atsushi Sawada[1]
1 Power Reactor and Nuclear Fuel Development Co., Tokai, Japan
2 Golder Associates Inc., Seattle, WA, USA
March 1994
Supported by PNC, Japan

ICR 94-10
Äspö Hard Rock Laboratory
International workshop on the use of tunnel boring machines for deep repositories
Äspö, June 13-14 1994
Göran Bäckblom (ed.)
Swedish Nuclear Fuel and Waste Management Co.
October 1994
Supported by SKB, Sweden

ICR 94-11
Data analysis and modelling of the LPT2 Pumping and Tracer Transport Test at Äspö.
Tracer experiment
Aimo Hautojärvi
VTT Energy
November 1994
Supported by TVO, Finland

ICR 94-12
Modelling the LPT2 Pumping and Tracer Test at Äspö. Pumping test
Veikko Taivassalo, Lasse Koskinen,
Mikko Laitinen, Jari Löfman, Ferenc Mészáros
VTT Energy
November 1994
Supported by TVO, Finland

ICR 94-13
Proceedings of The Äspö International Geochemistry Workshop, June 2-3, 1994, Äspö Hard Rock Laboratory
Peter Wikberg (chairman), Steven Banwart (proc. ed.)
December 1994
Supported by SKB, TVO, Nirex, ANDRA, CRIEPI

ICR 94-14
Hydrodynamic modelling of the Äspö HRL. Discrete fracture model
D Billaux[1], F Guérin[2], J Wendling[2]
1 ITASCA
2 ANTEA
November 1994
Supported by ANDRA, France

ICR 94-15
Hydrodynamic modelling of the Äspö Hard Rock Laboratory. ROCKFLOW code
M L Noyer, E Fillion
ANTEA
December 1994
Supported by ANDRA, France

ICR 94-16
Hydrodynamic modelling of the original steady state and LPT2 experiments. MARTHE and SESAME codes
Y Barthelemy, J Schwartz, K Sebti
ANTEA
December 1994
Supported by ANDRA, France